



BEDROCK GEOLOGY OF THE FULTON CHAIN-OF-LAKES AREA WEST CENTRAL ADIRONDACK MOUNTAINS, NEW YORK

BY PHILIP R. WHITNEY ■ ROBERT H. FAKUNDINY ■ YNGVAR W. ISACHSEN



MAP AND CHART 44
2002


NEW YORK State
Museum

**BEDROCK GEOLOGY OF
THE FULTON CHAIN-OF-LAKES AREA
WEST-CENTRAL ADIRONDACK MOUNTAINS, NEW YORK**

THE UNIVERSITY OF THE STATE OF NEW YORK

Regents of The University

ROBERT M. BENNETT, <i>Chancellor</i> , B.A., M.S.	Tonawanda
ADELAIDE L. SANFORD, <i>Vice Chancellor</i> , B.A., M.A., Ph.D.	Hollis
DIANE O'NEILL MCGIVERN, B.S.N., M.A., Ph.D.	Staten Island
SAUL B. COHEN, B.A., M.A., Ph.D.	New Rochelle
JAMES C. DAWSON, A.A., B.A., M.S., Ph.D.	Peru
ROBERT M. JOHNSON, B.S., J.D.	Huntington
ANTHONY S. BOTTAR, B.A., J.D.	North Syracuse
MERRYL H. TISCH, B.A., M.A.	New York
GERALDINE D. CHAPEY, B.A., M.A., Ed.D.	Belle Harbor
ARNOLD B. GARDNER, B.A., LL.B.	Buffalo
HARRY PHILLIPS, 3rd, B.A., M.S.F.S.	Hartsdale
JOSEPH E. BOWMAN, JR., B.A., M.L.S., M.A., M.Ed., Ed.D.	Albany
LORRAINE A. CORTÉS-VÁZQUEZ, B.A., M.P.A.	Bronx
JUDITH O. RUBIN, A.B.	New York
JAMES R. TALLON, JR., B.A., M.A.	Binghamton
MILTON L. COFIELD, B.S., M.B.A., Ph.D.	Rochester

President of The University and Commissioner of Education

RICHARD P. MILLS

Chief Operating Officer

RICHARD H. CATE

Deputy Commissioner for Cultural Education

CAROLE F. HUXLEY

Director of the New York State Museum

CLIFFORD A. SEIGFRIED

The State Education Department does not discriminate on the basis of age, color, religion, creed, disability, marital status, veteran status, national origin, race, gender, genetic predisposition or carrier status, or sexual orientation in its educational programs, services, and activities. Portions of this publication can be made available in a variety of formats, including braille, large print, or audio tape, upon request. Inquiries concerning this policy of nondiscrimination should be directed to the Department's Office for Diversity, Ethics, and Access, Room 530, Education Building, Albany, NY 12234. **Requests for additional copies of this publication may be made by contacting the Publications Sales, Room 3140 CEC, State Museum, Albany, NY 12230.**

**BEDROCK GEOLOGY OF
THE FULTON CHAIN-OF-LAKES AREA
WEST-CENTRAL ADIRONDACK MOUNTAINS, NEW YORK**

BY

PHILIP R. WHITNEY ■ ROBERT H. FAKUNDINY ■ YNGVAR W. ISACHSEN

NEW YORK STATE MUSEUM
MAP AND CHART SERIES NO. 44
2002

THE UNIVERSITY OF THE STATE OF NEW YORK
THE STATE EDUCATION DEPARTMENT

© The New York State Education Department, Albany, New York 12230

Published in 2002

Printed in the United States of America

Copies may be ordered from:

Publication Sales

New York State Museum

Albany, New York 12230

Phone: (518) 402-5344

FAX: (518) 474-2033

Library of Congress Control Number: 2002116877

ISBN: 1-55557-171-9

ISSN: 0097-3793

This book printed on acid free paper

Cover Photo:

Massive quartzite overlying amphibolite, unit BL, north bank of Moose River 4 miles west of McKeever.

Not a little (of Geology) consists of generalizations from incomplete data, of inferences hung on chains of uncertain logic, of interpretations not beyond question, of hypotheses not fully verified, and of speculations none too substantial. A part of this mass is true science, a part philosophy, . . . a part is speculation, and a part is yet unorganized material.

T. C. Chamberlain, 1904

Table of Contents

List of Figures	ix
List of Tables	xi
Acknowledgments	xiii
Introduction	1
Non-Technical Overview	3
Rocks of the Fulton Chain- of-Lakes Area	3
How Old Are These Rocks?	4
Geologic Structure	4
Regional Setting	5
The Last Billion Years	5
Geology and Landscape	6
Environmental Consequences	6
Chapter 1	
Metamorphosed Igneous Rocks	7
Charnockite-Granite Suite	7
Leucogranitic Gneiss	10
Megacrystic Biotite Granitic Gneiss	14
Granitic Gneisses within Other Units	14
Geochemistry of the Granitoids	15
Magmatic Temperatures and Pressures	21
Olivine Metagabbro	21
Anorthosite Suite	22
Amphibolite	23
Unmetamorphosed Diabase	24
Geochemistry of the Mafic Rocks	24
Chapter 2	
Metasedimentary Rocks	31
Calcsilicate Rocks and Marble	31
Metapelites	31
Quartzite	32
Quartzofeldspathic Metasedimentary Rocks	34
Metamorphosed Evaporites?	34
Regional Variation	35
Chapter 3	
Structure	37
Northwest Domain	37
West-central and East-central Domains	37
Moose River Domain	38
Southeast Domain	41
Jessup River Domain	43

Table of Contents, *continued*

Honnedaga Lake Domain	43
Flatfish Pond Domain	43
Inlet and Stillwater Zones	44
Domical Structures	44
Structural Synthesis	44
Brittle Structures	45
 Chapter 4	
Metamorphism	47
Metaigneous and Metavolcanic Rocks	47
Calcsilicates	51
Metapelites	53
Redox Equilibria	53
Anatexis	54
Relative Timing of Deformation and Metamorphism	54
Retrograde Metamorphic Effects	54
 Chapter 5	
Geochronology	57
 Chapter 6	
Geologic History and Tectonic Setting	59
Pre-1160 Ma	59
1160–1050 Ma	59
1050–990 Ma	60
 Chapter 7	
Glacial Geology	61
 Chapter 8	
Environmental Geology	63
 Tables	65
 References	99
 Appendices	
APPENDIX A Suggested Field Trip	107
APPENDIX B Notes on Mapping Units	115
APPENDIX C Lithology and Location of Analyzed Samples	117
APPENDIX D Abbreviations Used in Text, Figures, and Equations	123

List of Figures

Figure 1	FAM and SiO ₂ vs. FeO / (FeO + MgO) diagrams.....	8
Figure 2	Outcrops and thin sections of granitic rocks	9
Figure 3	Quartz-sillimanite segregations in leucogneiss.....	10
Figure 4	Normative quartz-albite-orthoclase in granitic rocks	11
Figure 5	Tectonic discrimination diagrams for granitoids	12–13
Figure 6	Amphibole and clinopyroxene compositions	14
Figure 7	Harker diagrams for granitoids	16–18
Figure 8	Rare Earth element (REE) distribution in granitoids	19–21
Figure 9	Q-mode factor model	22
Figure 10	Zircon saturation in granitoids	23
Figure 11	Outcrops of olivine metagabbro and jotunite	24
Figure 12	Geochemistry of mafic rocks	25–27
Figure 13	REE distribution in mafic rocks and anorthosite	29–30
Figure 14	Outcrops and thin sections, unit TH	32
Figure 15	Outcrops and thin sections, Mg-rich metasedimentary rocks of unit BL	33
Figure 16	Map of structural domains	38
Figure 17	Stereograms of structural data	39–41
Figure 18	Textures of deformed granitic rocks	42–43
Figure 19	T- X _{CO2} diagram for calcsilicate rocks	44
Figure 20	Photomicrographs of metamorphic features	49–50
Figure 21	Outcrops of migmatites	52
Figure 22	Effect of geology on lakewater pH	64

List of Tables

Table 1A	Geochemistry of granitoids, units CG and GA	65–73
1B	Geochemistry of granitoids, units BM, LD, BG, and KZ	74–77
1C	Geochemistry of granitoids within metasedimentary units	78–79
1D	Geochemistry of unit TH gneisses	80–82
1E	Geochemistry of mafic rocks and anorthosite	83–87
1F	Geochemistry of metasedimentary rocks	88–90
Table 2	Electron microprobe mineral analyses	91–93
Table 3	Varimax Rotated Q-modes (units CG and GA)	94
Table 4	Comparative geochemistry of mafic suites	95
Table 5	Lakewater pH and chemistry by bedrock map unit	96–97

Acknowledgments

This map and report are based on the field work of numerous geologists over nearly 40 years. In 1959 and 1960, reconnaissance mapping was done by Yngvar Isachsen and several assistants. In 1984, a second phase of mapping was begun under the supervision of Robert Fakundiny, Yngvar Isachsen, and Philip Whitney. The complete list of mappers for these projects follows.

Richard Berg (1959)	John Mihalik (1984)
Brian Brock (1984)	Timothy Mock (1990)
Jeffrey Chiarenzelli (1984, 1988)	Richard Nyahay (1992–1998)
Mark Davin (1984, 1987–1989)	Paul Ollila (1984)
Joseph DiPietro (1984–1986)	Karin Olson (1984–1985)
Louis Erhardt (1984)	James Pattee (1986–1987)
Robert Fakundiny (1984, 1996)	Khaled Rahman (1985)
Stewart Farrar (1988)	Carol Russ-Nabelek (1984)
Leo Hall (1959–1960)	Thomas Seal (1984–1985)
Jonathan Halpert (1984)	Richard Stenstrom (1959–1960)
Yngvar Isachsen (1959–1960, 1984)	Edward Stoddard (1984)
Steven Keating (1984)	Clifford Todd (1984)
Daniel Leavell (1984)	Philip Whitney (1984–1998)
Robert Lepak (1985)	

Published and unpublished maps of Dirk deWaard, and unpublished maps of Arthur Buddington, James McLelland, and Cleaves Rogers were also used in the compilation. We also thank numerous others who contributed significantly to the project, including Robert Darling, who first identified prismatine at the Moose River locality; Robert Dineen, who mapped the glacial geology; Gary Nottis, who organized the prodigious amounts of field data into usable files; and Janet Manchester, who produced the digital map and database. Pat Mulligan designed the text layout; Leigh Ann Smith designed the cover, and John B. Skiba managed the production of the publication. In addition to the field work, Mark Davin assisted with the chemical analyses, and Jonathan Halpert contributed logistical support and served as chef for the entire crew at the Deerhead “Inn” during the 1984 field season. Last but not least, “Chief” James McLelland helped initiate the 1984 field crew into the complexities of Adirondack geology.

Introduction

The mapped area comprises the west-central Adirondack Highlands of New York State between 43° 30' and 44° north latitude and 74° 45' and 75° 15' west longitude. It includes the following 15' quadrangles: Number Four (NFQ), Big Moose (BMQ), Raquette Lake (RLQ), McKeever (MKQ), Old Forge (OFQ), and West Canada Lakes (WCQ). The Adirondack Highlands is a multiply deformed, granulite facies metamorphic terrane of the Grenville Province. The Highlands, together with the Morin Terrane in Quebec, compose the Central Granulite Terrane of Wynne-Edwards (1972). In later subdivisions of the Grenville Province, the Adirondack Highlands were included within the Allochthonous Monocyclic belt of Rivers et al. (1989) and the southeastern Grenvillian belt of Davidson (1995).

The entire map area is underlain by Middle Proterozoic granulite facies metamorphic rocks intruded by a few thin, unmetamorphosed diabase dikes of probable latest Proterozoic or earliest Cambrian age. There are no published maps of the area, except for the 1:250,000 Adirondack sheet of the Geologic Map of New York State (Isachsen and Fisher, 1970), and a map of the Little Moose Mountain Syncline (WCQ) by deWaard (1962). Unpublished reconnaissance maps of the RLQ by Cleaves Rogers (ca. 1941) and the central BMQ by A.F. Buddington (undated) are in the New York State Geological Survey Open File. Adjacent areas to the north have been mapped by Dale (1935) and Buddington and Leonard (1962). Parts of the Blue Mountain Lake 15' Quadrangle (east of RLQ) have been mapped by Geraghty (1978) and Fallon (1990). Parts of the Indian Lake 15' Quadrangle (east of WCQ) were mapped by deWaard and Romey (1963), and an unpublished map of the entire quadrangle by M.H. Krieger (ca. 1940) is in the Open File of the New York State Geological Survey. The northern half of the Piseco Lake

15' Quadrangle (south of WCQ) was mapped by Glennie (1973), and the entire quadrangle by Cannon (1937). The Ohio 15' Quadrangle (south of OFQ) was mapped by Nelson (1968), and the Remsen 15' Quadrangle (south of MKQ) by Miller (1909). To the west, the Port Leyden Quadrangle (west of MKQ) and Lowville 15' (west of NFQ) Quadrangles are described by Miller (1910) and Buddington and Ruedemann (1934), respectively.

Field notes and unpublished maps of more than thirty geologists (see Acknowledgments) have been used to compile the Fulton Chain-of-Lakes map. These have been synthesized and field checked by the senior author, who is solely responsible for the northern half of the RLQ. We have attempted to maximize the usefulness of the map as an empirical representation of the bedrock underlying any given location, and to avoid forcing the data to fit particular structural or tectonic models.

Two factors, well known to Adirondack geologists, have complicated the mapping. In over 95% of the area, the bedrock is mantled with Pleistocene (Wisconsinan) glacial deposits, recent alluvium, and wetlands. With few exceptions, bedrock exposures are scattered and contacts are rarely exposed. More challenging is the failure of nature to provide convenient mapping units, with the result that map units described in the legend are necessarily somewhat arbitrary. With the exception of CG and OG, all units are mixtures of two or more lithologies. Moreover, a single outcrop may contain insufficient information for assignment to a specific lithologic unit, since all the defining characteristics may not be present.

Lithologic units, represented by two- or three-letter symbols, are described in the explanation on the map and in Appendix B. Abbreviations for mineral names used in the text, figures, equations, and tables are explained in Appendix D.

Non-Technical Overview

Rocks of the Fulton Chain-of-Lakes Area

Bedrock exposed at the surface in the map area consists almost entirely of metamorphic rocks. The only exceptions are a few small diabase dikes, at most about 15 feet (5 m) thick, that occupy fractures in fault zones. During metamorphism, high temperatures and pressures caused recrystallization of the existing minerals as well as chemical reactions that produced new minerals. The rocks we now see at the earth's surface in the Adirondacks contain sets of minerals that, based on laboratory experiments, were formed at temperatures as high as 800°C (1470°F) and pressures of 7000 to 8000 times atmospheric. These conditions are equivalent to depths of roughly 20 to 25 kilometers (12–16 mi.) in the earth's crust. Rocks originally formed at or near the earth's surface were somehow buried at depths up to 16 miles. This can happen when two continents collide and thick slices of one continent are thrust over the other. A similar collision is occurring now between the Indian subcontinent and Asia. Adirondack scenery one billion years ago, shortly after a major mountain-building event known as the Grenville Orogeny, may have resembled today's Himalaya Mountains and Tibetan Plateau.

Former sedimentary rocks, now metamorphosed, are the dominant constituents of map units CM, MU, BL, KZa, and TH and account for nearly half of the bedrock in the map area. These included limestones, quartz-rich sandstones, shales, and evaporites (rocks consisting of soluble minerals such as salt, formed by evaporation of seawater), with some inter-layered lavas and volcanic ash deposits. The presence of evaporites suggests deposition in a shallow marine basin cut off from the open ocean, together with an arid climate that facilitated evaporation. Limestones,

quartz sandstones, and shales were metamorphosed to marble, quartzite, and gneiss, respectively. The gneiss of map units KZa and BL is composed chiefly of biotite (black mica), quartz, and feldspar, and commonly also contains red or lavender crystals of garnet and tiny white needles of sillimanite. White or pink streaks and veins composed of quartz and feldspar were formed by partial melting of the gneiss during metamorphism. In some places, the gneisses contain unusually large amounts of the elements potassium, magnesium, boron, and fluorine, derived from the former evaporites.

Gneisses in unit TH, composed chiefly of quartz and feldspar, may be a metamorphosed arkose, a feldspar-bearing sandstone derived from the erosion of granite. Calcsilicate rocks with abundant pale- to dark-green pyroxene and varying amounts of feldspar, quartz, scapolite (a feldspar-like mineral), tremolite, and mica are metamorphic products of impure limestones or dolostones (rocks composed chiefly of the mineral dolomite) that initially contained substantial amounts of sand, chert, or clay. The pyroxene was formed by reaction of dolomite (calcium-magnesium carbonate) with quartz. Thinly laminated rocks consisting of alternating quartz- and pyroxene-rich layers are found in several locations. These are similar to carbonate-bearing rocks in the northwest Adirondack Lowlands that contain fossil stromatolites, layered structures produced by ancient cyanobacteria ("blue-green algae"), although no stromatolites have been found in the map area.

Igneous rocks that intruded the sedimentary rocks prior to metamorphism are mainly granite and charnockite. The latter is a feldspar-quartz rock similar to granite but with more dark minerals; its gray-green color, turning to "maple sugar" brown when weathered, distinguishes it from the gray, pink, or white granites. Gneisses derived by metamorphism of

the granites and charnockites occur both as sheets within the metamorphosed sedimentary rocks and as larger dome-like masses. They appear on the map as units CG, GA, and BG. Similar granitic gneisses in units BM, LD, and KZb are generally finer grained and more strongly layered than those in units CG and GA, and probably are metamorphosed volcanic rocks. Collectively, granitic and charnockitic gneisses underlie approximately half of the map area. Small amounts of anorthosite (a pale, coarse-grained igneous rock rich in plagioclase feldspar that underlies much of the Adirondack High Peaks region) and dark, iron-rich gneiss ("jotunite") compose unit JA, which occurs as layers in unit BM in the Big Moose and Raquette Lake Quadrangles. Small bodies of metamorphosed gabbro (unit OG) occur in the southeastern third of the area. Amphibolite, formed by metamorphism and deformation of basalt, diabase, or gabbro, is found in a few thick layers (shown on the map unit AM) and numerous thinner layers in other units. Thin amphibolite layers in the granitic gneisses of unit GA are probably metamorphosed diabase dikes that were intruded into the original granite and deformed along with it.

How Old Are These Rocks?

The rocks of the Fulton Chain-of-Lakes area were formed in the Mesoproterozoic Era, the time interval that followed development of an oxygen-bearing atmosphere on earth. This era marks the first appearance of complex (eucaryotic) single-celled organisms, but precedes the evolution of multicellular life.

The ages of rocks can be measured using naturally occurring radioactive isotopes* that break down into stable isotopes at known rates. One of the most widely used methods involves the mineral zircon (zirconium silicate), found in small grains in

most rocks. Zircon contains traces of the radioactive element uranium. Two isotopes of uranium (^{238}U and ^{235}U) break down to lead isotopes ^{206}Pb and ^{207}Pb , respectively, at rates sufficiently slow for use as geologic "clocks." Measurements of the relative amounts of these isotopes in zircon can, under favorable circumstances, give the age of the zircon and of the rock that contains it with a precision of 0.1% or better. However, in rocks from areas with a complex geologic history, such as the Adirondacks, measured ages tend to be less precise and more difficult to interpret. Numerous ages for metamorphosed igneous rocks in the Adirondack Highlands have been obtained by this and other methods, including a few from the map area. The results indicate that most are between 1.35 and 1.05 Ga (billion years old), roughly one-quarter the age of the earth. Most of these rocks originated during a period of intense igneous activity between 1.15 and 1.09 Ga. The rocks of sedimentary origin are more difficult to date, but probably fall in the 1.4 to 1.15 Ga range. Some contain mineral grains derived from much older rocks. The most recent metamorphism, a result of the continental collision, reset some of the atomic clocks between 1.06 and 0.99 Ga.

Geologic Structure

All rocks in the area, with the exception of the scattered late diabase dikes, have been folded into a series of complex anticlines (upfolds) and synclines (downfolds), so that originally horizontal layers are now tilted. In many parts of the area the folded rock layers have been rotated into a nearly vertical position or even turned upside-down. The orientation of the folds suggests that the area was compressed by forces acting in a S-N or SE-NW direction, most likely during the same collisional event that caused the metamorphism. Some rocks in the southeastern third of the area also may have been affected by an earlier deformation and metamorphism between 1.25 and 1.18 Ga.

Most fractures and faults (fractures along which relative movement has occurred) in the area follow a NE-NNE trend that is roughly parallel to numerous faults found in the eastern Adirondack Highlands. These vertical to steeply dipping faults probably formed near the end of the Proterozoic or in earliest

* Atoms of a chemical element all have the same atomic number but may differ in atomic weight. For example, all atoms of the element oxygen have atomic number 8 (the number of protons in the nucleus), but oxygen atoms may have atomic weights of 16, 17, or 18 (the number of protons plus neutrons). Atoms with the same atomic number and atomic weight are called isotopes. Thus, oxygen consists of three isotopes, oxygen 16, oxygen 17, and oxygen 18.

Cambrian time, perhaps as a result of the same extensional forces that caused the opening of the Iapetus Ocean to the east of the Adirondacks. Some of these faults remained active at least into the middle part of the Ordovician Period, about 450 Ma (million years ago); none are known to be active today. A few faults with other orientations include the WNW-trending Independence River Fault in the western part of the map area. Some of the NE-trending faults contain dikes (thin, tabular bodies) of diabase, an igneous rock which intruded along the faults in latest Proterozoic time. These dikes are the only rocks in the area that have not been metamorphosed or folded.

Regional Setting

The igneous activity and the subsequent collision-induced deformation and metamorphism of the bedrock over a billion years ago were part of a complex series of events known as the Grenville Orogeny, which occurred between 1.4 and 1.0 Ga during assembly of the supercontinent Rodinia. Rocks exposed at the surface from southern Labrador southwestward through Quebec and eastern Ontario as far as Lake Huron were formed, deformed, and metamorphosed at this time. Collectively, the area where these rocks occur is known to geologists as the Grenville Province. Parts of northernmost Ireland and Scotland and southern Norway and Sweden also appear to be an eastern extension of the Grenville Province, detached from the rest by the opening of the Atlantic Ocean about 200 Ma. Grenville rocks, now covered by younger sedimentary strata, have also been traced in deeply drilled wells thousands of miles southward and westward from the Adirondacks; surface exposures are found as far away as the Llano Uplift in Texas and Oaxaca Province in southern Mexico. The Adirondack Dome, connected at the surface to the Ontario segment of the Grenville Province at the Thousand Islands, is a “window” to the Grenville through younger rocks. Similar windows occur in the Hudson Highlands in southeastern New York, the Berkshires in Massachusetts, and the core of the Green Mountains of Vermont, and the Long Range of western Newfoundland.

The Last Billion Years

Following the Grenville Orogeny, a long period of uplift and erosion removed the 12 to 16 miles (20–25 km) of rock that once lay above the present surface. Little is known in detail about this process, save that it was substantially completed by the beginning of the Cambrian Period, roughly 540 Ma. At this time the erosion surface was near sea level. Later in the Cambrian, sea level rise led to deposition of sandstones of the Potsdam Formation, which overlies the metamorphic rocks and forms outcrops around the north, east, and south margins of the Adirondacks. Deposition of sand and lime sediments continued at least through Ordovician time (ca. 510–440 Ma) and perhaps well into the Devonian (ca. 410–360 Ma).

Much later, during the Tertiary Period (65–2 Ma), the Adirondack region began to be uplifted in the form of a roughly circular dome. Erosion removed the sedimentary blanket over the dome and carved the present Adirondack Mountains from the underlying metamorphic rocks. An imaginary plane drawn through the tops of the highest hills and ridges in the map area slopes gently toward the southwest, away from the center of the dome. This plane is probably not far below the Cambrian erosion surface; it projects close to the contact (unconformity) between Proterozoic metamorphic rocks and Cambrian and Ordovician sedimentary rocks in the Black River valley.

The entire area was covered by continental glaciers over a mile thick several times during the Pleistocene Epoch, which began about 1.6 Ma and ended roughly 10,000 years ago, when the last ice retreated from the area. Glacial striae (scratches on bedrock surfaces made by rock fragments embedded in moving ice) show that the ice in the map area moved in a NE–SW direction, in contrast to the more nearly N–S movement in the Champlain valley to the east or the Black River valley to the west. It is likely that ice movement in the map area was steered by ridges and valleys on the underlying rock surface. Most of the bedrock is now covered with unsorted rock debris, called till. Till consists of rock fragments that range in size from microscopic clay particles to house-sized boulders. It includes both lodgement till smeared onto the land surface at the base of advancing glaciers, and ablation till left behind by melting

ice. Outwash deposits consisting of layers of well-sorted sand and gravel deposited by water from melting ice and sediments deposited in glacial lakes, occur locally in valley areas. Nearly all of the McKeever Quadrangle southwest of White Lake is covered with a thick blanket of these outwash materials; only one bedrock outcrop has been found there.

Geology and Landscape

The land surface in the Fulton Chain of Lakes area was modified to some extent by the continental glaciers, but the present-day landscape is controlled chiefly by the structure of the bedrock and by differential resistance of the rocks to erosion. All of the highest elevations in the area, including Wakely Mountain, Blue Ridge, and West Mountain, are underlain by erosion-resistant granitic gneiss or charnockite. Most ridges and valleys reflect the trend of the major folds, roughly NE-SW in the western part of the area, swinging gradually to nearly E-W in the eastern part. Steeply tilted layers of gneiss form ridges, whereas softer, more easily eroded layers of metasedimentary rocks underlie most valleys, lakes, and bogs. The Fulton Chain of Lakes and Route 28, as well as the villages of Old Forge, Eagle Bay, Inlet, and Raquette Lake, occupy a valley in the center of a major syncline of relatively soft and soluble marble. By contrast, Bald Mountain, the elongate ridge parallel to Route 28 on the north side of Fourth Lake (between Old Forge and Inlet), is underlain by a thick, tilted layer of erosion-resistant charnockite. Layers of highly resistant quartzite in the syncline form the cliffs near Bug Lake, north of the carry between Seventh and Eighth Lakes. The outline of Raquette Lake reflects the alternation of resistant gneisses that form the points and islands in the lake, and softer metamorphosed sedimentary rocks that underlie the bays.

Bedrock shattered and weakened by faults is also more susceptible to erosion. As a result, the larger faults tend to be marked by linear valleys occupied by rivers, such as the Red and Independence Rivers, or

by lakes. North Lake is in a fault valley that can be traced northeastward as far as the High Peaks and southwestward to the Mohawk River. Long Lake, well to the northeast, lies on the trace of the same fault. Similarly, the elongate northeastern arm of Raquette Lake is fault-controlled, as are the northwestern and southeastern arms of Brandreth Lake.

Environmental Consequences

Both bedrock and glacial geology affect the susceptibility of ponds and lakes to damage by acid precipitation, a serious concern in the Adirondacks. Weathering of most rock-forming minerals involves chemical reactions that tend to neutralize acidity. Minerals such as calcite and dolomite react rapidly and are very efficient neutralizers. Calcsilicate minerals, pyroxenes, hornblende, and micas react more slowly, feldspars more slowly still, and quartz only to a negligible extent. Thus, the proportions of these minerals in the bedrock and soils of the watershed affect the degree to which water from acid rain and snow is neutralized before reaching the lake. Lakes and ponds in areas underlain by granitic or charnockitic gneiss, composed chiefly of feldspars and quartz, tend to be moderately to strongly acidic. At the other extreme, lakes in areas of marble bedrock with abundant, easily weathered calcite are ordinarily weakly acidic to somewhat alkaline.

Because glacial till is a mixture of fragments from local and more remote bedrock sources, its mineral content and neutralizing capacity do not correlate precisely with that of the local bedrock. Where the till is thick and somewhat permeable, groundwater moving through it will react with a much greater surface area of mineral grains, and be more effectively neutralized, than either surface runoff or groundwater in fractured bedrock. This effect is even more pronounced in highly permeable outwash deposits. The neutralizing capacity of glacial soils may, however, diminish as easily weathered minerals become exhausted.

Chapter 1

Metamorphosed Igneous Rocks

The granitic, anorthositic, and associated mafic rocks of the Adirondack Highlands have been called the anorthosite-mangerite-charnockite-granite (AMCG) suite (e.g., McLelland and Whitney, 1990). In the map area, the AMCG suite is represented by granitic rocks in units CG, GA, and BM, and jotunites and anorthosites in units BM and JA. In the map area, as elsewhere in the Highlands, AMCG rocks are distinctly bimodal (Fig. 1A); the felsic and mafic rocks are approximately coeval but probably not comagmatic. The criteria of Irvine and Baragar (1971) and Anderson (1983) indicate that the AMCG suite as a whole has a tholeiitic rather than a calc-alkaline character (Figs. 1A, B). Absent from the map area are the monzodiorites, mangerites, ferrogabbros, and ultramafic rocks that form part of the AMCG suite in the Adirondack High Peaks region. Amphibolites and olivine metagabbros in units OG, AM, GA, KZ, and MU may be coeval with or slightly younger than the AMCG suite.

Charnockite-granite suite (units CG, GA, and subordinate layers in most other units) — Charnockitic and granitic gneisses occur as stratiform bodies up to several kilometers thick, as elongate domes, and as layers or lenses within metasedimentary rocks. They are present throughout the map area, but become increasingly abundant from SE to NW. They are presumed to be intrusive, but deformation has obscured any original crosscutting relations. Xenoliths of other rocks in granites and charnockites are rare, but do occur in a few locations (Fig. 2A). Charnockitic and granitic lithologies are not separately mappable and may occur together in the same outcrop. Those in unit GA are chemically and lithologically indistinguishable from their counterparts in unit CG (Table 1A), but tend to be more heterogeneous and strongly foliated. Foliation is present in most exposures (Figs. 2B, C), but is poorly developed or absent in the less

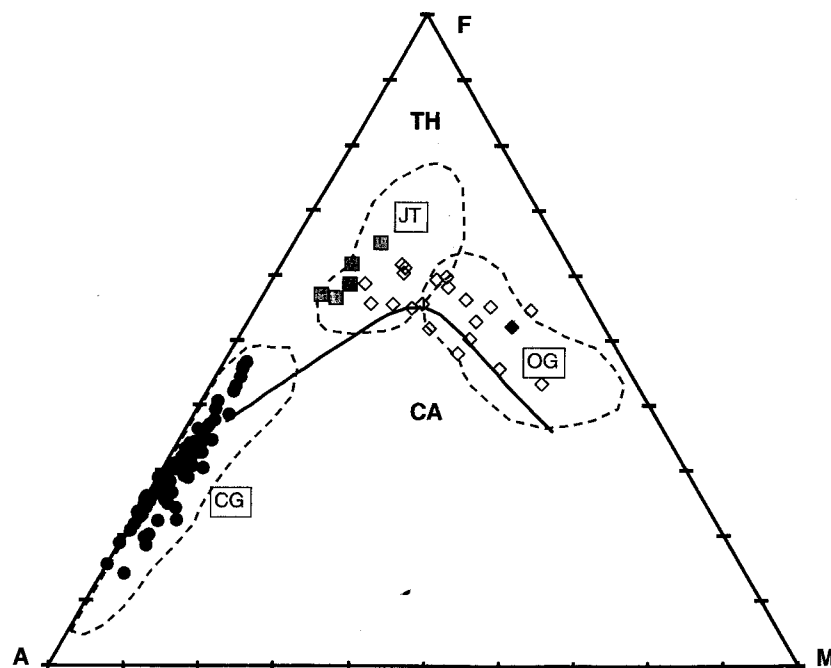
deformed interiors of large bodies of CG. Pronounced grain-shape fabrics, including mineral lineations, are uncommon in these and other granitoids in the map area, but do occur locally in areas of strong foliation. Both granitic and charnockitic gneisses commonly contain foliation-parallel, millimeter- to centimeter-scale layers and lenses of coarser granitic material that were probably formed by partial melting during or prior to deformation. Less commonly, crosscutting granitic veins are also present.

Unit GA is distinguished from unit CG chiefly by the presence of centimeter- to meter-scale amphibolite or biotite amphibolite layers parallel to foliation (Fig. 2D). These amphibolites, present in most exposures of GA, are well foliated and locally lineated except in the interiors of thick layers. Differential weathering of amphibolite layers locally causes prominent hogback topography that is clearly visible on aerial photographs.

In both units CG and GA, mesoperthite is the principal alkali feldspar, and its modal abundance is nearly constant throughout the suite. Less deformed rocks in the interiors of larger CG bodies commonly are inequigranular with rounded to ovoid mesoperthite megacrysts that suggest a deformed rapakivi texture, although rarely with intact plagioclase rims. The rock grades from charnockite to granitic gneiss to leucogneiss with increasing silica content. Plagioclase and mafic mineral contents decrease and the mafic assemblage changes from (Hbl + Cpx + Opx) to (Hbl \pm Cpx) to (Hbl + Bt) to (Bt). Fayalite, partly or wholly altered to iddingsite, is locally present over the entire range of compositions, but is most common in evolved felsic rocks, where it may be accompanied by fluorite (Fig. 2E). Fayalite-bearing rocks are ordinarily deep olive-green on fresh surfaces, and are easily mistaken in the field for charnockites.

In most granites and charnockites, the opaque

A.



B.

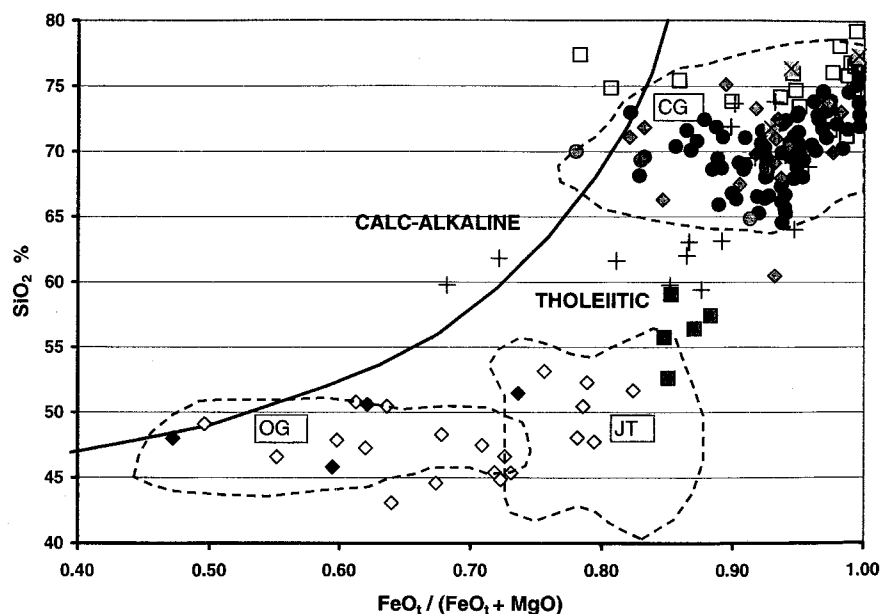


Figure 1. FAM and SiO_2 vs. $\text{FeO}_t / (\text{FeO}_t + \text{MgO})$ diagrams. **(A)** F (total Fe as FeO)–A ($\text{Na}_2\text{O} + \text{K}_2\text{O}$)–M (MgO) for mafic rocks (excluding anorthosites and plagioclase-rich cumulates) and CG and GA suite granitoids from the map area. Solid line separating the CA (calc-alkaline) and TH (tholeiitic) fields is from Irvine and Baragar (1971). **(B)** SiO_2 vs. $\text{FeO}_t / (\text{FeO}_t + \text{MgO})$ diagram (after Anderson, 1983) for granitic and mafic rocks from the map area. Envelopes in both figures (A and B) show fields for charnockites and granite (CG), olivine metagabbros (OG), and jotunites (JT) from the Adirondack High Peaks region. Symbols: Granitic rocks: Solid circles, charnockites and granites (CG and GA); open squares, leucogneisses (unit BM); shaded Xs = sillimanite-nodular leucogneisses (unit BM); shaded circles, megacrystic biotite granites (unit BG); shaded diamonds, granitoids in other units (LD, MU, KZa, KZb); +s, quartzofeldspathic gneisses of unit TH. Mafic rocks: solid squares, jotunite (unit JA); open diamonds, amphibolite; solid diamonds, olivine metagabbro (unit OG).

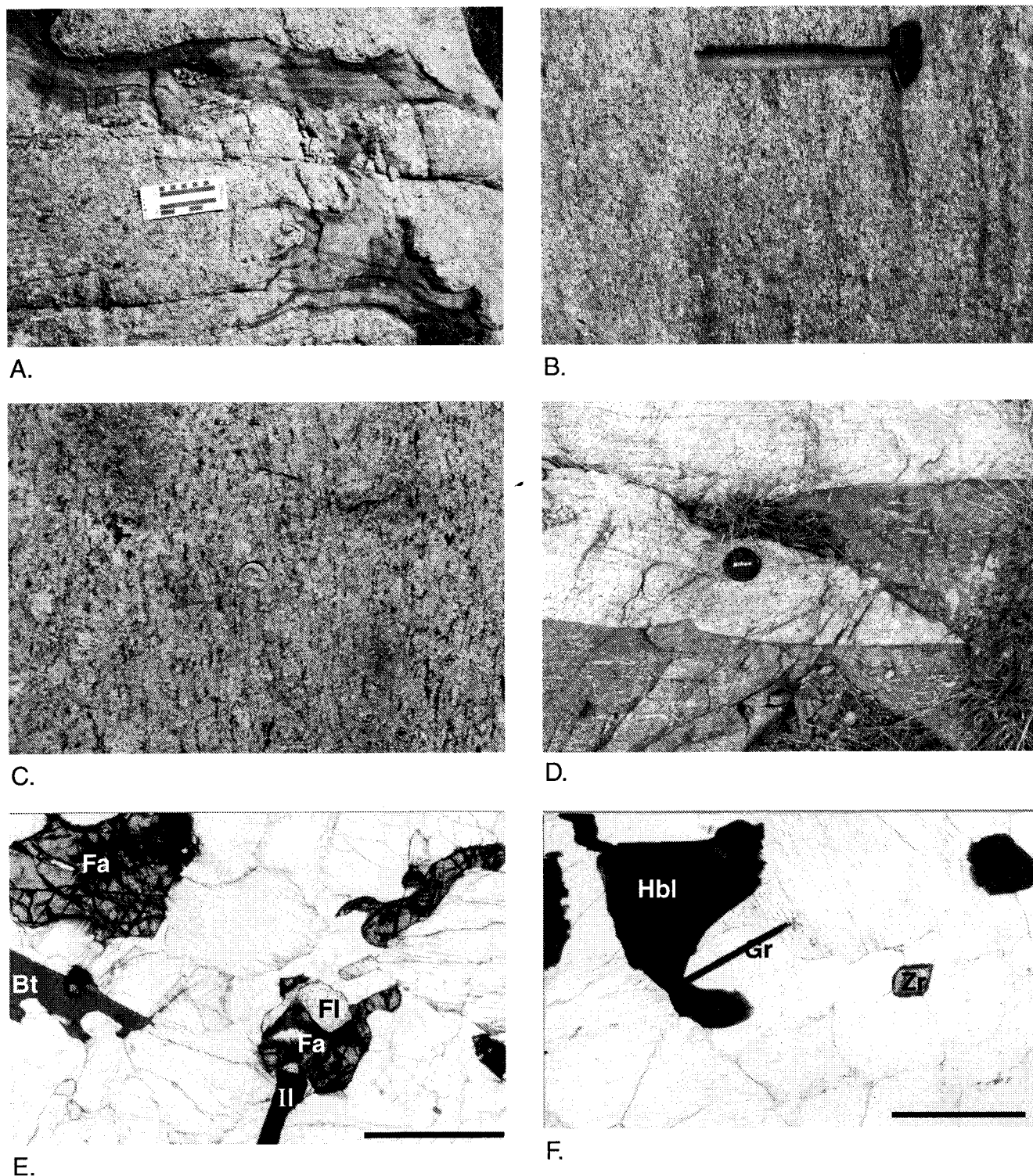


Figure 2. Outcrops and thin sections of granitic rocks. (A) Foliated xenoliths of calcsilicate granulite in hornblende granite gneiss. Unit CG, 0.3 mi. S. of Raven Lake, NFQ. (B) Weathered surface of charnockitic gneiss. Unit CG, roadcut on Rte 28, 3 mi. E of Old Forge, OFQ; site of sample OFY01 (Appendix A, Stop 7). (C) Weathered surface of hornblende granitic gneiss. Unit CG, roadcut at Big Moose Station, BMQ (Appendix A, Stop 8A). (D) Faulted contact between amphibolite layer and granite gneiss. Unit GA, 1 mi. NE of Flatfish Pond, RLQ. (E) Fayalite (Fa), partially altered to iddingsite, and fluorite (Fl) with biotite (Bt) and ilmenite (Il) in fayalite-quartz-mesoperthite granite, unit CG, 0.5 mi. NE of Cellar Mtn, WCQ; sample WCG41. Scale bar 1 mm, plane light. (F) Graphite (Gr), zircon (Zr), and hornblende (Hbl) in granitic gneiss of unit CG, Ice Cave Mtn, OFQ; sample OFS20. Scale bar 1 mm, plane light.

oxide phase is ilmenite, although magnetite occurs locally and is the dominant oxide in a few samples. Graphite (Fig. 2F) in trace amounts is widespread, especially where fayalite is present. Metamorphic garnet occurs intergrown with plagioclase as symplectic rims around orthopyroxene and oxides in some charnockites in the eastern third of the area.

Leucogranitic gneiss (in units BM, LD, and KZb; local layers in KZa and MU) — Unit BM in the Northwest, West-central, and East-central domains consists largely of (magnetite)-(garnet)-(sillimanite)-biotite leucogneisses. Perthite is the principal alkali feldspar in most thin sections, but microcline is locally present, especially where sillimanite and magnetite are abundant. Local concentrations of magnetite cause a discontinuous aeromagnetic high over some parts of units BM and LD (Balsley and Bromery, 1965b, d). Common accessory minerals include fluorite and hercynitic spinel. Zircon grains are sparse but commonly large, euhedral, and visibly zoned. Foliation is ordinarily well developed, but is obscure where mafic minerals are scarce. BM leucogneisses are geochemically similar to felsic members of the charnockite-granite suite and may be volcanics or

shallow intrusives associated with it.

Quartz-sillimanite segregations in the form of stringers, lenses, and elongate nodules, some with garnet, mark a distinctive facies of leucogneiss that occurs locally throughout unit BM (Figs. 3A, B). Exceptional exposures are present along the Moose River near Lyonsdale (Appendix A, Stop 2) and at Agers Falls, both in the Port Leyden 7.5' Quadrangle immediately west of the map area. At these locations, two sets of stringers appear to intersect at a low angle, the earlier of which is subparallel to foliation in the leucogneiss (Fig. 3B).

The principal lithology in unit LD is magnetite-biotite-plagioclase-quartz-microcline gneiss. Much of the iron in these rocks is sequestered in magnetite rather than mafic silicates. This gives them the appearance of leucogneisses although their bulk chemistry and normative color index is in the same range as that of CG and GA granitoids. The outcrop belt is marked by a prominent aeromagnetic high (Balsley and Bromery, 1965a). The geochemical similarity of these LD "leucogneisses" to CG and GA, together with the presence of amphibolite and metasedimentary layers, suggests that LD is a more



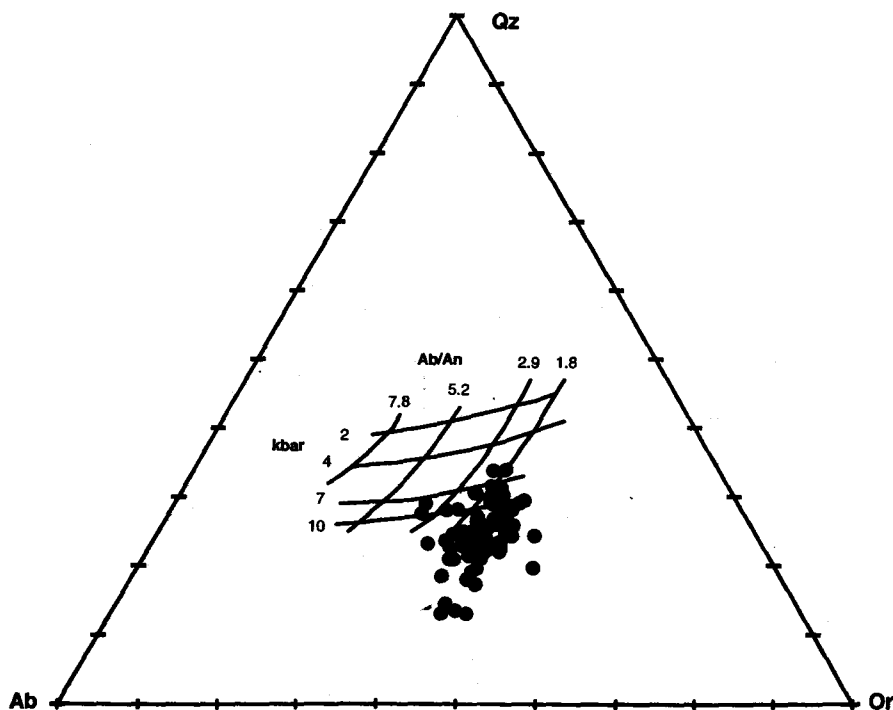
A.



B.

Figure 3. Quartz-sillimanite segregations in leucogneiss, unit BM. (A) Elongate Qz-Si segregations on weathered surface. Note that some appear to be isoclinically folded. N side of Moose River downstream from dam at Lyonsdale, Port Leyden 7.5' Quadrangle (Appendix A, Stop 2). (B) Weathered surface, S side of Moose River at Agers Falls, Port Leyden 7.5' Quadrangle. Qz-Si segregations are both parallel to foliation (small ovoid features under hammer) and crosscutting (elongate ridges parallel to hammer handle).

A.



B.

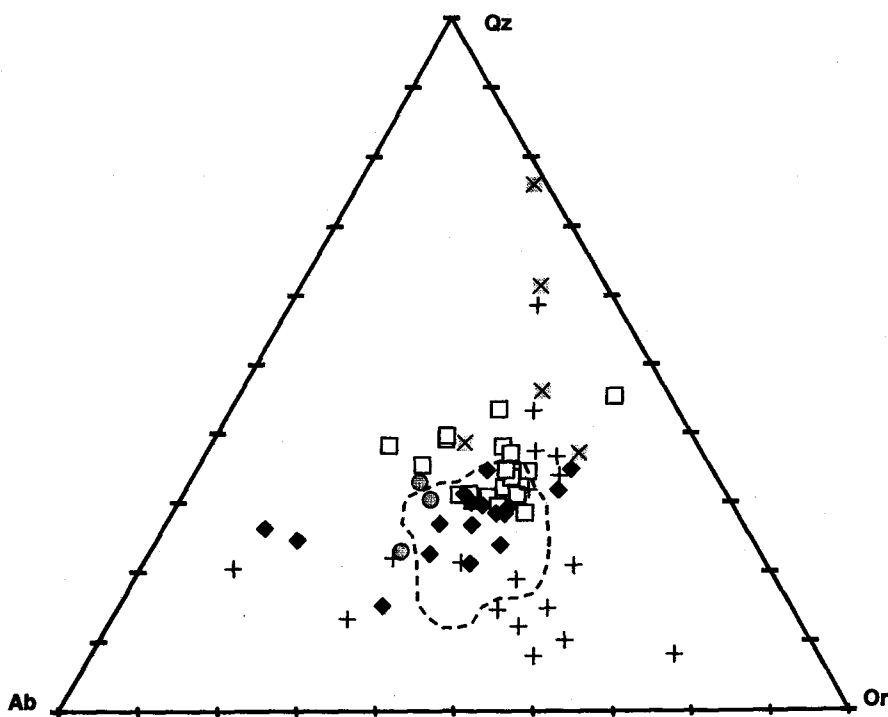


Figure 4. Normative quartz (Qz), albite (Ab), and orthoclase (Or) in granitic rocks. (A) Units CG and GA (solid circles). Grid showing experimental compositions of partial melts as a function of pressure and plagioclase composition of source rock after Anderson (1983). (B) Other granitoids. Dashed line: Envelope for units CG and GA from Fig. 4A. Symbols as in Fig. 1.

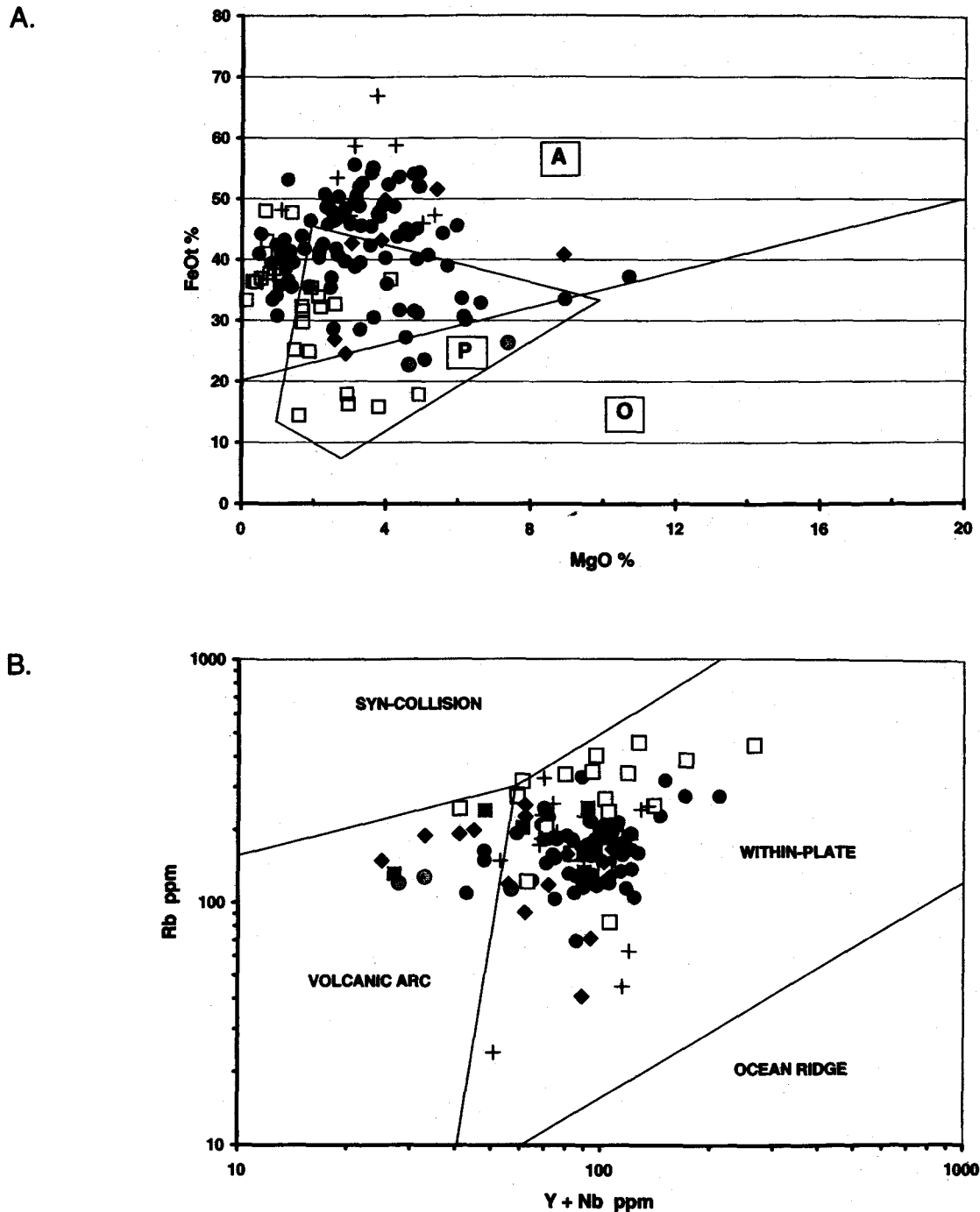


Figure 5. Tectonic discrimination diagrams for granitoids. (A) $100 \cdot \text{FeO}_t / (\text{Al}_2\text{O}_3\text{-K}_2\text{O-Na}_2\text{O} + \text{MgO} + \text{FeO}_t)$ vs. $100 \cdot \text{MgO} / (\text{Al}_2\text{O}_3\text{-K}_2\text{O-Na}_2\text{O} + \text{MgO} + \text{FeO}_t)$ diagram after Maniar and Piccoli (1989). Axis labels on diagram are abbreviated as FeO_t % and MgO % respectively. Labeled fields A (anorogenic), P (postorogenic), and O (orogenic). (B) Rb vs. (Y + Nb) diagram after Pearce et al. (1984). Labeled squares: Average compositions of granite types A, I, M, and S of Whalen et al. (1987). (C) (Zr + Nb + Y + Ce) vs. $10000 \cdot \text{Ga} / \text{Al}$ discrimination diagram after Whalen et al. (1987). (D) Nb-Y-3*Ga diagram after Eby (1992). Field A1, granitoids from hotspots, plumes, and continental rifts. Field A2, granitoids from post-collisional and anorogenic (within-plate) settings, including rapakivi granites. Symbols as in Fig. 1.

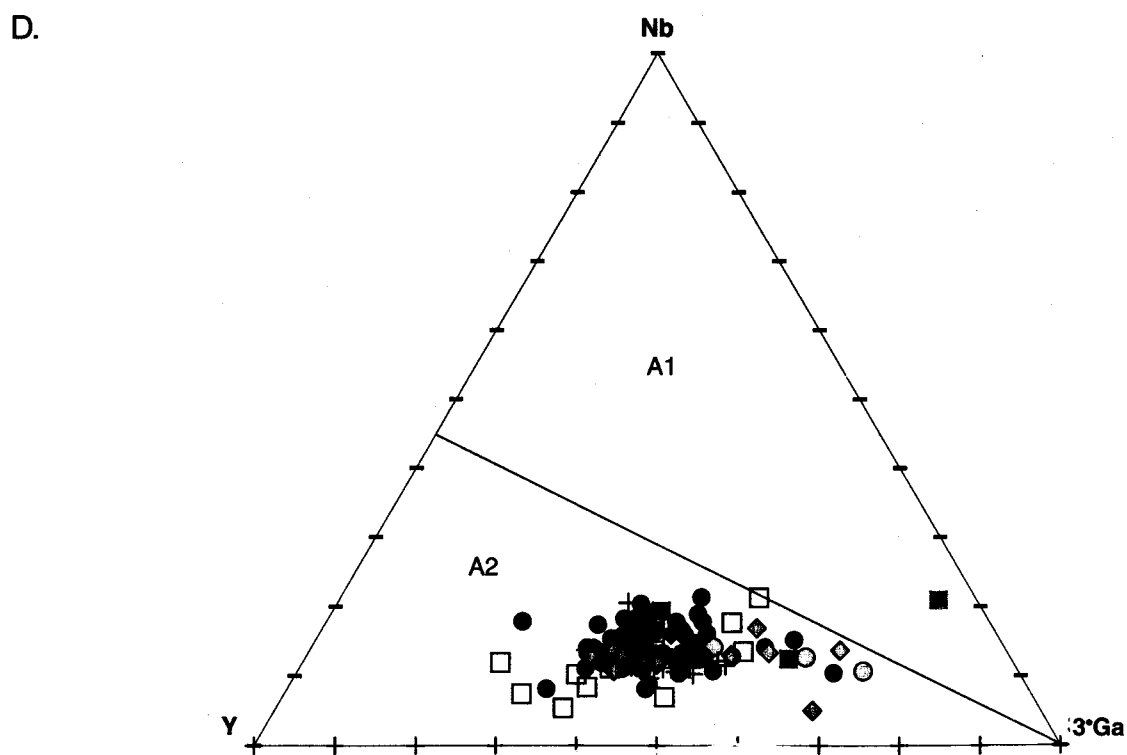
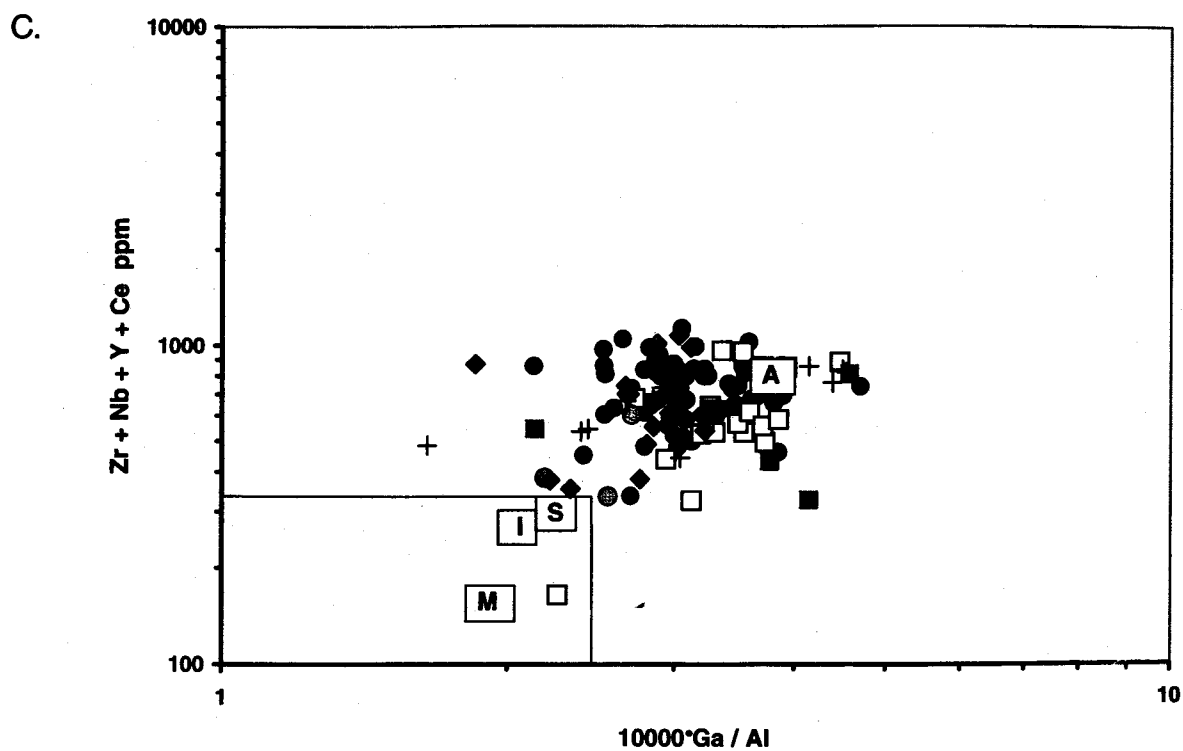


Figure 5. continued

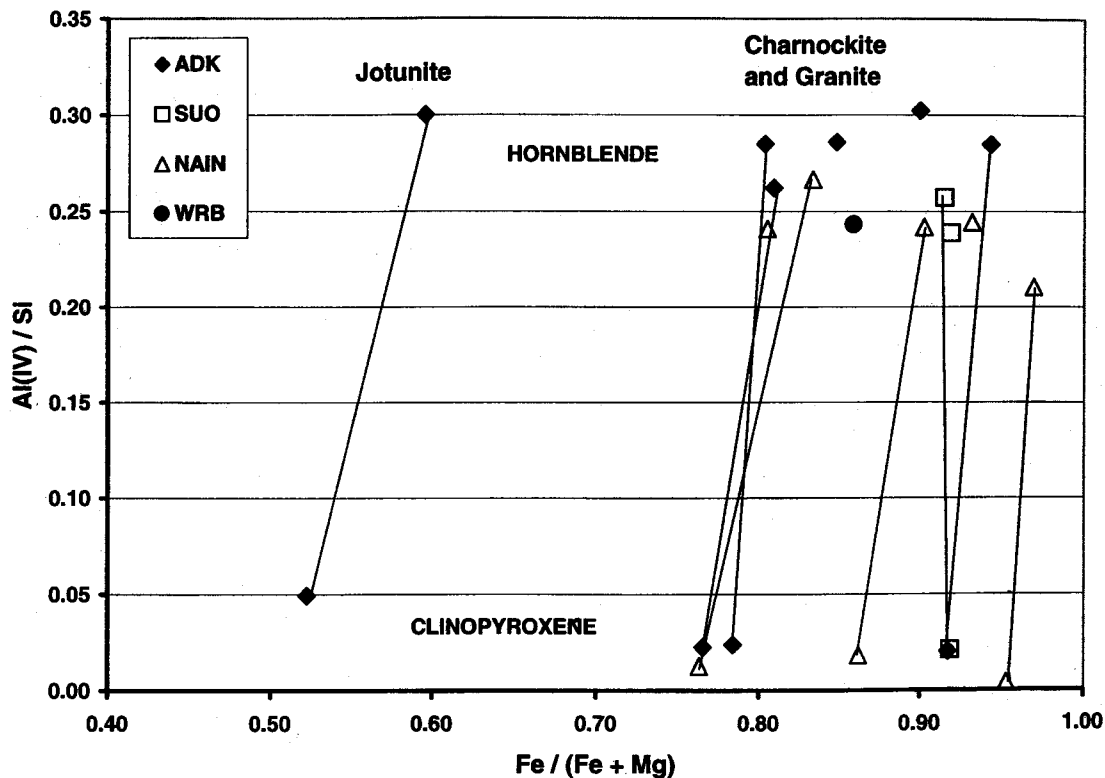


Figure 6. Amphibole and clinopyroxene compositions. Mafic mineral compositions in unit CG compared to those from selected type A granitoids. ADK: Adirondack CG suite (Table 2); NAIN: Nain Province, Labrador (Emslie and Stirling, 1993); SUO: Suomenniemi Batholith, Finland (Ramo, 1991); WRB: Wolf River Batholith, Wisconsin (Anderson and Culler, 1978).

deformed, oxidized, and locally altered equivalent of GA. K / Na ratios vary widely and, at several locations, sodic plagioclase is the predominant feldspar, probably resulting from metasomatic alkali exchange.

Leucogneisses in unit KZb are similar in appearance to those in BM, but commonly contain more biotite and plagioclase. They lack fluorite and quartz-sillimanite segregations. KZb leucogneisses resemble the dominant rocks of unit LD, but contain less magnetite and lack the pronounced aeromagnetic anomaly of the latter. In the field, distinction between leucogneisses of units BM, LD, and KZb and felsic granitoids of units CG and GA is often difficult, and is based on the generally finer-grained texture and greater heterogeneity of the former.

Megacrystic biotite granitic gneiss (unit BG, locally in MU and KZa) — Except for an isolated stratiform body southwest of Old Forge, unit BG is confined to

the southern third of WCQ. These biotite-rich granitoids with salmon-pink megacrysts of mesoperthite or microcline are typically strongly foliated, and augen or flaser textures are common. Megacrysts are subrounded, augen-shaped, or severely flattened depending on the intensity of deformation. The rock is commonly inhomogeneous, with wide variation in the modal abundances of biotite, quartz, and megacrystic feldspar.

Granitic gneisses within other units — Units MU and KZa, and less commonly, BL and CM, contain layers of quartzofeldspathic gneiss. These layers are ordinarily too thin to map separately, although they may be the dominant or exclusive lithology in some outcrops. The gneisses vary in composition, but in general are sufficiently similar to the CG unit to suggest an origin as sills or transposed dikes intruded concurrently with the larger granitoid bodies of units

CG and GA. Some granitic sheets within unit KZa may be partial melts derived from the host biotite-quartz-plagioclase gneisses.

Geochemistry of the granitoids — Tables 1A–C list X-ray fluorescence analyses of 119 granitic and charnockitic rocks within and adjacent to the map area. These include 74 samples from units CG and GA, 24 from BM, 6 from LD, 3 from BG, and 12 from granitic layers in KZa, KZb, and MU. Quartzofeldspathic rocks of unit TH are represented by 18 analyses (Table 1D).

Samples from units CG and GA form a compact group in the normative quartz-albite-orthoclase diagram (Fig. 4A). Those from units BM and LD (Fig. 4B) are more scattered, probably as a result of localized metasomatism ranging from alkali exchange in LD to loss of alkalis relative to silica and alumina in the sillimanite-nodular facies of BM. Data from metasedimentary quartz-feldspar gneisses of unit TH (Fig. 4B) are also scattered.

The CG-GA suite is metaluminous with high $K_2O / (K_2O + Na_2O)$ and $FeO / (FeO + MgO)$ ratios, characteristic of type A granitoids (Whalen et al., 1987). In Figure 5A, most samples fall within the anorogenic (A) or postorogenic (P) fields of Maniar and Piccoli (1989). Trace element distributions (Figs. 5B, C) are typical of within-plate (Pearce et al., 1984), and type A (Whalen et al., 1987) granitoids. In Figure 5D, nearly all plot within the A2 field of post-collisional and rapakivi granites in the classification of Eby (1992). Strong iron enrichment is also evident in the mafic minerals of the CG-GA suite (Table 2). Amphiboles are Fe-rich ($0.04 \leq MgO / (MgO + FeO) \leq 0.13$) ferrohastingsite or hastingsitic hornblende in the classification of Hawthorne (1981). Amphiboles and clinopyroxenes from several CG granitoids are similar to those from other Proterozoic type A suites despite the metamorphic overprint (Fig. 6).

The chemistry of the granitoids of units CG, GA, and LD is consistent with an origin as a single differentiated suite (Whitney, 1992) or as multiple intrusions derived through partial melting of similar source rock and subsequent fractionation. In general, the charnockites are lower in silica (SiO_2 65–70%) than the granites (69–75%) despite considerable overlap. The granites also overlap with leucogneisses of unit BM, which may be strongly fractionated volcanic

equivalents of the same suite. Biotite granites (unit BG) are weakly peraluminous, richer in Sr and poorer in the high field strength (HFS) trace elements than the charnockite-granite suite, and may be unrelated.

Least-squares mixing models indicate that fractionation of an assemblage of cumulate minerals, dominated by alkali feldspar, can account for most of the observed geochemical variation (Whitney, 1992). Crystallization of plagioclase, mafic silicates, ilmenite, apatite, and zircon results in decreasing FeO_t (Fig. 7A), TiO_2 (Fig. 7B), CaO (Fig. 7C), MgO , P_2O_5 , and Zr, and increasing Rb / Sr (Fig. 7D) with increasing SiO_2 . The trends in K / Ba and K / Rb (Figs. 7E, F) reflect the fractionation of alkali feldspar. The exponential increase in K / Ba with SiO_2 is a consequence of the strong preference of Ba for K feldspar relative to the liquid ($KD_{Ba}^{Kf/L} \approx 6$; Long, 1978).

Rare earth element (REE) distribution in the plutonic granites of units CG and GA shows consistent relative light REE (LREE) enrichment and distinct negative Eu anomalies. Figures 8A–E show the limited range of REE distributions in 13 samples of CG and GA as heavy lines. Similar REE distributions occur in other Proterozoic A-type granitic suites (Fig. 8A). Unit BM leucogneisses (Fig. 8B) show deep negative Eu anomalies and more variable REE distributions, attributable to stronger fractionation and, in some samples, REE-rich phases such as allanite or fluorite. In the sillimanite-nodular facies of unit BM (Fig. 8C), some REE distributions are anomalous, possibly due to mobilization of REE during partial melting in the presence of reactive fluids (Nabelek, 1997). The REE patterns of quartzofeldspathic gneisses in unit TH (Fig. 8D) are indistinguishable from those of CG and GA. Biotite granites (unit BG), and leucogneiss from unit KZb show relative heavy rare earth (HREE) depletion with respect to units CG and GA (Fig. 8D), suggesting different source rocks and/or conditions of origin. Within the CG-GA suite, Eu / Eu^* decreases with increasing SiO_2 (Fig. 8E), consistent with fractionation of Eu-enriched alkali feldspar and plagioclase.

Not all of the geochemical variation in the CG-GA suite can be explained by magmatic fractionation. Q-mode factor analysis (Miesch, 1976) yields three varimax rotated factors (Table 3). Factors Q1 and Q2 approximately correspond to the cumulate

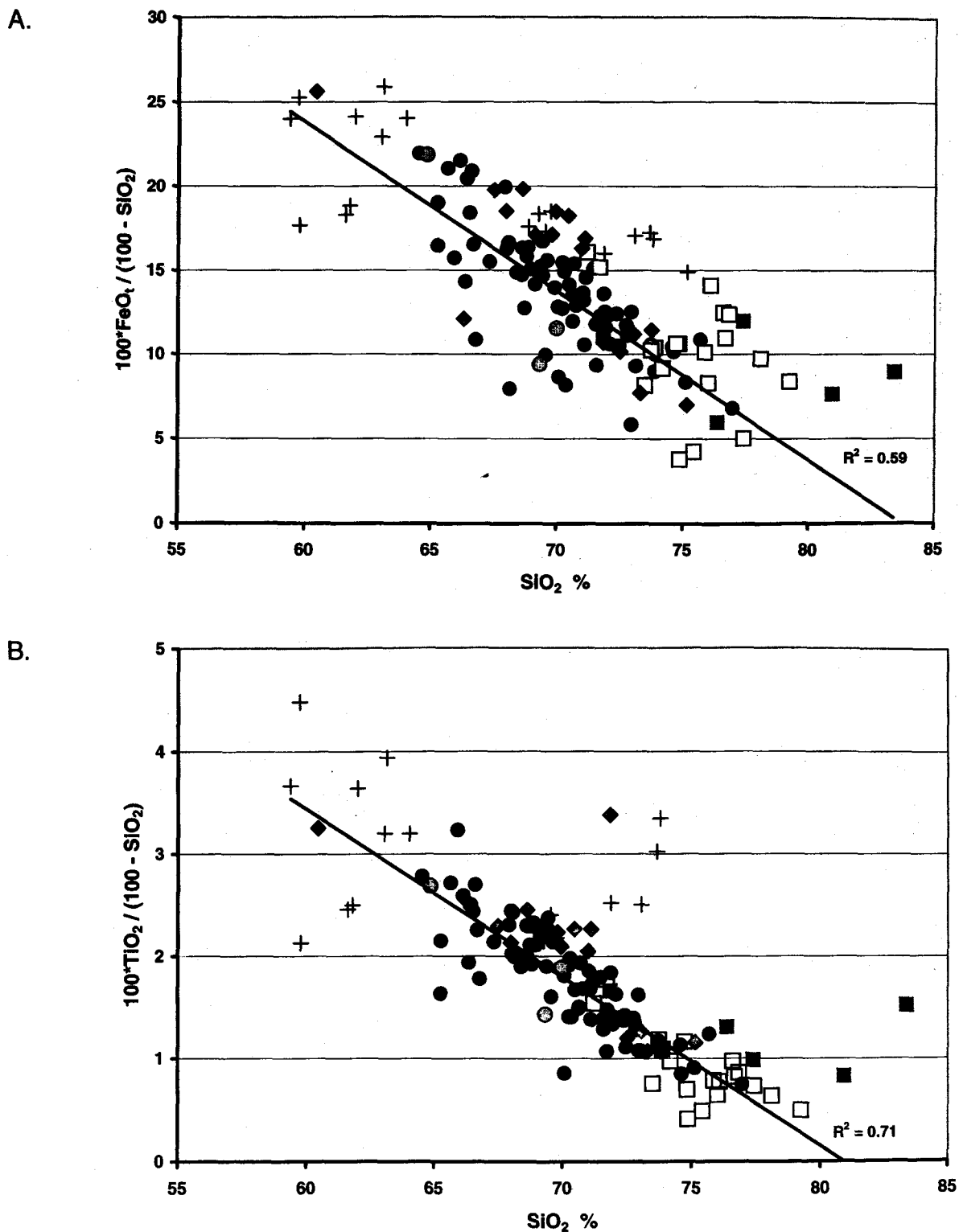


Figure 7. Harker diagrams for granitoids. Variation of selected elements and ratios with percentage of silica in granitoids. (A) Total Fe as FeO. (B) TiO₂. (C) CaO. (D) Rb / Sr. (E) K / Ba. (F) K / Rb. In Figs. A–C, oxides are plotted as percentages of total excluding silica, to avoid spurious trends resulting from the constant-sum effect. Symbols as in Fig. 1.

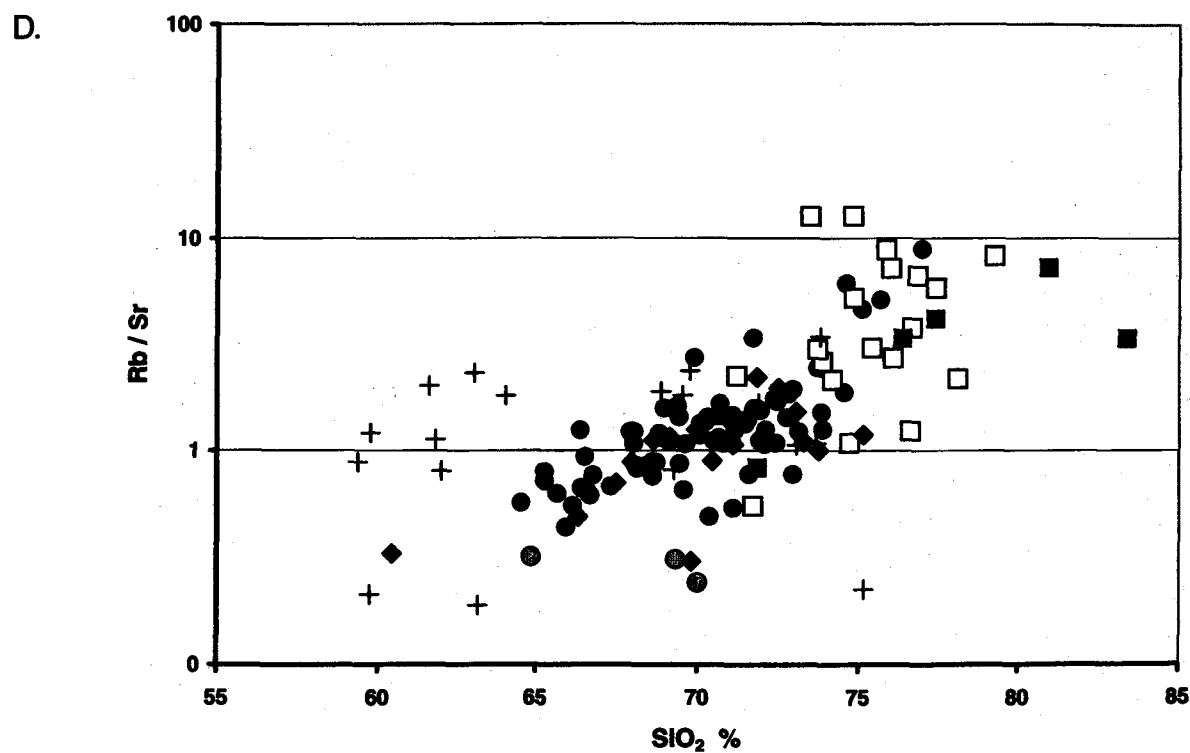
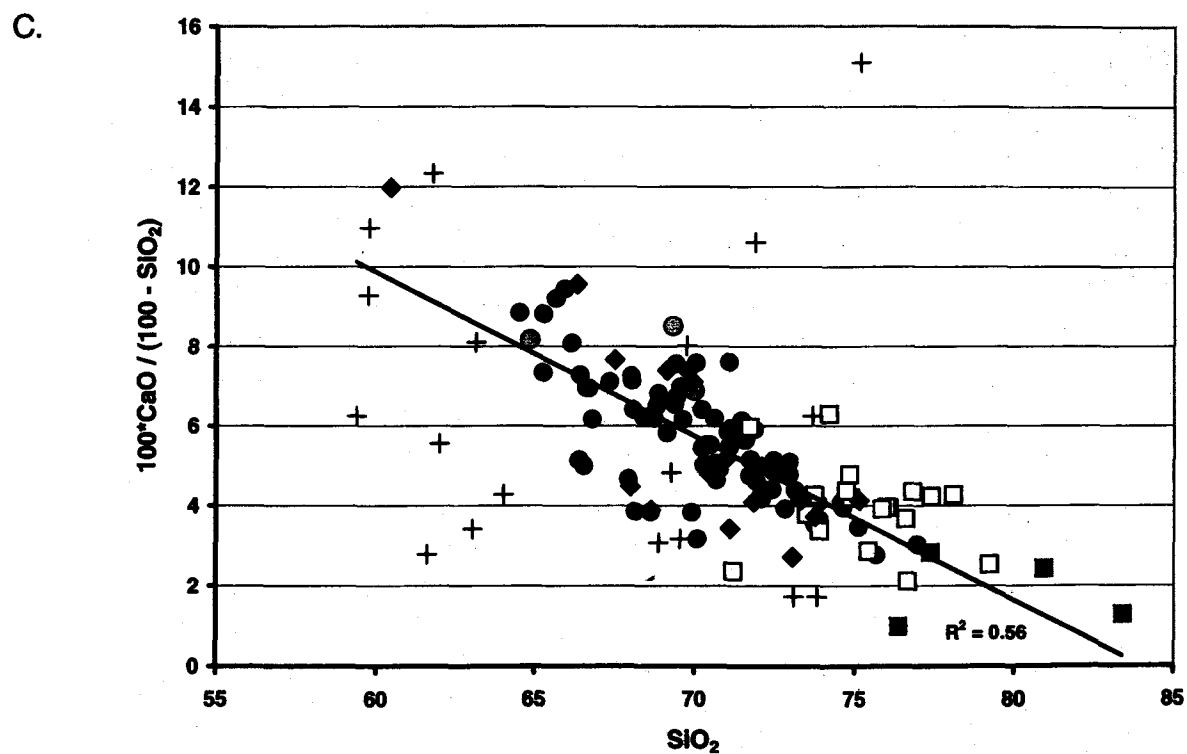


Figure 7. continued

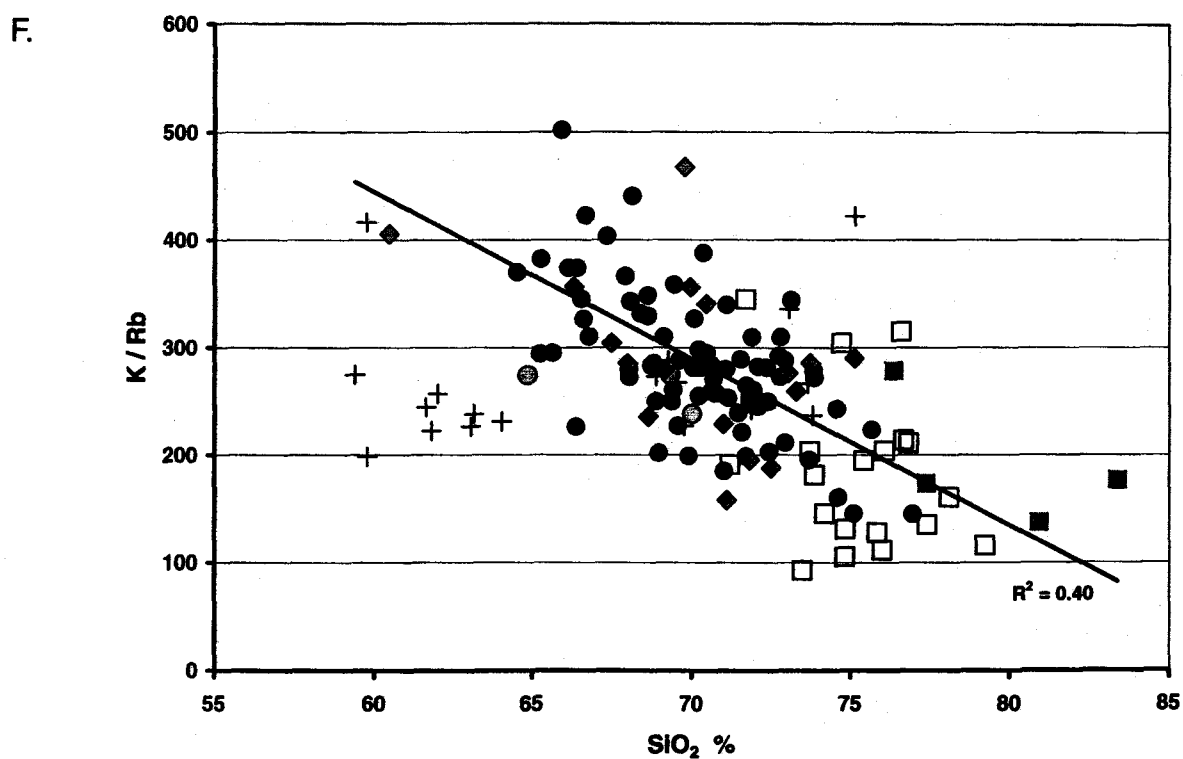
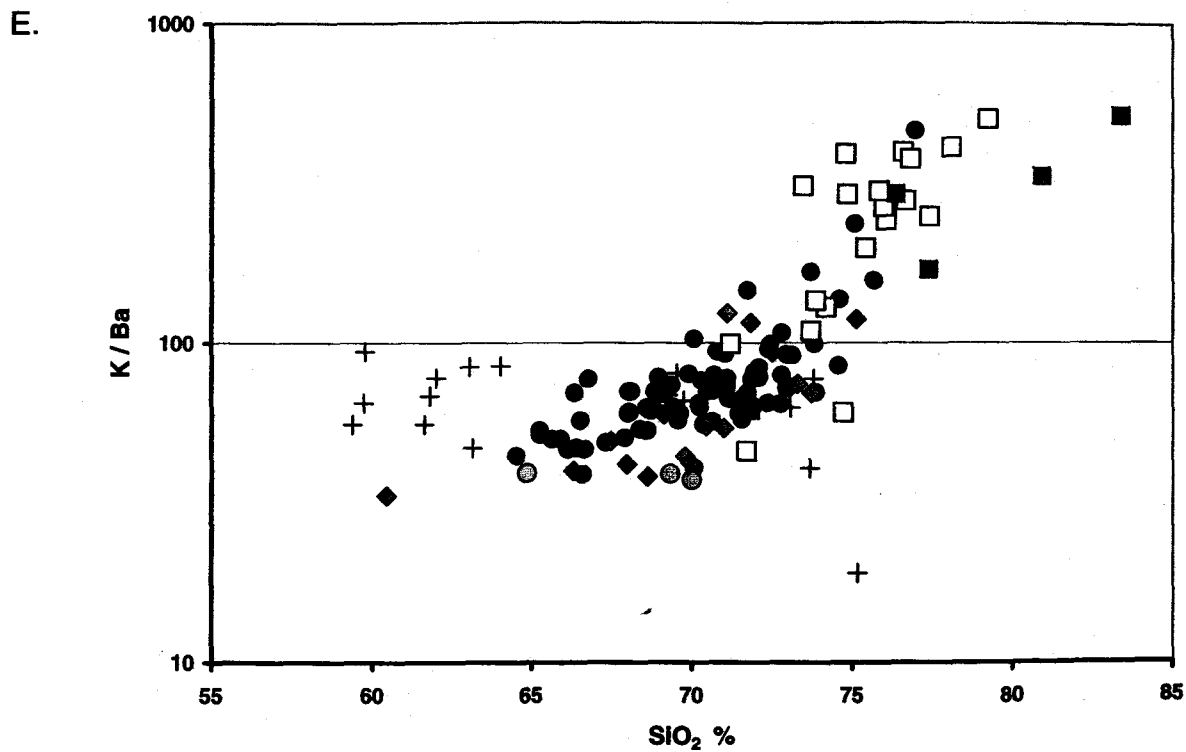


Figure 7. continued

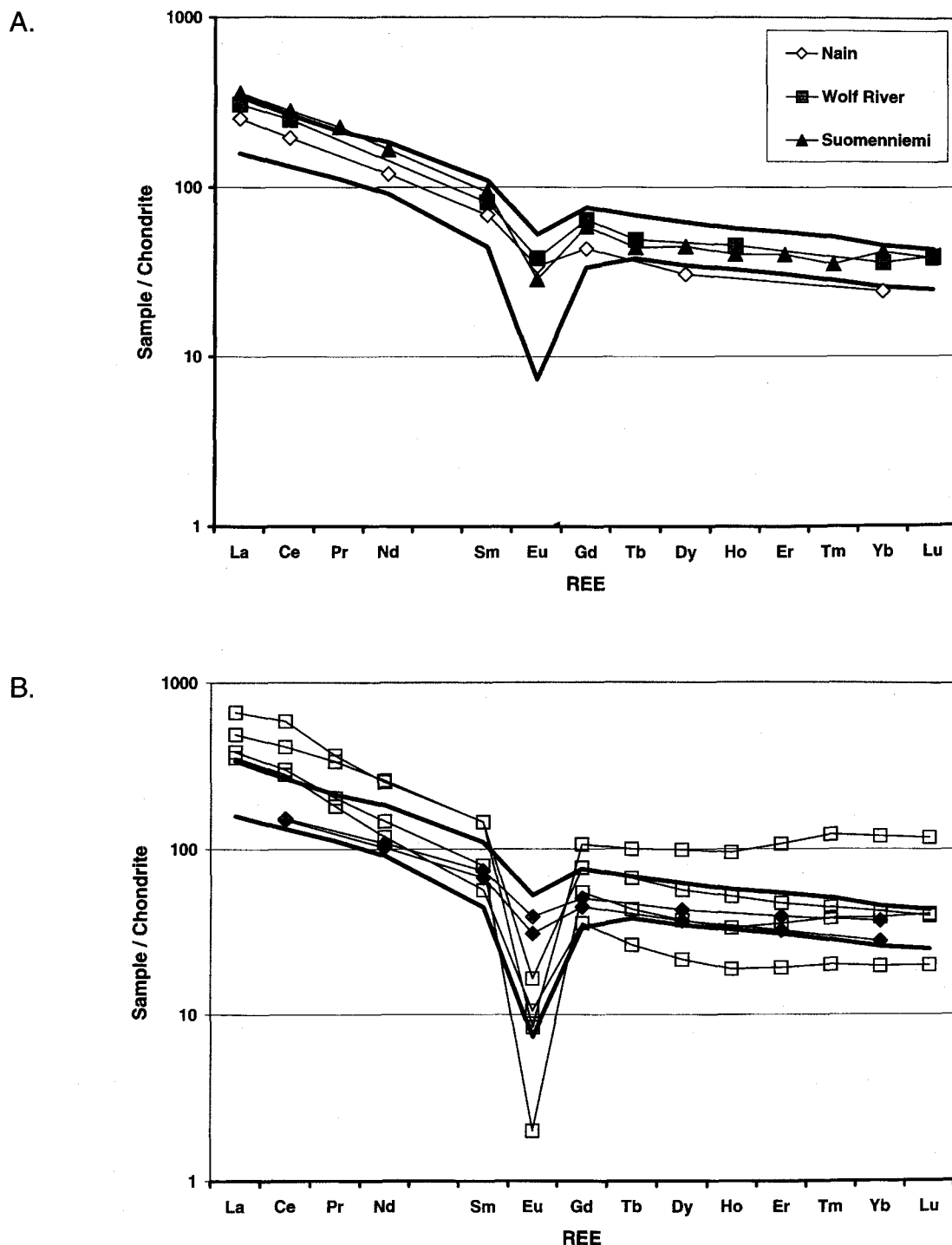


Figure 8. Rare earth element (REE) distribution in granitoids. Heavy lines in Figs. A–D show limits of variation in 13 samples of units CG and GA (A) Averages from other type A suites: Nain (Emslie and Stirling, 1993), Wolf River Batholith (Anderson and Cullers, 1978), Suomenniemi Batholith (Ramo, 1991). (B) Units BM (squares) and LD (diamonds). (C) Sillimanite-nodular facies of unit BM. (D) Units TH (crosses), BG (circles), and KZb (triangles). (E) Eu / Eu^* vs. SiO_2 ($\text{Eu}^* = \text{SQRT}[\text{Sm}_N \cdot \text{Gd}_N]$). Filled circles: units CG and GA; other symbols as in Figs. 8A–8D. REE data are normalized to the recommended chondrite values of Henderson (1984),

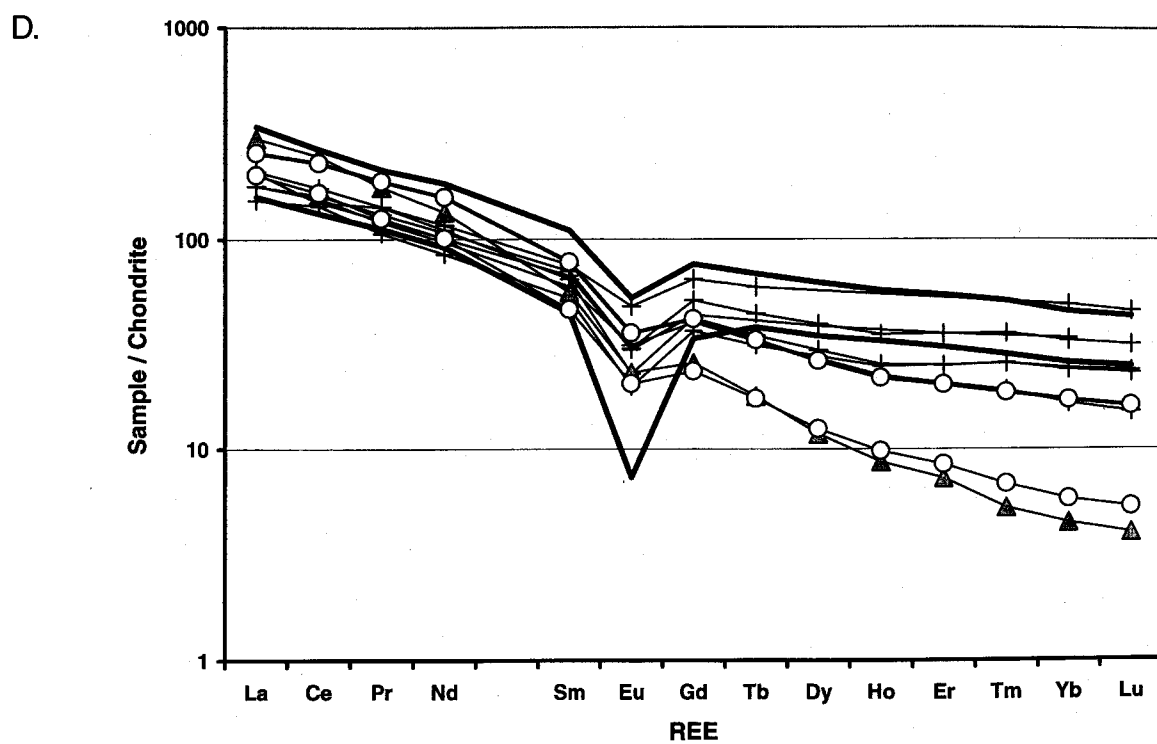
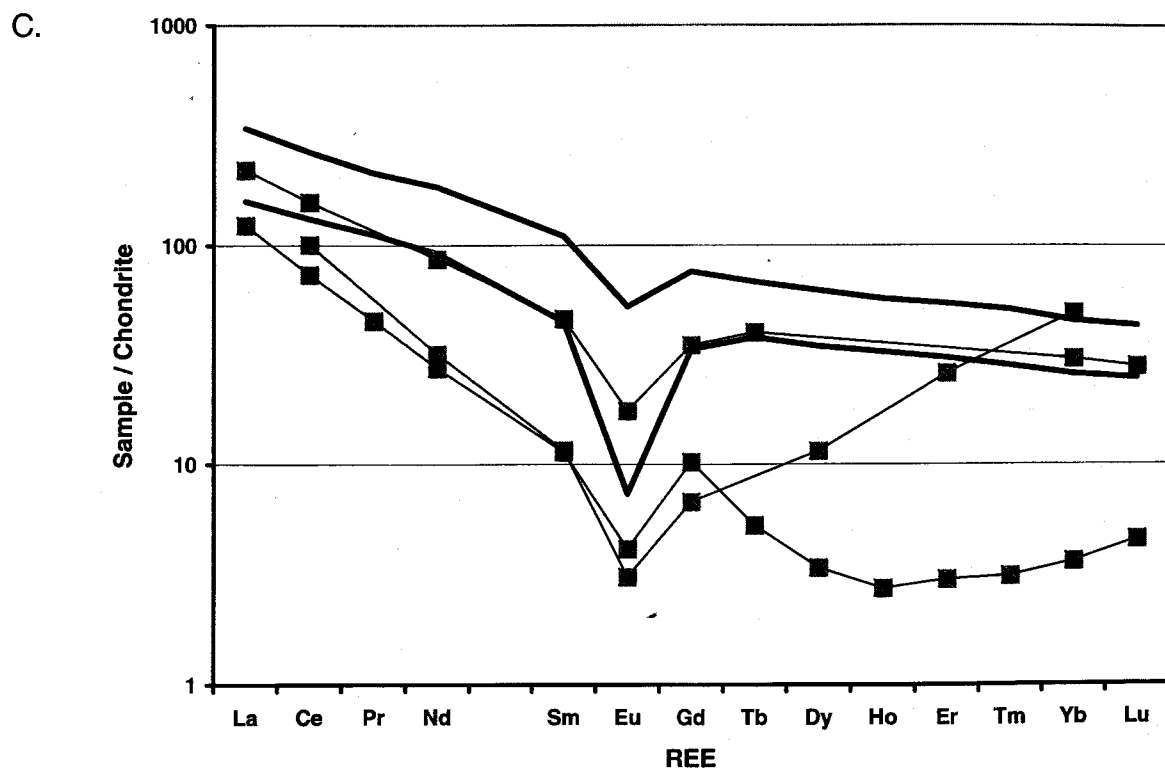
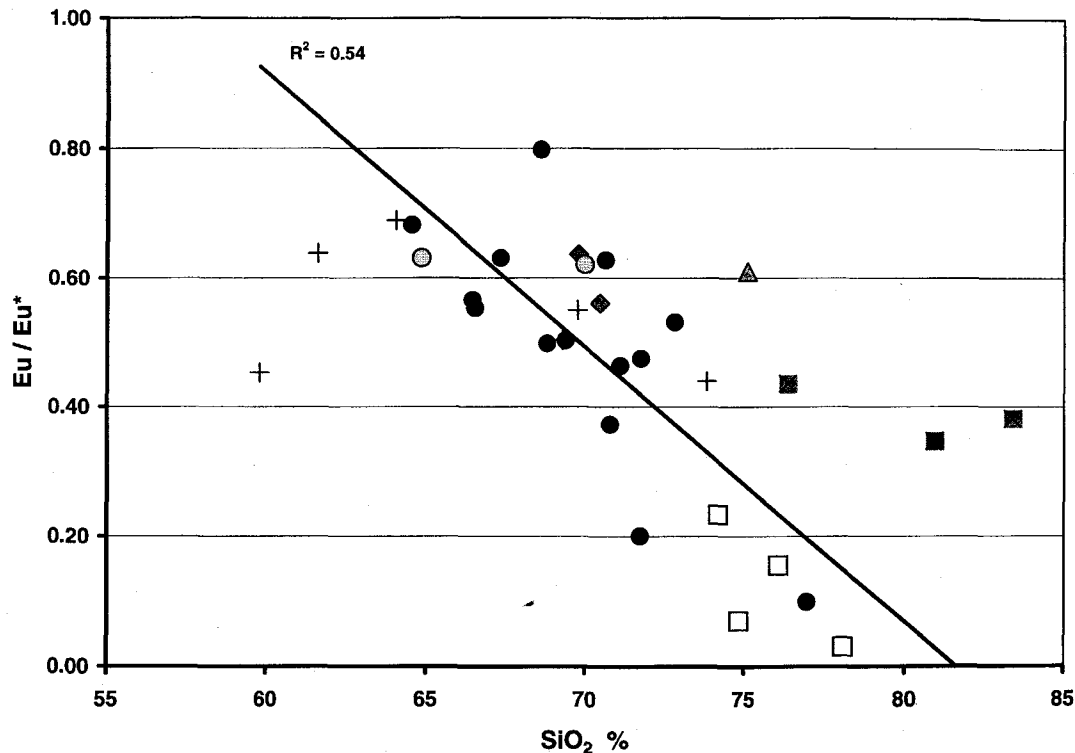


Figure 8. *continued*

Figure 8. *continued*

fraction and to the most evolved liquid, respectively (Fig. 9). Samples below the trend in Figure 9 are enriched in factor Q3. Nearly all of these are from bodies of CG and GA in the westernmost part of the map area (open symbols on Fig. 9). Relative to other rocks of the suite, they have slightly higher Mg / Fe ratios, lower K / Na ratios, lesser amounts of incompatible trace elements, and more Sr. The differences suggest derivation from more mafic source rocks, or more extensive partial melting, or both. The effect is, however, relatively small compared to that of fractionation.

Magmatic temperatures and pressures — The presence of hypersolvus alkali feldspars throughout the CG-GA suite suggests relatively hot, dry magmas. Use of the zircon saturation model of Watson and Harrison (1984) with Zr abundances in rocks of the CG-GA suite yields temperatures in the range of 800–900°C (Fig. 10). The trend of data is oblique to the isotherms, with lower model temperatures in the more felsic rocks, consistent with cooling during fractionation. This trend may be augmented by enrich-

ment of the more mafic rocks in cumulus zircon. The use of suite-average values of M and Zr yields a temperature of $874 \pm 25^\circ\text{C}$, which is very approximate due both to the experimental uncertainties (Watson and Harrison, 1983) and the likely presence of inherited zircon, leading to erroneously high model temperatures. Hornblendes in granite (Table 2, BMS10X, MKU05, OFY01, RLS45, WCS33) yield average pressures of 1.15 ± 0.32 , 2.03 ± 0.33 , and 2.83 ± 0.35 kbar at 875° , 850° , and 825° , respectively, using the Al-in-hornblende geobarometer of Anderson and Smith (1995). These pressures are consistent with shallow intrusion (< 10 km depth) and limited re-equilibration during granulite facies metamorphism.

Olivine metagabbro (unit OG; layers and lenses in GA, LD, KZ, and BG) — Metamorphosed gabbro, troctolite, and leucotroctolite occur in relatively small bodies and layers in the southeastern half of the map area. Most occurrences are too small to appear at map scale. The best exposures are on Wakely Mountain (Fig. 11A), Payne Mountain, and Sturge Hills in the northeastern corner of WCQ. Isolated small bod-

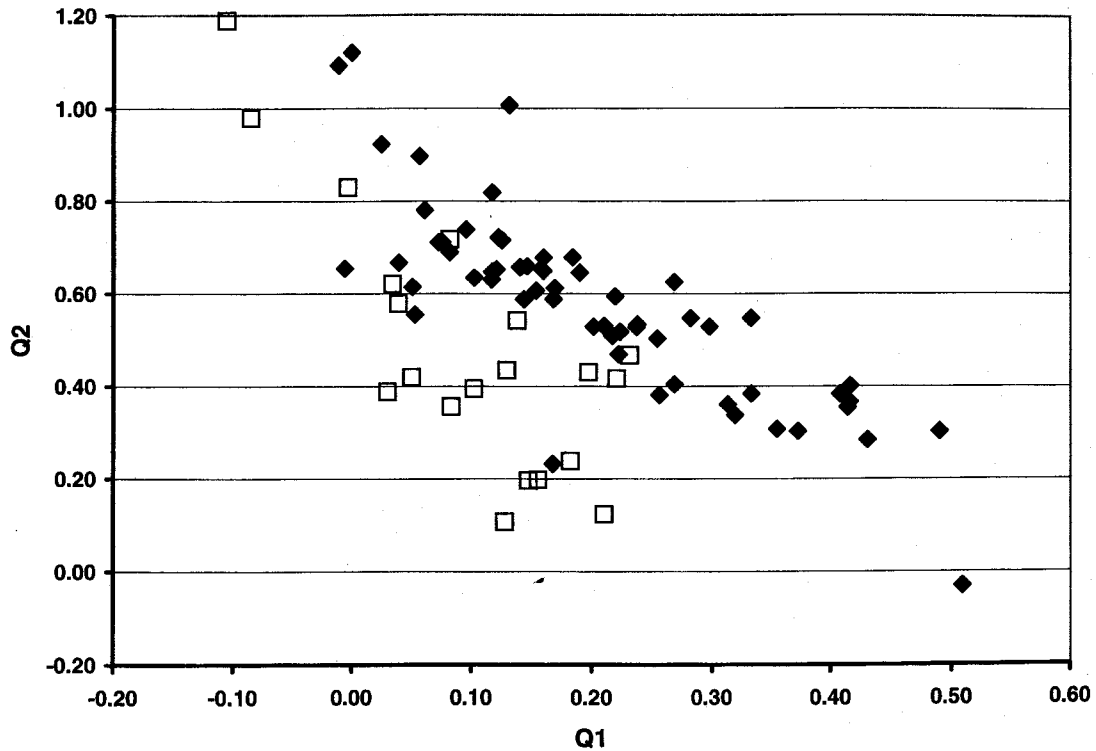


Figure 9. Q-mode factor model. Plot of the first two Q-mode factors of a three-factor model for units CG and GA. See text and Table 3 for details. Solid symbols: Samples of charnockite and granite from the eastern 5/6 of the map area and westernmost Blue Mountain Lake 15' Quadrangle. Open symbols: Samples from the western 1/6 of the map area and eastern Port Leyden 7.5' Quadrangle.

ies occur just north of the junction of First Stillwater and South Branch Moose River (OFQ); on Cool Mountain, southeast of Atwells (OFQ); and approximately 1 mile south-southeast of Helldiver Pond (WCQ). The latter body was described by deWaard (1961) and interpreted as a laccolith. Alternatively, it may be a lens-shaped body with its northwest side truncated by shearing along the Moose River Deformation Zone (see Structure section, this volume).

The massive interiors of large olivine metagabbro bodies preserve subophitic igneous textures; near their contacts they grade into foliated amphibolite or garnet amphibolite. Metamorphic minerals including garnet, secondary clinopyroxene, orthopyroxene, hornblende, and biotite form reaction coronas around grains of olivine and oxides (Whitney and McLelland, 1973, 1983). Plagioclase is clouded with green, micron-scale metamorphic spinels. Garnet is absent

in the Cool Mountain body. Biotite-hornblende rims around ilmenite grains give the rock a distinctive spotted appearance in many outcrops. Southwest of South Lake (WCQ), a body of coarse-grained metagabbro, amphibolite, and olivine-normative leuconorite has been mapped as OG, although it is distinct in appearance and texture. It includes a coarse-grained anorthositic facies that differs from other anorthosites in the map area in being strongly olivine normative (Table 1E, WCC25 and WCC26).

Anorthosite suite (unit JA, and local thin layers and lenses in BM) — These heterogeneous rocks are chiefly jotunite (as defined by Owens et al., 1993), with lesser amounts of gabbroic anorthosite gneiss and metanorthosite. Blocky to rounded andesine megacrysts up to 5 centimeters across and enclaves of anorthosite are common in the jotunite (Fig. 11B). These rocks occur as relatively thin, laterally exten-

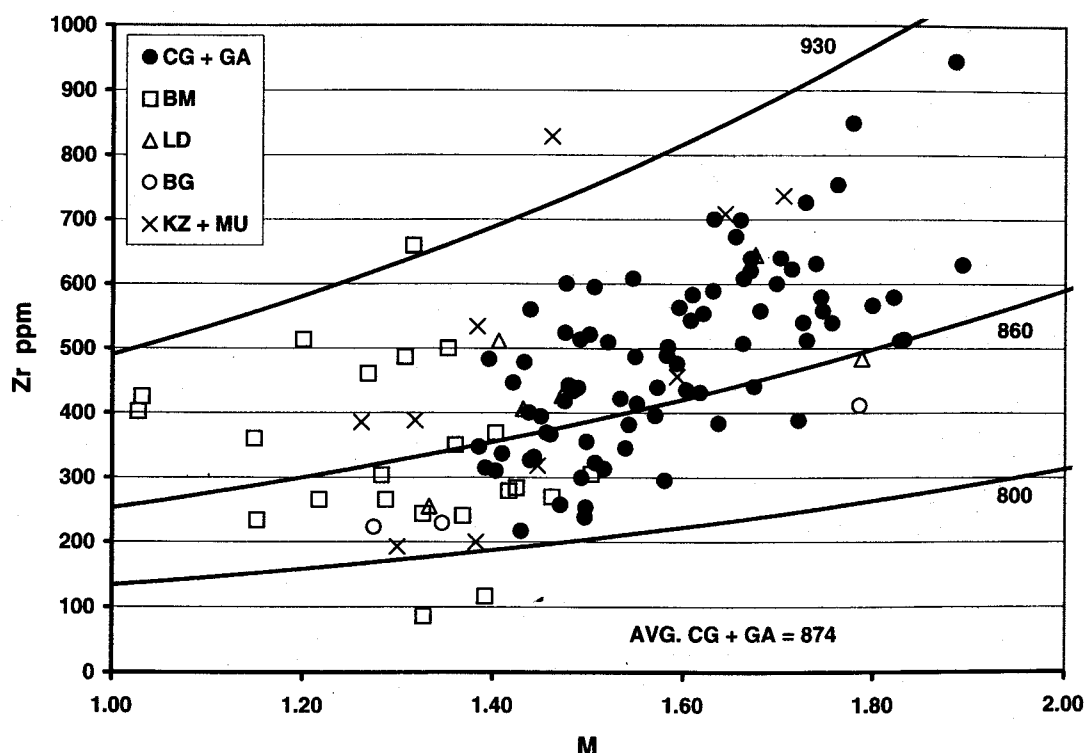


Figure 10. Zircon saturation in granitoids. Temperature calculated using the zircon saturation model of Watson and Harrison (1983, 1984). $M = (Na + K + 2Ca) / (Al + Si)$ cation ratio. Isotherms are in degrees Celsius.

sive stratiform bodies suggestive of an origin as shallow, sill-like intrusions of relatively fluid ferrodiorite or leuconorite magma. Individual layers of unit JA, rarely more than a few hundred meters thick, are traceable up to 40 kilometers along strike. Most occur within or adjacent to unit BM, except in northeastern RLQ, where they occur with unit GA. Small bodies of coarse gabbroic metanorthosite occur in units BG and CG south of Little Moose Pond (SE WCQ), near Pillsbury Mountain on the periphery of the Snowy Mountain Dome. These may be deformed dikes or sills related to the Snowy Mountain anorthosite (deWaard and Romey, 1969).

Anorthosite in unit JA may have originated as local concentrations of plagioclase that formed by flow differentiation or crystal settling. Both jotunitites and anorthosites contain somewhat more quartz and alkali feldspar than similar rocks in the Adirondack High Peaks region, perhaps due to assimilation of felsic

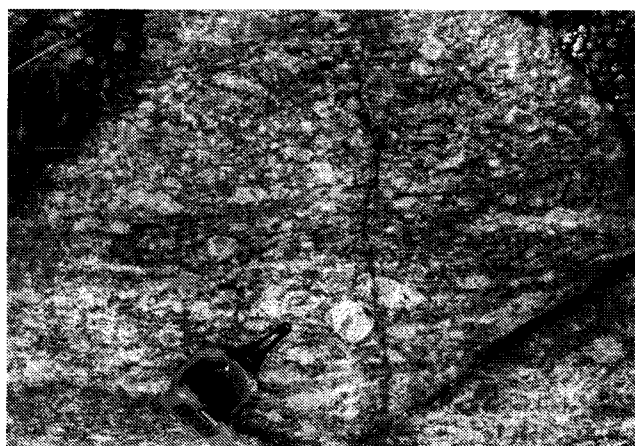
host rocks. In many locations, the felsic components occur as quartz-alkali feldspar leucosomes oriented parallel to foliation, probably as a result of pre- or syn-deformation anatexis. Garnet is present as reaction rims around oxides and orthopyroxene in some jotunitites in the easternmost third of the map area.

Amphibolite (unit AM, and layers in GA, LD, KZ, BL, and MU) — Amphibolite occurs principally as relatively thin (from a few mm up to 10 m) layers in granitic and metasedimentary rocks. A few thicker layers are mapped as unit AM. Garnet amphibolite occurs locally at contacts of olivine metagabbro (unit OG) with other units in the southeastern third of the area.

Mafic silicate assemblages in the amphibolites include Hbl + Cpx, Hbl + Bt, Hbl + Cpx + Bt, Hbl + Cpx + Opx, Hbl + Cpx + Opx + Bt, and Hbl + Cpx + Bt + Grt. Opaque oxides are normally present, and a few samples contain titanite. Plagioclase is ubiqui-



A.



B.

Figure 11. Outcrops of olivine metagabbro and jotunite: (A) Weathered surface of olivine metagabbro. Rough surface is due to uneven distribution of garnet in the rock. Summit of Wakely Mtn, WCQ. (B) Foliated jotunite with plagioclase megacrysts, approximately 0.5 mi. E of Hitchcock Lake, NFQ.

tous, but may be partially or wholly replaced by scapolite in amphibolites hosted by marble. Rarely, a few blocky plagioclase megacrysts similar to those in the jotunites are present. Some amphibolites contain varying amounts of alkali feldspar and trace to minor amounts of quartz. Mafic layers in unit BL locally contain the assemblage $Bt + Cpx + Opx \pm Grt$ with little or no hornblende. Except for enrichment in potassium, these biotite-rich rocks (e.g., Table 1E, RLS134) are similar in composition to other amphibolites.

Unmetamorphosed diabase — Fine- to medium-grained mafic dikes up to 5 meters wide occur locally along and parallel to the major faults and fracture zones. These rocks are poorly exposed due to their location in fault- or fracture-controlled valleys. A particularly good exposure is in Golden Stair Creek; a short distance upstream from North Lake, OFQ. This thick (ca. 5 m), plagioclase-phyric dike with chilled margins is parallel to the trace of the North Lake–Long Lake Fault. A similar dike, 1 to 2 meters wide, is exposed in the bed of the Red River at the southern edge of the RLQ, along the trace of the same fault. These dikes are similar in lithology and orientation to the more abundant, latest Proterozoic or earliest Cambrian diabase dikes of the eastern and

northeastern Adirondack Highlands (Isachsen et al., 1988; Coish and Sinton, 1991).

Geochemistry of the mafic rocks — Geochemical data from 36 samples of mafic and anorthositic rocks (Table 1E) indicate a generally tholeiitic character (Figs. 1A, B). Table 4 and Figures 12 A and B compare the average composition of 27 mafic rocks (excluding anorthosites) from the map area with the corresponding suite of mafic rocks from the Adirondack High Peaks region. In general, map area rocks are slightly more felsic and enriched in K, Rb, and Zr, consistent with assimilation of granitic host rocks. The average major element chemistry of both suites (Table 4) is similar to continental tholeiite flood basalts such as those of the Proterozoic Keweenaw (Basaltic Volcanism Study Project, 1981) and Tertiary Columbia River–Snake River (Carlson and Hart, 1988) provinces, as well as to dike swarms associated with rapaki intrusives, for example, the Proterozoic Suomenniemi Batholith (Ramo, 1991).

Olivine metagabbros, amphibolites, jotunites, and anorthosites from the map area are compared with olivine metagabbros (envelopes labeled OG) and jotunites (JT) from the Adirondack High Peaks region in Figures 12C–F. In the R1-R2 diagram of de la Roche et al. (1980), olivine metagabbros and

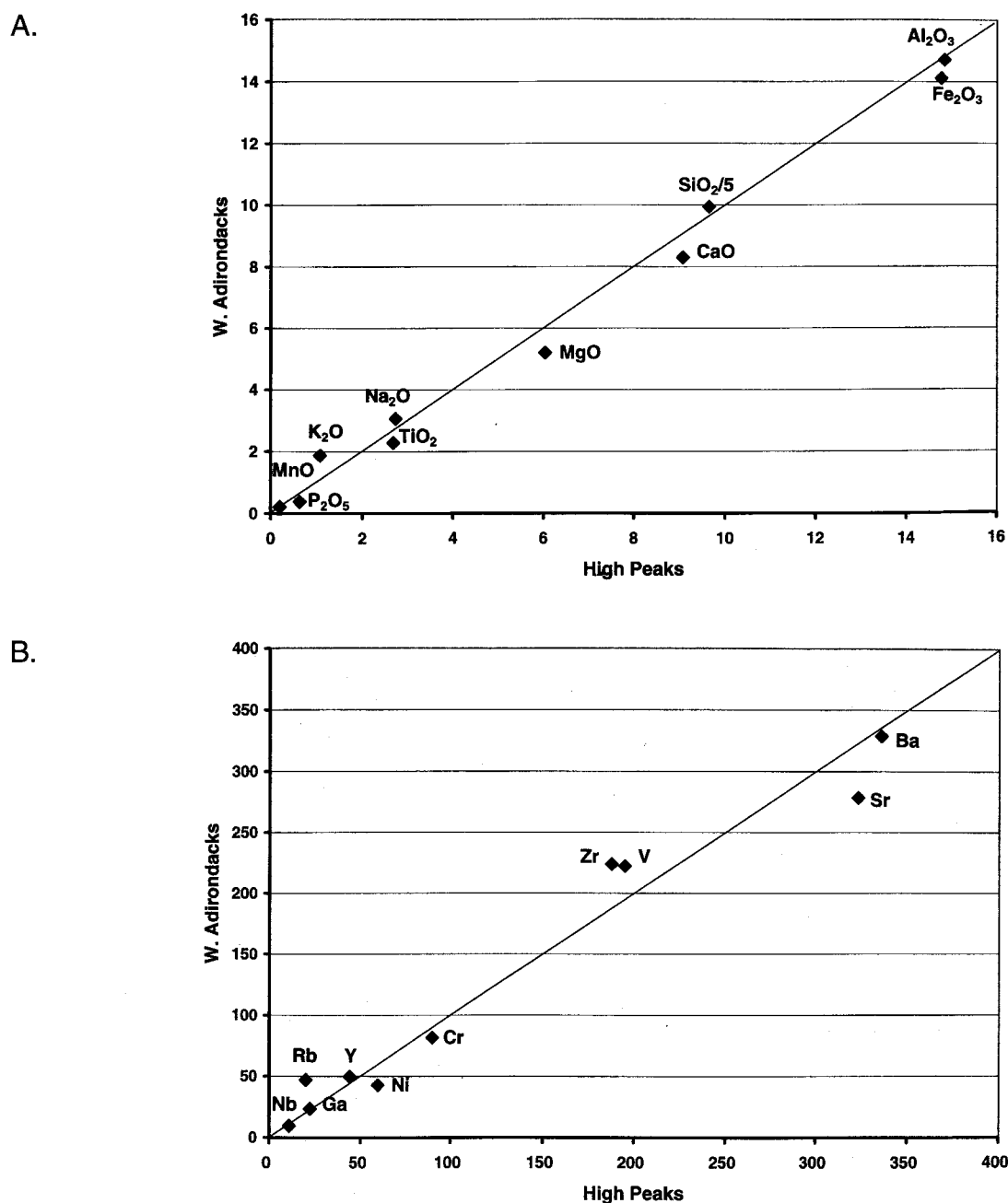


Figure 12. Geochemistry of mafic rocks. **(A)** Comparison of average major element contents of the western Adirondack mafic suite (27 samples), excluding plagioclase-rich compositions, with analogous rocks from the Adirondack High Peaks region (78 samples). Scales in weight percentages. **(B)** Comparison of trace element contents of the same sample sets as in Fig. 12A; scales in parts per million. **(C)** R1–R2 diagram (de la Roche et al., 1980) for mafic rocks of the map area. $R1 = 4000 \cdot Si - 11000 \cdot (K + Na) - 2000 \cdot (Fe + Ti)$. $R2 = 6000 \cdot Mg + 2000 \cdot Ca + 1000 \cdot Al$. Symbols as in Fig. 1; shaded diamonds distinguish group B amphibolites. Solid envelopes show fields for olivine metagabbros (OG) and jotunites (JT) from the High Peaks area; dashed envelope is for all High Peaks mafic rocks. **(D)** Variation of TiO_2 (normalized to percentage of mafic minerals) with mg number ($Mg / [Mg + Fe]$); envelopes and symbols as in Fig. 12C. **(E)** Variation of Y with mg in mafic rocks; envelopes and symbols as in Fig. 12C. Trends for Zr, Nb, P_2O_5 , and Ga / Al are similar to that for Y. **(F)** Variation of $K / (K + Na)$ with mg in mafic rocks; envelopes and symbols as in Fig. 12C. Outliers result from alkali exchange between thin amphibolites and their host rocks.

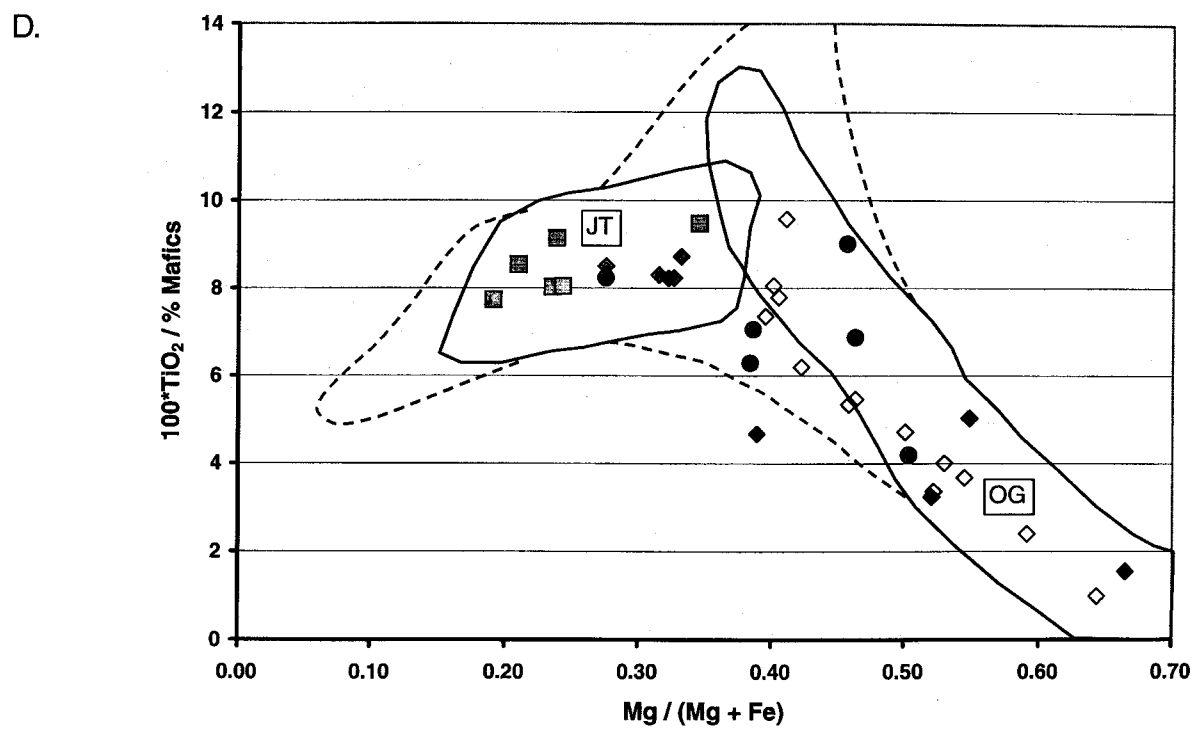
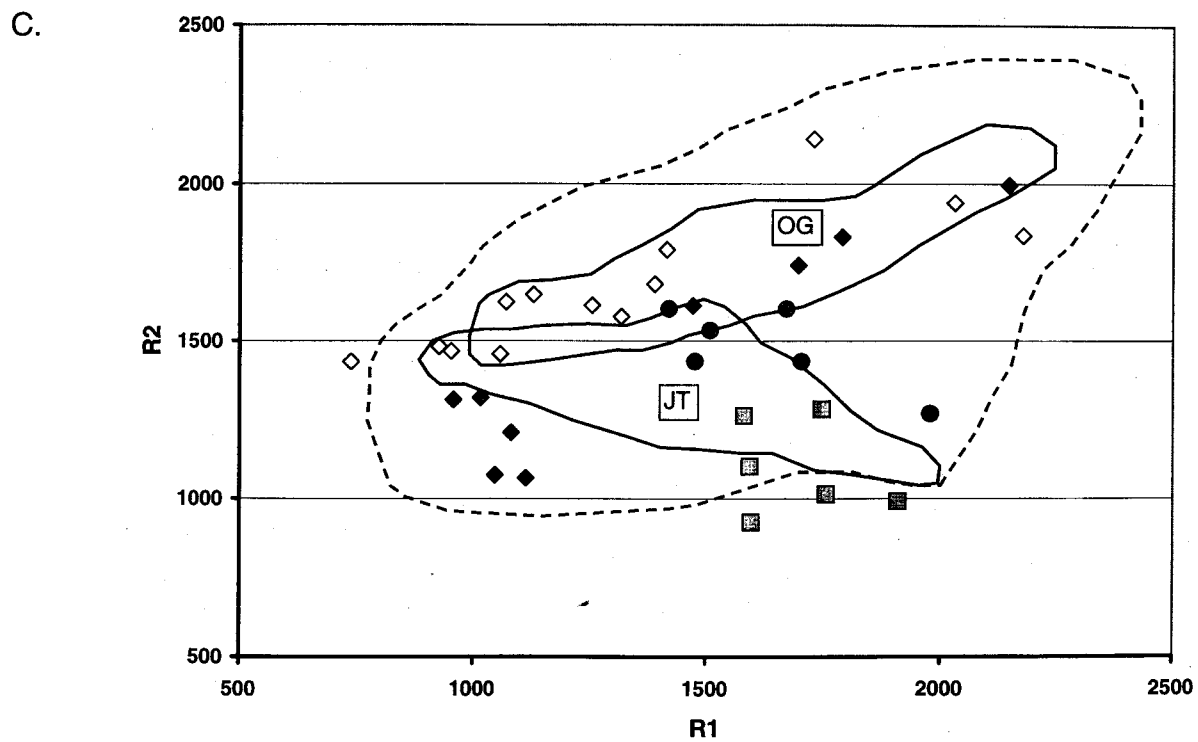
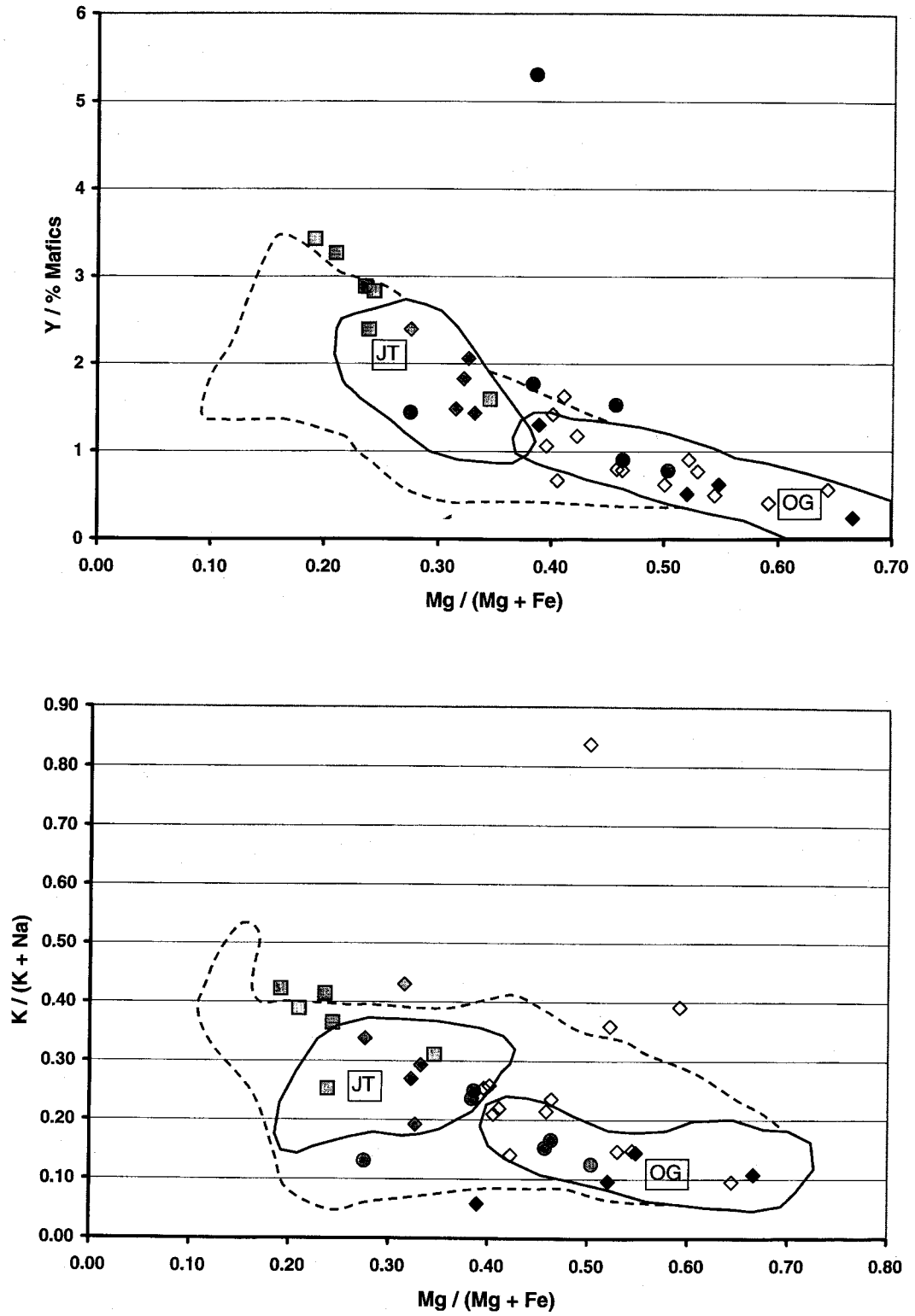


Figure 12. *continued*

Figure 12. *continued*

amphibolites form a roughly linear array parallel to that of the High Peaks gabbros, consistent with fractionation of olivine and plagioclase in an undersaturated basaltic magma (Fig. 12C). A separate group of amphibolites (shaded diamonds in Figs. 12C–F) indicates a plurality of magma sources or varying conditions of fractionation. Incompatible components such as TiO_2 (Fig. 12D) and Y (Fig. 12E) consistently increase with decreasing mg ($\text{mg} = \text{Mg} / [\text{Mg} + \text{Fe}]$). Similar trends are shown by P_2O_5 , Zr, Nb, and Ga / Al. In Figures 12D and E, the incompatible elements are normalized to the percentage of normative mafic minerals to correct for the effects of cumulus plagioclase. The outlier in Figure 12E is a gabbroic anorthosite that contains traces of a metamict phase (allanite?) that may account for the anomalous Y value. The ratio $\text{K} / (\text{K} + \text{Na})$ also increases with mg (Fig. 12F), consistent with a progressive concentration of K in the liquid during fractionation and/or assimilation of felsic host rocks. Outliers in Figure 12F probably result from metasomatic alkali exchange between amphibolite layers and their host rocks, either at the time of emplacement or during metamorphism. The most K-rich sample (Table 1E, RLS134) is a biotite-2 pyroxene-garnet gneiss layer associated with meta-evaporites of unit BL. The presence of leucite in the norm of this rock and of nepheline in several other amphibolites is consistent

with metasomatic addition of alkalis.

Substantial in situ fractionation is unlikely in small mafic dikes, and the fractionation indicated in these diagrams probably occurred in a subcrustal or lower crustal reservoir from which batches of magma were intruded at higher levels. Jotunites form a distinct group that does not appear to be related to the gabbros and amphibolites by simple fractionation (Figs. 12C, D). Their consistent association with anorthosite in unit BM suggests an origin by plagioclase fractionation from a quartz-saturated gabbroic anorthosite liquid (McLelland et al., 1994). Assimilation of felsic host rocks or mixing with granitic magma may explain why several of the jotunites fall outside the envelope defined by their High Peaks counterparts.

REE patterns of anorthosites (Fig. 13A), jotunites (Fig. 13B), and olivine metagabbros (Fig. 13C) are also comparable to those of the corresponding rocks in the High Peaks. Amphibolite REE patterns (Fig. 13D) resemble those of the metagabbros, the greater total REE content and the distinct negative Eu anomalies of the more evolved samples are consistent with fractionation of Eu-enriched plagioclase. Plagioclase cumulates, both anorthosites (Fig. 13A) and plagioclase-rich metagabbros (Fig. 13C, lower two patterns), have positive Eu anomalies.

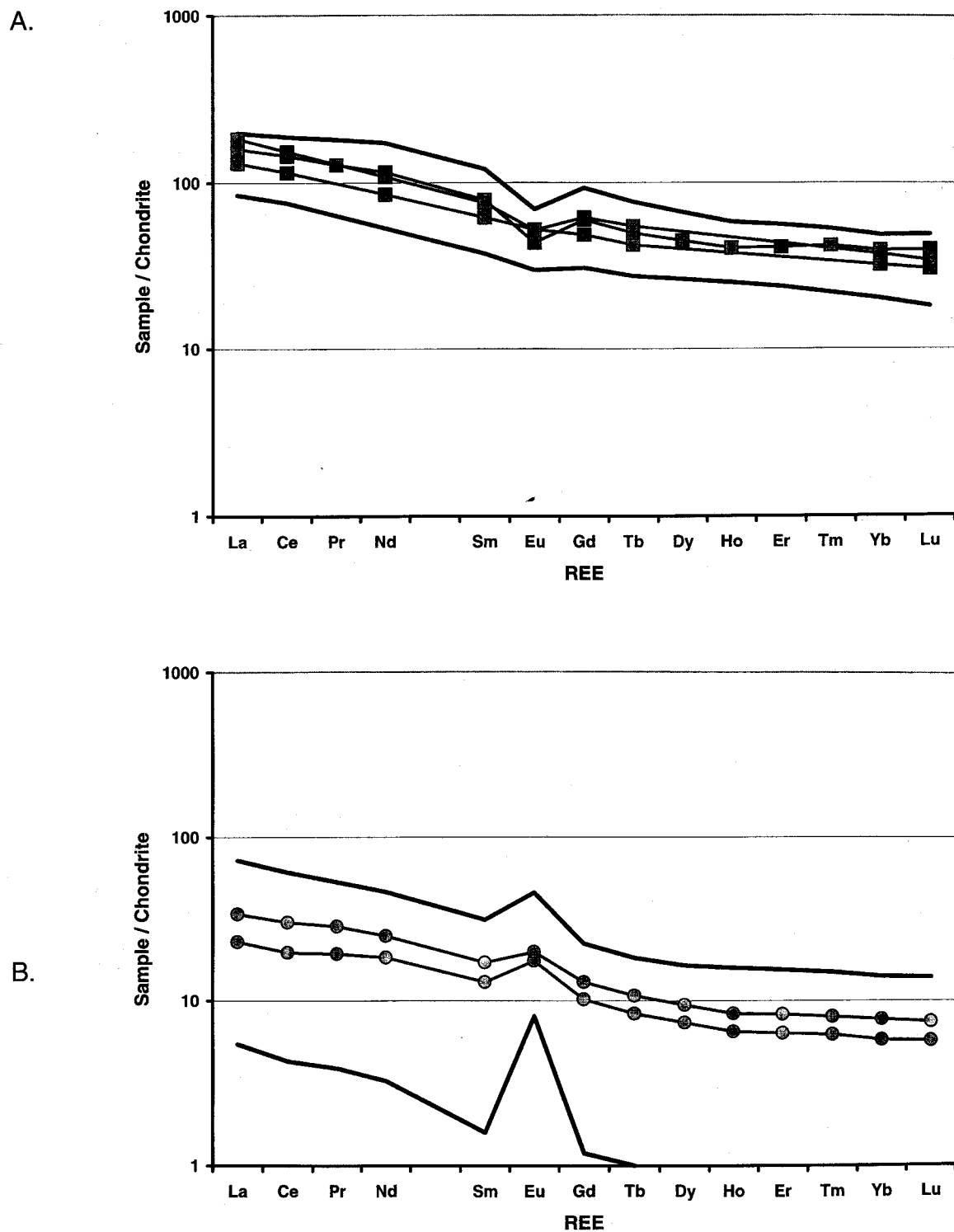
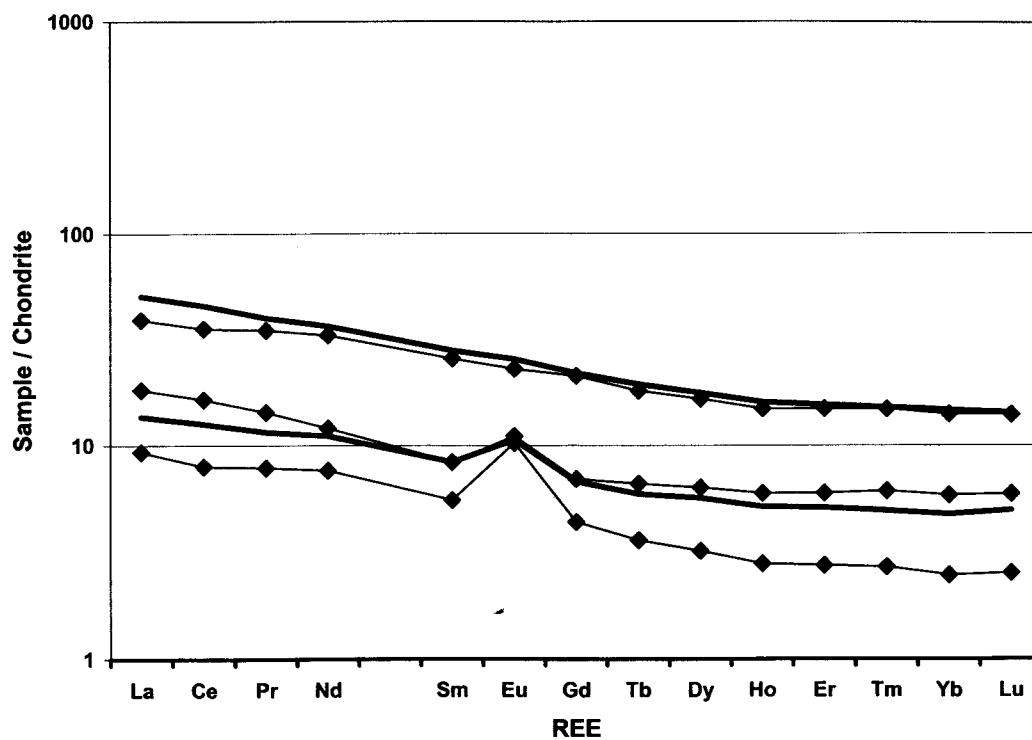


Figure 13. REE distribution in mafic and anorthositic rocks. Heavy lines show extent of variation in analogous rocks from the Adirondack High Peaks region. (A) Jotunite. (B) Anorthosite and gabbrioc anorthosite. (C) Olivine metagabbro and associated plagioclase cumulates. (D) Amphibolites and biotite amphibolites. Symbols as in Fig. 2. All REE data are normalized to the recommended chondrite values of Henderson (1984).

C.



D.

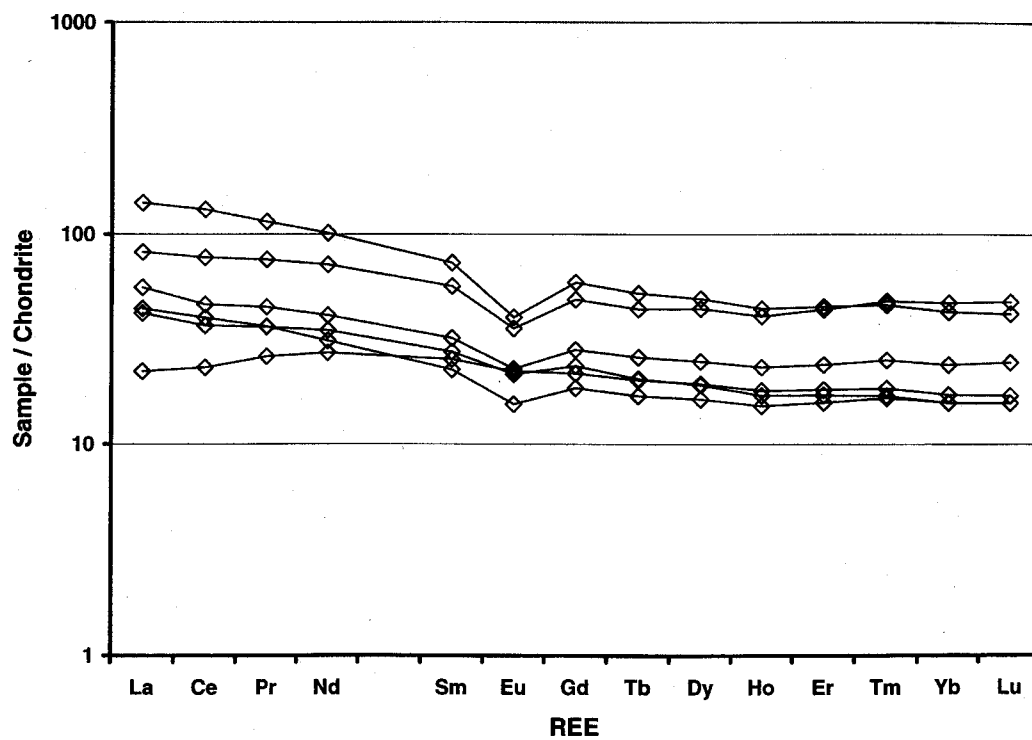


Figure 13. *continued*

Chapter 2

Metasedimentary Rocks

Calcsilicate rocks and marble — Metamorphosed calcareous rocks dominate unit CM, are abundant in MU, and occur locally in GA, BM, LD, TH, KZ, and BL. Diopsidic clinopyroxene ($\text{Di}_{80}\text{--Di}_{90}$) is the most common silicate mineral in carbonate rocks throughout the area. Diopside-rich rocks range from nearly pure diopsidites to combinations of diopside with microcline, plagioclase, scapolite, or quartz in various proportions. Tremolite, phlogopite or Mg-biotite, enstatite, epidote, and grossular-andradite garnet also occur in some calcsilicates. Wollastonite is rare and has been found in only three locations (see discussion under Metamorphism). Titanite is nearly ubiquitous, occurring in minor amounts as discrete anhedral grains or as rims on opaque oxides. Graphite and pyrite or pyrrhotite are common accessories. In the northwestern third of the map area, where calcsilicates occur principally as thin layers or isolated remnants within granitic gneisses, a brown amphibole, relatively pale in thin section, commonly occurs with clinopyroxene, feldspars, and quartz. Textures of most calcsilicate rocks tend to be fine-grained and equigranular except where micas or tremolite predominate.

Potassium feldspar in the calcsilicate rocks ordinarily ranges from clear, untwinned grains to microcline with well-developed twinning; perthitic alkali feldspars are less common. Most are quite K-rich ($\text{Or} > 90$), and several samples of K feldspar-rich calcsilicates show elevated Ba (Table 1F). Microprobe analysis of microcline from a typical diopside-K feldspar-quartz rock yielded 0.8% Ba (Table 2). The K-rich feldspars may be the metamorphic equivalent of illitic clays or authigenic microcline.

Mineral assemblages in marble consist of variable combinations of calcite, diopsidic clinopyroxene, phlogopite, quartz, scapolite, microcline, titanite, or (less commonly) tremolite. Forsterite, partially

altered to serpentine, is an uncommon constituent of relatively pure calcite marbles. Accessory minerals include graphite, pyrrhotite, and pyrite. Dolomite marbles, consisting of nearly monomineralic dolomite, are rare, and confined to the southeastern third of the area. Amphibolite, quartzite, and quartzofeldspathic gneiss occur as discrete layers, rootless small folds, or blocks within marble.

Metapelites (units KZa, BL, and locally in MU, KZb, and BM) — The most abundant rocks in unit KZa are biotite-quartz-plagioclase gneisses (“kinzigites”) that commonly contain garnet and/or sillimanite and varying amounts of perthitic alkali feldspar. The kinzigites are interlayered with substantial amounts of granitic and charnockitic gneiss, amphibolite, olivine metagabbro, and marble. deWaard (1962) mapped these rocks as separate units in the Little Moose Mountain Syncline (northeastern WCQ), and subdivided the kinzigite according to the dominant feldspar. Migmatitization is nearly ubiquitous in the kinzigites, with quartzofeldspathic leucosomes both parallel to and locally crosscutting foliation.

These rocks are probably metamorphosed pelitic or semipelitic sediments. Less aluminous varieties that lack sillimanite resemble the Popple Hill gneiss of the Adirondack Lowlands, which may have a dacitic volcanic protolith (Carl, 1988). In unit BL, kinzigite, biotite-sillimanite schist, and biotite-two pyroxene amphibolite are interlayered with massive to finely laminated quartzites up to several meters thick. On Flatrock Mountain (central MKQ), (pyroxene)-biotite-quartz-plagioclase gneiss without garnet or sillimanite alternates with feldspathic quartzites in what appears to be primary sedimentary bedding. Metapelitic (graphite)-(plagioclase)-sillimanite-garnet-quartz-K feldspar gneisses with little or no biotite occur locally as thin layers in KZa and MU. Unit BM contains scattered occurrences of

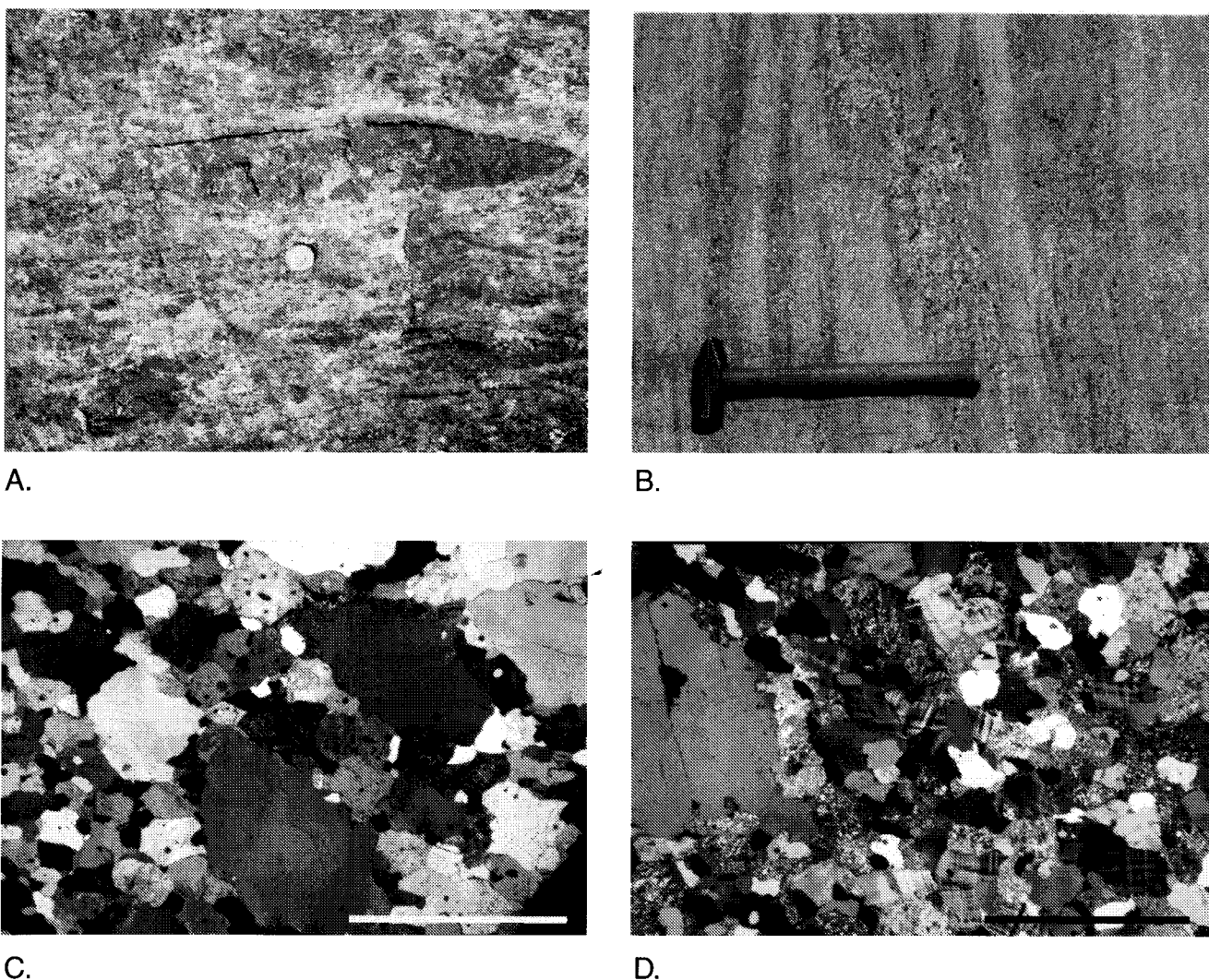


Figure 14. Outcrops and thin sections, unit TH. (A) Deformed quartz lens (stretched cobble?) in impure quartzite, Hill 2120, 1.2 mi. WSW of Thendara RR station, MKQ (Appendix A, Stop 5). (B) Compositional layering in quartzofeldspathic gneiss of unit TH; outcrop on N side of Rte 28, 1.2 mi. SW of Thendara RR station, MKQ (Appendix A, Stop 6); top to left, looking N. (C) Large rounded quartz grains in a matrix of finer-grained quartz, plagioclase, and ilmeno-hematite. Hill 2320, ca. 0.7 mi. N of Terror Lake, BMQ. Scale bar 5 mm, crossed polars. (D) Typical quartzofeldspathic gneiss of unit TH. Large rounded quartz grain at left of photo, in matrix of finer-grained quartz, microcline, altered plagioclase, and ilmeno-hematite. Roadcut on N side of Rte 28, 0.1 mi. E of Thendara RR station, MKQ; sample MKB07. Scale bar 55 mm, crossed polars.

(garnet)-(biotite)-sillimanite-quartz-K feldspar gneiss that locally grade into the sillimanite-nodular leucogneiss facies.

Quartzite (in units BL, TH, and MU, rarely CM) — Quartzites in the map area occur as relatively thin layers in other metasedimentary rocks, but in unit BL massive to finely laminated quartzites up to tens of

meters in thickness are common. Lenses and thin layers of diopside-rich calcsilicate granulite are locally common in the laminated facies. These quartzites contain trace to major amounts of biotite, phlogopite, microcline, plagioclase, tremolite, diopside, enstatite, garnet, or tourmaline. In unit TH, quartzite, grading into quartz-rich calcsilicate rocks, occurs

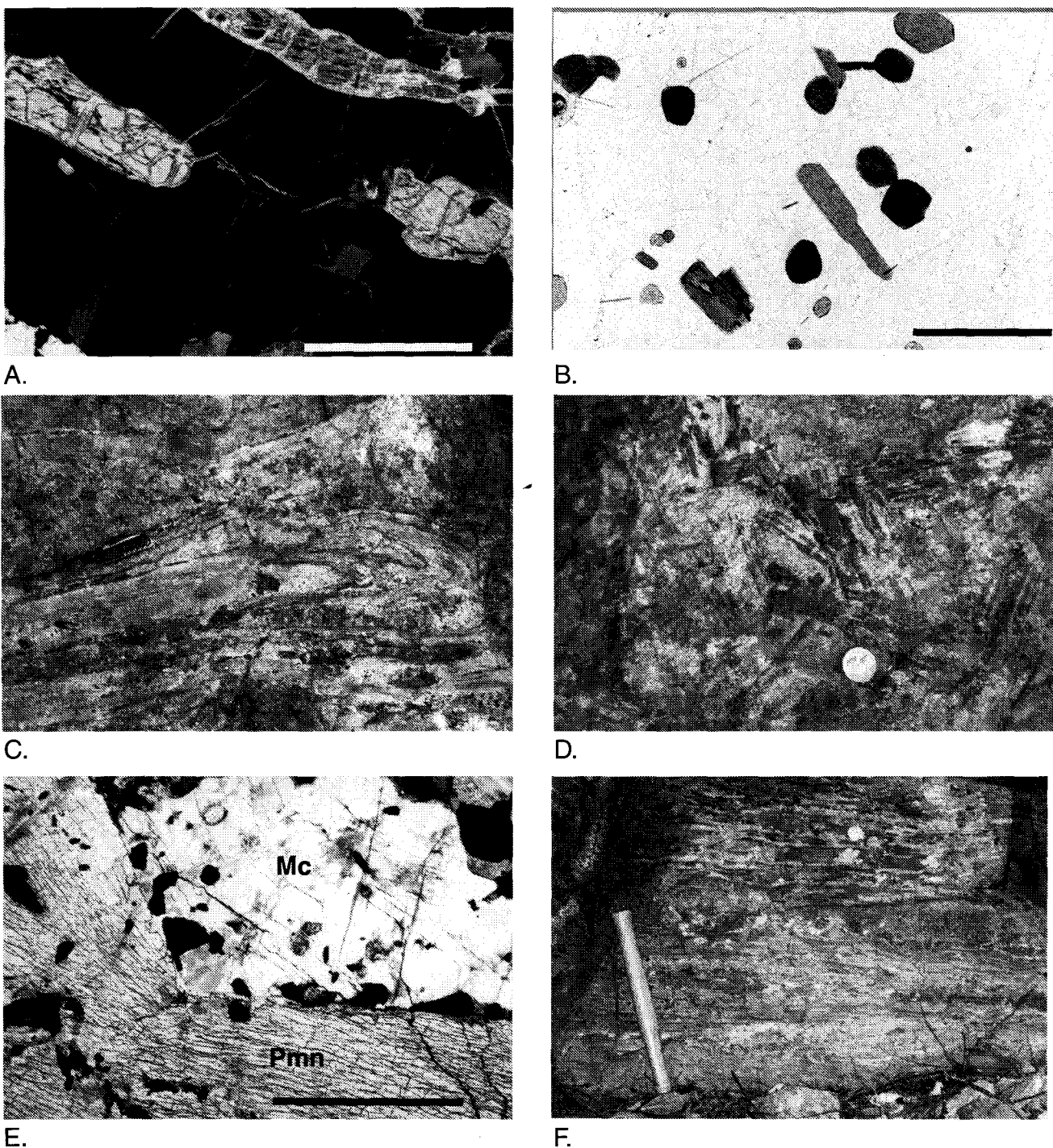


Figure 15. Outcrops and thin sections, Mg-rich metasedimentary rocks of unit BL. (A) Enstatite (gray), partially altered to talc, in quartzite. The enstatite shows strong preferred orientation that defines a lineation in the rock. Unit BL, Inlet Zone, 0.6 mi. SW of Black Bear Mtn, BMQ. Scale bar 5 mm, crossed polars. (B) Tourmaline (rounded) and biotite (elongate) in rutiled quartzite. Unit BL, 0.1 mi. NW of Big Lake, RLQ. Scale bar 1 mm, plane light. (C) Mg-rich paragneiss and quartzite. Large dark spots in lower half of photo are prismatic crystals. Note the recumbent isoclinal fold, possibly F_1 . Looking W, pocketknife for scale. Outcrop on S bank of Moose River ca. 0.5 mi. WMW of the hamlet of Moose River, MKQ (Appendix A, Sto3). (D) Prismatic crystals in foliation plane of Mg-rich paragneiss. Quarter for scale. Same location as Fig. 15C. (E) Large prismatic crystal (Pmn) with microcline (Mc) and quartz. Small dark grains are rutile. Same location as Figs. 15C, D. Scale bar 5 mm, plane light. (F) Laminated quartzite with alternating quartz- and diopside-rich layers. S bank of Moose River ca. 0.1 mi. upstream from the outcrop in Fig. 15C. Looking W.

locally as layers in the dominant quartzofeldspathic gneisses. A distinctive quartzite layer, up to 20 meters thick, is well exposed at the top of an unnamed 2120-foot hill, 1.2 miles west-southwest of the railroad station at Thendara, MKQ (Appendix A, Stop 5). This layer varies from quartzite to quartz-rich gneisses with diopside, grandite garnet, epidote, calcite, sphene, microcline, plagioclase, and scapolite in varying combinations and proportions. Rounded or lenticular masses of quartz up to 30 centimeters long, some flattened parallel to foliation, are present in some outcrops (Fig. 14A).

Quartzofeldspathic metasedimentary rocks (unit TH; locally in MU, BM, and LD) — A distinctive quartz-plagioclase-microcline gneiss is the principal lithology in unit TH. It occurs at two locations within the map area, in the northeastern MKQ north and west of the village of Thendara, and in the central BMQ between Rose Pond and Terror Lake. Meter- to decimeter-scale layers and lenses of quartz-rich calcsilicate rocks and quartzite occur in both areas but are more abundant and thicker in the Thendara body, where they form locally prominent hills.

Compositional layering is prominent (Fig. 14B), and even seemingly homogeneous samples show centimeter-scale crypto-layering defined by relative abundances of plagioclase, microcline, quartz, and pyroxene. Foliation-parallel leucosomes of salmon-pink microcline and quartz are locally abundant, as are concordant or crosscutting quartz veins and pegmatites. Mafic minerals include diopside, magnesiohastingsite (Table 2, MKS36), phlogopite or pale biotite, and, rarely, andraditic garnet. Titanite is nearly ubiquitous and locally abundant; zircons are scarce, small, rounded, and pink. Texture in thin section is commonly inequigranular (Figs. 14C, D), and many samples contain scattered large quartz grains up to several millimeters in diameter. Pyroxenes and amphiboles tend to be poikiloblastic, enclosing quartz and, less commonly, microcline. Ferric iron dominates in these strongly oxidized rocks, sequestered in steel-gray ilmenohematite that consists of titanohematite with exsolution lamellae of ferrian ilmenite (Buddington and Lindsley, 1964); magnetite is uncommon. Scattered strong negative aeromagnetic anomalies in both areas (Balsley and Bromery, 1965d, e) coincide with ilmenohematite

concentrations. Because of the scarcity of ferrous iron, pyroxenes, amphiboles, and micas are Mg-rich and pale in color; hence the rocks resemble leucogneisses where compositional layering is inconspicuous, even though the normative color index commonly exceeds 10%.

The average composition of unit TH gneisses (Table 1E) is granitic, but the extreme variation in modal and normative quartz, albite, and orthoclase (Fig. 4B), the distinct compositional layering in most exposures, the uniformly high oxidation state of iron, and the presence of metasedimentary quartzite and calcsilicate interlayers all suggest a sedimentary protolith such as arkose. REE patterns in quartzofeldspathic gneisses of unit TH (Fig. 8D) differ only slightly from the pattern for CG, consistent with an arkosic protolith.

Metamorphosed evaporites? — Calcsilicate rocks at several locations in units BL, CM, and MU are dominated by Mg-rich phases such as diopside, tremolite, phlogopite, or magnesian biotite. These include tremolite-phlogopite-diopside schists with as much as 16% MgO (e.g., Table 1F, RLS135). In the eastern part of the Fulton Lakes Synform and in the southern WCQ, calcsilicate assemblages locally include enstatite, partly replaced by talc (Fig. 15A). Many quartzites in unit BL also are relatively Mg-rich, containing assemblages such as Bt + Qtz, Bt + Di + Qtz, Bt + Grt + Qtz, Tr + Phl + Di + Qtz, En + Phl + Di + Qtz, and En + Phl + Qtz. Biotite quartzites locally contain accessory to major amounts of brown tourmaline (dravite) as small, equant, strongly pleochroic grains (Fig. 15B). Biotite schists and gneisses interlayered with the quartzites contain up to 50% biotite with quartz, sillimanite, clino- and orthopyroxenes, garnet, plagioclase and, rarely, cordierite. Mg- and B-rich metapelites (Table 1F, MKS102) occur in unit BL on the Moose River about 1 kilometer west of the hamlet of Moose River (MKQ; Appendix A, Stop 3). These contain Mg-biotite, cordierite, garnet, tourmaline, alkali and plagioclase feldspars, rutile, quartz, and the uncommon Mg-B-Al silicate prismatine (Darling et al., 2000), which occurs in laths up to 20 centimeters in length, oriented in the foliation plane (Figs. 15C–E). Thinly laminated (mm- to -cm scale) quartzites with interlayered diopside-rich calcsilicates (Fig. 15F) occur in the same section as the prismatine-bearing rocks, as do schists and quartzites with F-

rich tremolite and phlogopite (Table 2, MKB124). The presence of metasedimentary rocks enriched in Mg, K, B, and F suggests the presence of evaporites in the protolith (Moine et al., 1981). Evidence of evaporite protoliths is present elsewhere in the Adirondack Highlands (Lamb and Valley, 1988; Grew et al., 1991; Whitney and Olmsted, 1993), as well as in the Northwest Lowlands (Brown and Ayuso, 1985; Whelan et al., 1990; Hauer, 1995). Laminated quartzites in the Moose River section resemble those in stromatolite-bearing units of the Upper Marble of the Northwest Adirondack Lowlands (Isachsen and Landing, 1983; Carl et al., 1990). The latter are associated with evaporites and have oxygen isotope ratios consistent with diagenetic replacement of carbonates by chert (Whelan et al., 1990; Hauer, 1995; deLorraine and

Johnson, 1997), a process favored by the high dissolved silica content of evaporitic fluids (Siever, 1992).

Regional variation — There is a pronounced regional variation of the metasedimentary suite across strike in the map area. In the southeastern third of the area, the dominant rock is migmatitic kinzigite with subordinate amounts of marble, calcsilicates, and quartzite. In the Fulton Lakes Synform, the abundant rocks are calcsilicates, quartzite, and marble, with subordinate biotite-rich gneisses and schists, and the meta-arkosic rocks of unit TH. In the northwest, metasedimentary rocks occur as scattered, relatively thin layers or synclinal keels in granitic gneisses, and consist chiefly of feldspar-rich calcsilicate rocks with minor, local metapelite and quartzite.

Chapter 3

Structure

The map area has been divided into four large and four smaller structural domains (Fig. 16). Changes in structural style and orientation across domain boundaries are gradational and placement of the boundaries is somewhat arbitrary. Density-contoured stereographic plots of poles to foliation for the several zones are shown in Figures 17A, D, G, J, M, P, S, and U. Foliation throughout the region is almost invariably parallel to compositional layering where both are measurable. Lineations (Figs. 17B, E, H, K, N, Q, and T) include quartz rods, elongate clusters of pyroxene, hornblende, oxides, and/or garnet, and oriented grains of hornblende, tremolite, sillimanite, or, in one location, enstatite. Minor fold axes (Figs. 17C, F, I, L, O, and R) are not contoured.

Northwest (NW) domain — The regional foliation pattern (Fig. 17A) indicates that the dominant structural trend is NE to NNE with a gentle NE plunge. One major fold, an open, N-plunging synform east of Soft Maple Reservoir appears to be an exception to this trend. This fold may be part of the F_4 fold set of McLelland and Isachsen (1986). It is outlined by differentially eroded amphibolite layers of unit GA and is clearly visible on aerial photographs.

Arcuate, E-dipping foliations in the westernmost NFQ and northwesternmost MKQ may be due to a buried anorthosite-cored dome west of the area, centered near the village of Denmark. Except for anorthosite exposures mapped by Buddington and Ruedemann (1934) near Carthage, the hypothetical dome is concealed under Paleozoic sedimentary rocks, but its presence is suggested by a prominent gravity low (Revetta and Diment, 1973). If present, the anorthosite may be the source of the Port Leyden Nelsonite deposit (Darling and Florence, 1995).

The lineation maximum in Figure 17B is subparallel to the axis of the great circle defined by the foli-

ations. Few minor folds were observed in the NW domain, probably due to the prevailing homogeneous granitic lithology. Those measured, however, form a tight cluster close to the lineation maximum (Fig. 17C).

West-central (WC) and East-central (EC) domains — A large majority of foliations strike NE to ENE (Figs. 17D, G). This reflects the presence of large, tight-to-isoclinal, ENE-trending folds (F_2 and F_3 of McLelland and Isachsen, 1986). Many of these folds are overturned toward the south, producing a concentration of poles in the southern halves of the stereoplots. Axes of major folds are subhorizontal and trend NE in the WC domain; they gradually swing to the ENE in the EC domain. All rock units are folded, with the exception of the unmetamorphosed diabase dikes. The most prominent major fold, cored by unit BL, is the complex Fulton Lakes Synform that trends NE to ENE from near McKeever to the eastern edge of the map area. Route 28 parallels the axis of the synform, which is overturned toward the south. Three basins are aligned along the axis at Utowana Lake, Bug Lake, and Nelson Lake. They may be synclinal troughs of open F_4 crossfolds (McLelland and Isachsen, 1986), or large NNW-plunging sheath folds. A second major fold is a tight, nearly upright, doubly plunging anticline extending from near Big Moose Station ENE to Forked Lake, where it is bifurcated by a minor syncline that plunges steeply NE. This structure is outlined by anorthosite-suite rocks (unit JA) and leucogneisses (unit BM), and cored by granitic gneisses of unit CG.

In the WC and EC domains, two poorly defined lineation maxima are present (Figs. 17E, H). Several additional clusters are of doubtful significance. The strongest maximum is subhorizontal and trends ENE, subparallel to the major fold axes and to lineation in the adjacent Moose River domain. A secondary max-

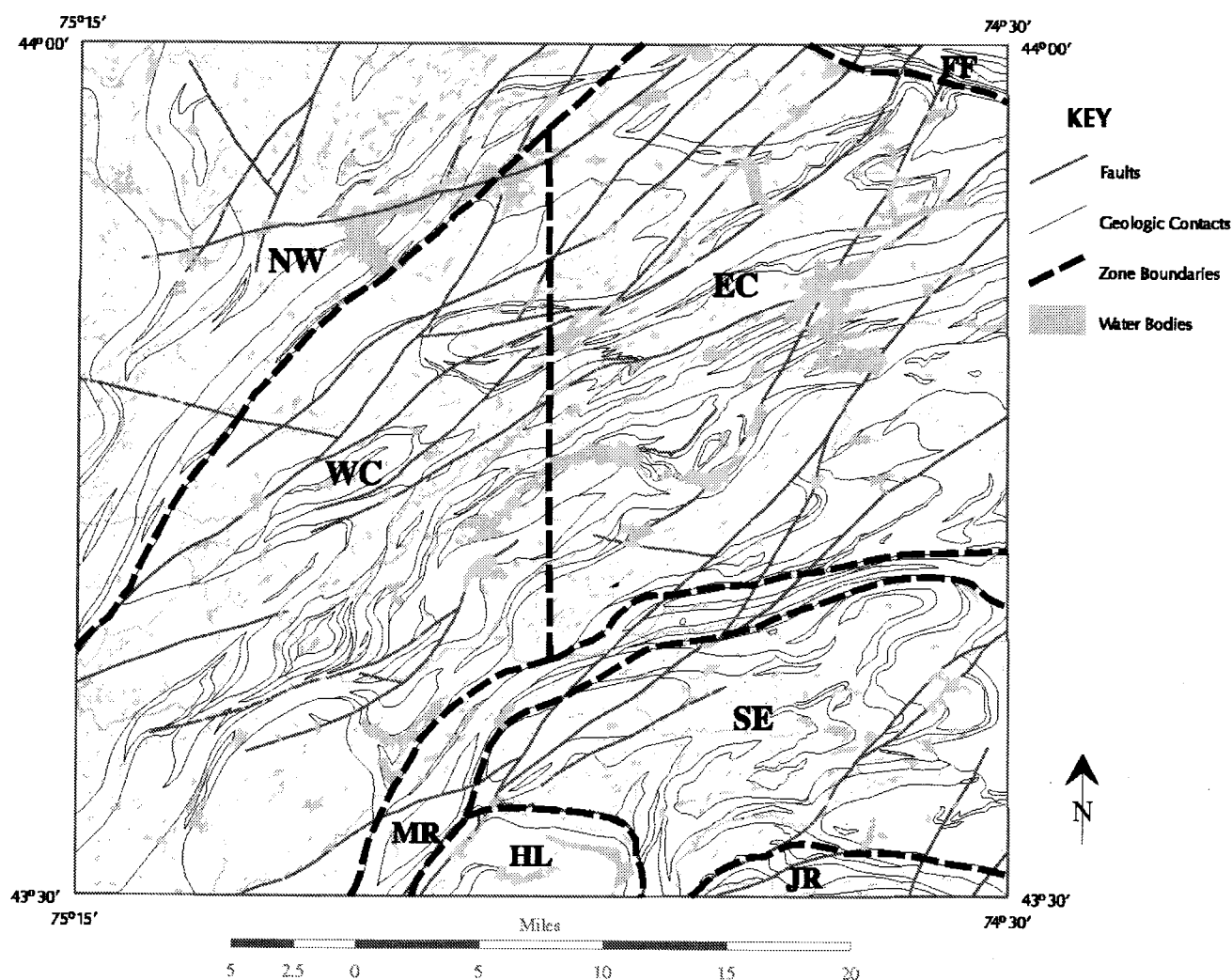


Figure 16. Map of structural domains. NW, Northwest; WC, West-central; EC, East-central; SE, Southeast; MR, Moose River; HL, Honnedaga Lake; JR, Jessup River; FF, Flatfish Pond. Changes in structural style and/or orientation across domain boundaries are gradational and the placement of the boundaries on this map is approximate only.

imum plunges gently NW (WC domain) and NNW (EC domain), nearly perpendicular to the main trend. This NW trend is well developed in the Inlet deformation zone (Appendix A, Stop 9). Minor folds axes (Figs. 17F, I) are scattered. However, many appear to be roughly aligned with lineation maxima, such as the recumbent (F_1 ?) isocline in Figure 15C.

Moose River domain (Moose River deformation zone) — The Moose River deformation zone (MRDZ), forms the boundary between the SE domain and the WC and EC domains. It is a narrow (ca. 1–2 km thick), curvilinear zone of strong to extreme defor-

mation within granitic gneisses, amphibolites, and metasedimentary rocks. The zone trends approximately E-W to WSW in the WCQ and eastern OFQ, following the South Branch of the Moose River, and curves southwest in the western OFQ. Foliation (Fig. 17M) and compositional layering strike parallel to this trend with moderate N or NW dips. Foliation is intense (Fig. 18A) in the eastern two thirds of the domain but is less pronounced in the southwestern OFQ. The intensity of foliation gradually decreases both north and south of the zone and well-defined contacts with less deformed rocks are absent. The

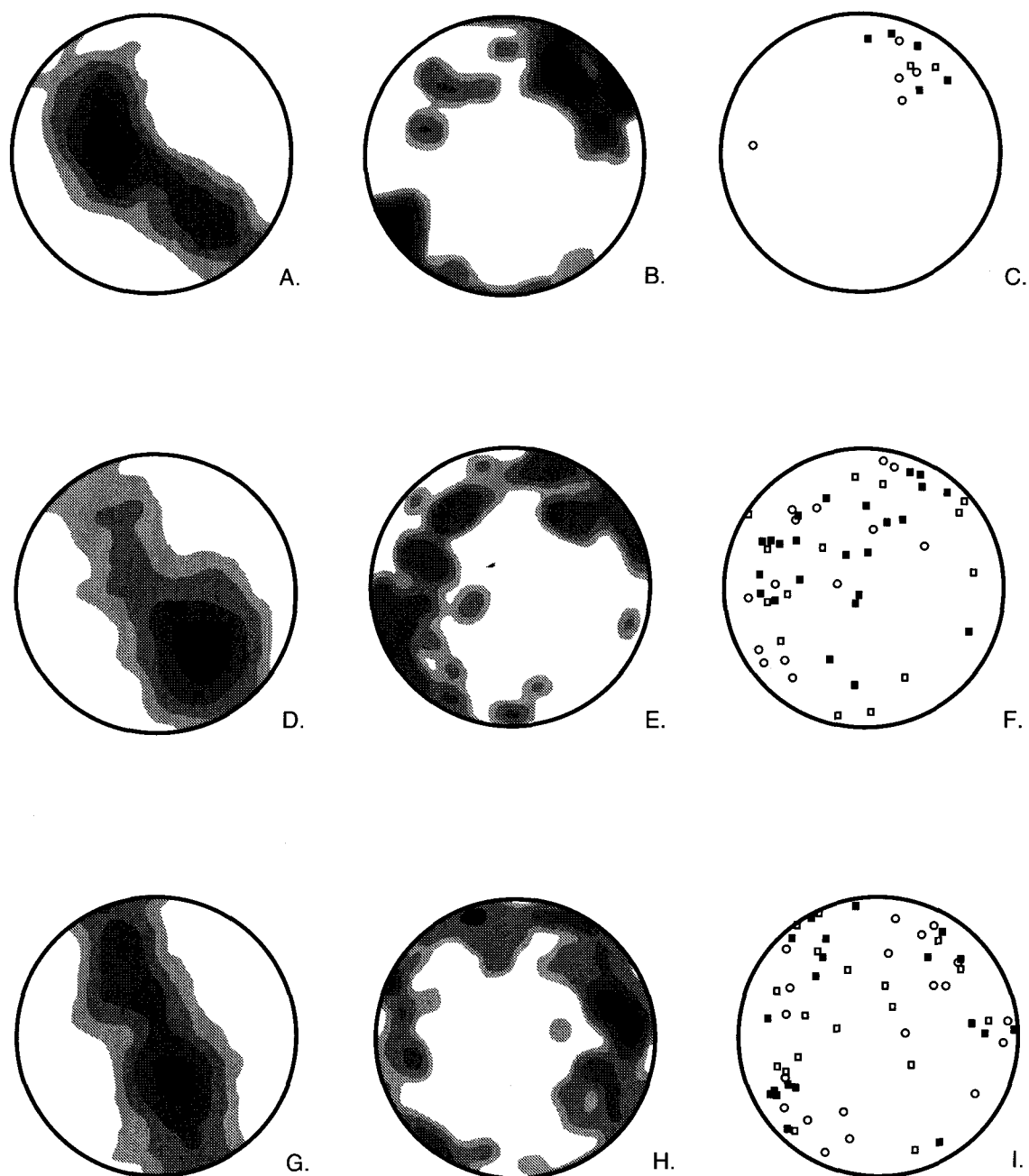


Figure 17. Stereograms of structural data. Lower-hemisphere stereographic projections of poles to foliation, lineation, and outcrop-scale fold axes. Projections are calculated using the program Stereo™ (Rockware Inc., Wheat Ridge, CO). Density contours for foliation and lineation at 0.5, 1.0, 2.0, 4.0, 8.0, and 16.0%. Symbols for minor fold axes (not contoured): Solid squares, tight to isoclinal folds; open squares, open folds; open circles, other or type not recorded. (A) Northwest domain (NW) foliations, $n = 1151$. (B) NW lineations, $n = 60$. (C) NW fold axes, $n = 12$. (D) West-central domain (WC) foliations, $n = 2240$. (E) WC lineations, $n = 81$. (F) WC fold axes, $n = 53$. (G) East-central domain (EC) foliations, $n = 2031$. (H) EC lineations, $n = 100$. (I) EC fold axes, $n = 58$. (J) Southeast domain (SE) foliations, $n = 1604$. (K) SE lineations, $n = 163$. (L) SE fold axes, $n = 90$. (M) Moose River domain (MR) foliations, $n = 444$. (N) MR lineations, $n = 29$. (O) MR fold axes, $n = 14$. (P) Jessup River domain (JR) foliations, $n = 390$. (Q) JR lineations, $n = 45$. (R) JR fold axes, $n = 5$. (S) Honnedaga Lake domain (HL) foliations, $n = 137$. (T) HL lineations, $n = 17$. (U) Flatfish Pond domain foliations, $n = 63$.

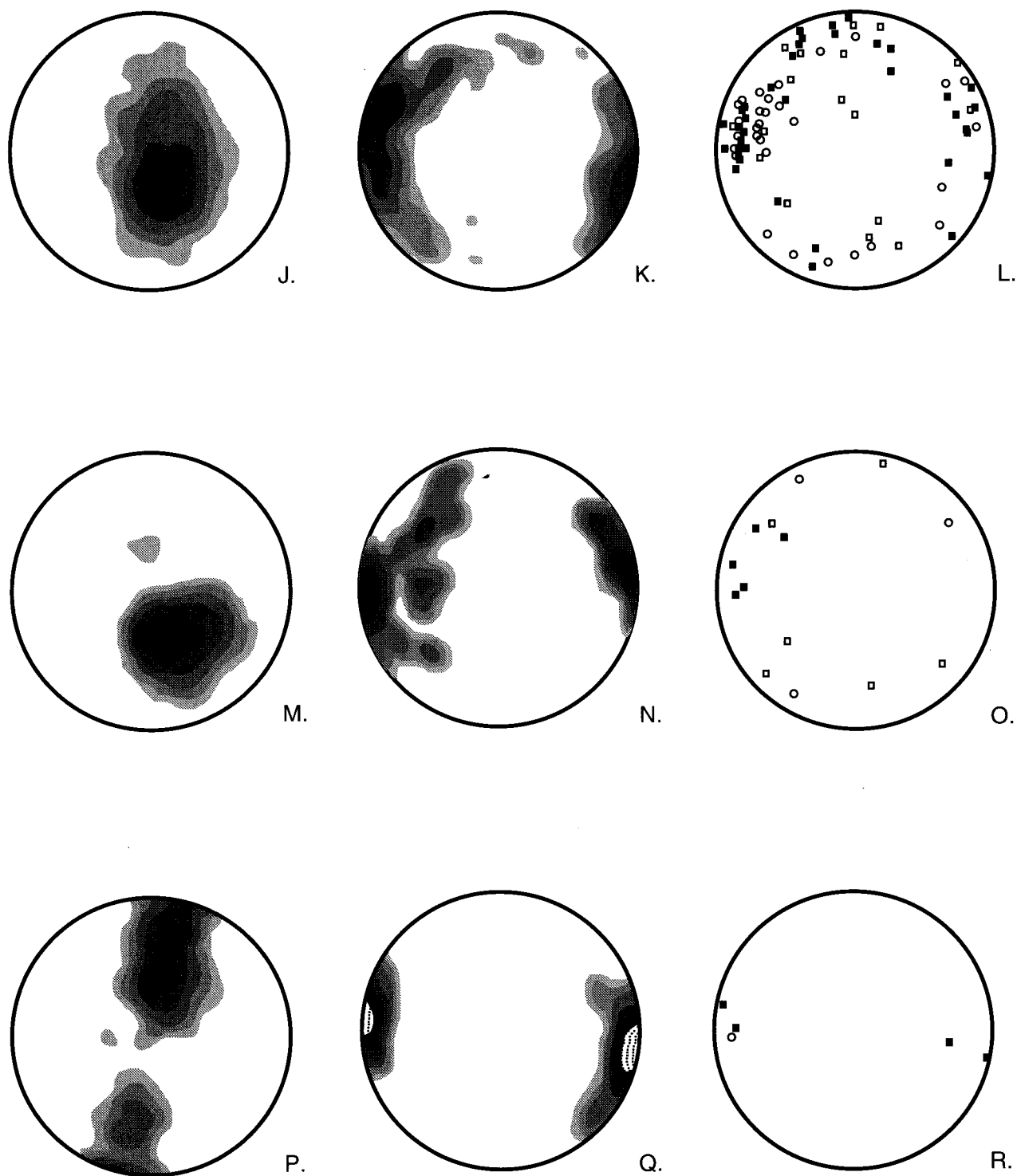
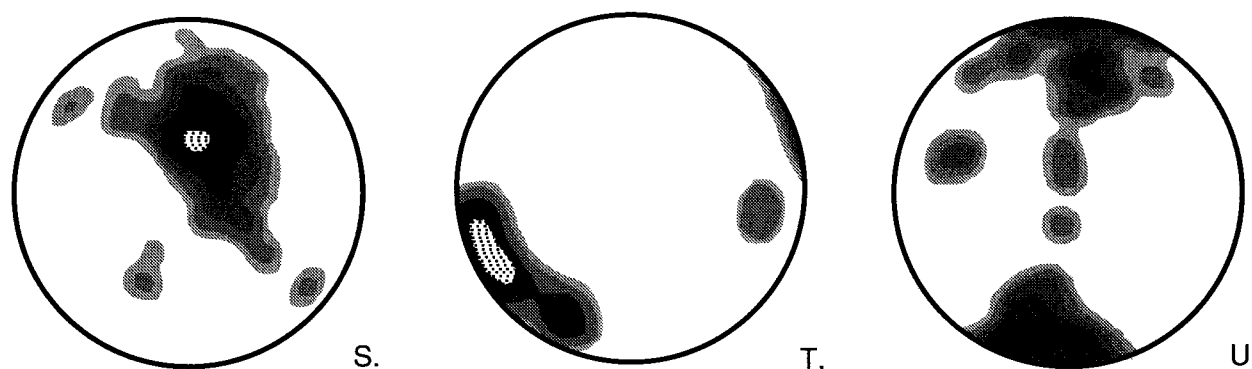


Figure 17. *continued*

Figure 17. *continued*

zone appears to truncate regional trends at a low angle in the EC and SE domains.

Prominent lineations are near-horizontal and approximately parallel to strike (Fig. 17N). Most consist of quartz rods, oriented hornblende grains, and elongate mafic aggregates. If these are stretching lineations, movement along the zone was primarily strike-slip. Thin amphibolite layers (Fig. 18B) locally form recumbent intrafolial isoclinal folds; thicker amphibolites are locally boudinaged. Foliation in the granitic gneisses also shows boudinage in some outcrops, suggesting some compositional inhomogeneity with resulting ductility contrast. Coarse quartzofeldspathic segregations (Fig. 18A) both crosscut and parallel the foliation. Viewed down-dip, as in the photo, the cross-cutting segregations suggest melt-filled tension fractures oblique to foliation, with an orientation consistent with sinistral shear. Other kinematic indicators also suggest primarily sinistral displacement. Rock exposures within the zone of intense deformation are scarce; the most complete section is on the steep southern slope of Mitchell Ponds Mountain, immediately north of the Moose River near the western edge of WCQ. Smaller, more accessible exposures are present on hogback ridges on both sides of the main east-west road through the Moose River Plains recreation area (Appendix A, Stop 10).

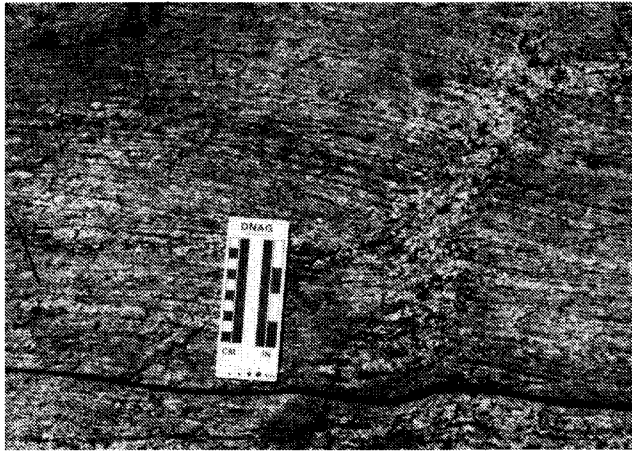
Southeast (SE) domain — The foliation pattern in this area suggests subhorizontal E-W to WSW-trending folds strongly overturned to the south (Fig. 17J). In general, the foliation is more pronounced than in the EC, WC, or NW domains. Lineation (Fig. 17K) is also more strongly developed in the SE domain,

and shows a strong WNW maximum at a small angle to the W or WSW orientation of major fold axes.

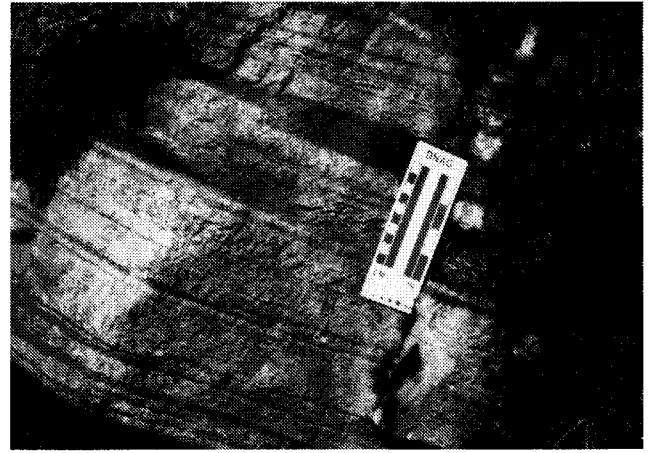
The most prominent major fold is the Little Moose Mountain Syncline (deWaard, 1962), clearly visible in aerial photographs in the north-central WCQ. The precise configuration of this complex fold is, however, difficult to determine in detail. Throughout most of the area south and west of Little Moose Mountain, foliation and compositional layering dip moderately NNW, with pronounced irregularities near bodies of gabbro or granite. The dips are consistent with a tight to isoclinal synform overturned to the south, the north limb merging with, and partially sheared out by, the MRDZ. However, the structure in the area west of Little Moose Lake, marked by prominent arcuate ridges readily visible in aerial photographs, suggests a relatively open syncline. The apparent discrepancy is resolved if the map pattern results from dragging of isoclinally folded rocks during sinistral shearing on the MRDZ.

North of the MRDZ, the overturned, granite-cored Wakely Mountain Antiform plunges WSW, intersecting the MRDZ at a low angle. The Wakely Mountain and Little Moose Mountain folds appear to be a conjugate antiform/synform pair, plunging gently W, their mutual limb replaced by the MRDZ. There is no evidence that the Wakely Mountain structure is a nappe, as suggested by deWaard and Walton (1967).

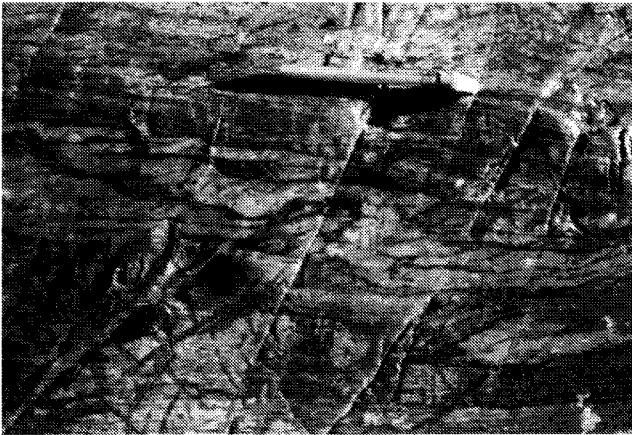
The gently W-plunging major folds of the SE domain are approximately coaxial with a cluster of E-W oriented, tight to isoclinal minor folds (Fig. 17L) that may have resulted from the same deforma-



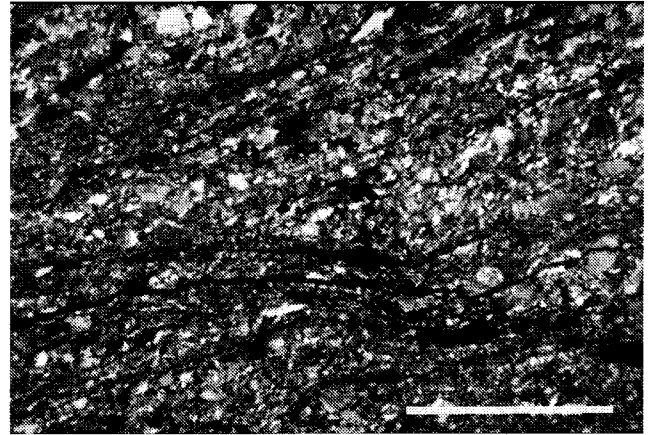
A.



B.

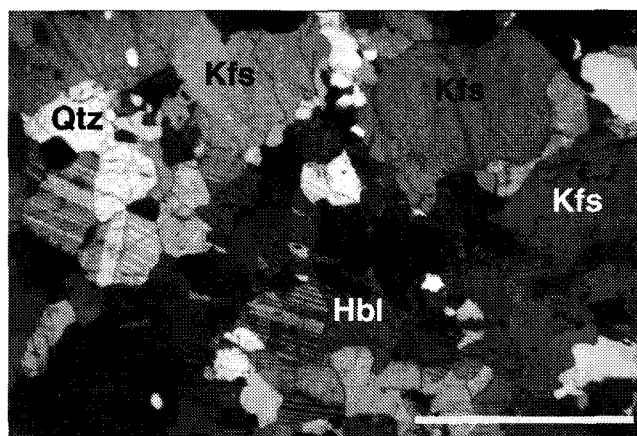


C.

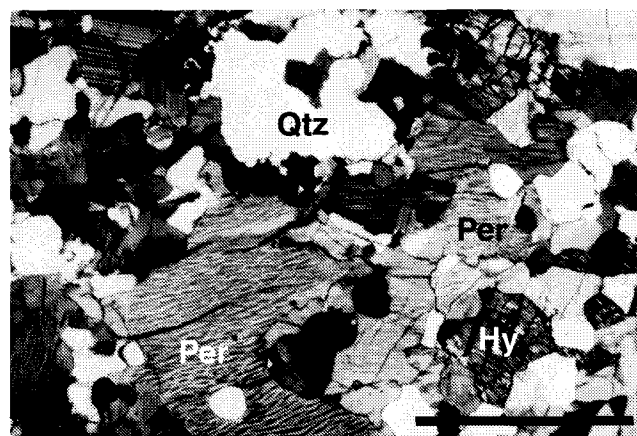


D.

Figure 18. Textures of deformed granitic rocks. (A) Chamockitic gneiss in the Moose River deformation zone (MRDZ). Note crosscutting leucosome and thin amphibolite layer. 2.2 mi. WNW of Sly Pond, WCQ (Appendix A, Stop 10), looking down-dip (NNW). (B) Straight gneiss comprising intensely foliated and lineated charnockite and amphibolite. MRDZ, S face of Mitchell Ponds Mtn, WCQ, looking N. (C) Mylonite, Stillwater zone, 0.7 mi. SE of Stillwater Mtn, NFQ, looking SW. (D) Photomicrograph of mylonite, Stillwater zone 0.5 mi. SE of Stillwater Mtn, NFQ. Scale bar 5 mm, crossed polars. (E) Photomicrograph of charnockitic gneiss, MRDZ, 1.7 mi. NW of Sly Pond, WCQ. Kfs: Alkali feldspar; Hbl: Hornblende; Qtz: Quartz. Hypersthene, plagioclase (twinned), and ilmenite are also present. Compare the absence of well-developed perthitic intergrowths in the alkali feldspar with the strongly perthitic feldspar in typical charnockite (Fig. 18F), and note coarser texture relative to the Stillwater mylonite (Fig. 18D). Scale bar 5 mm, crossed polars. (F) Photomicrograph of charnockitic gneiss, Unit CG, 0.9 mi. SW of West Canada Mtn, WCQ. Per: Perthite; Qtz: Quartz; Hy: Hypersthene. Plagioclase, hornblende, and ilmenite are also present. This texture is typical of charnockite in most of the map area. Scale bar 5 mm, crossed polars.



E.



F.

Figure 18. *continued*

tion. A second cluster of NNW-plunging tight to isoclinal minor folds may represent pre-Ottawan deformation, or result from drag during transpressional shearing along the MRDZ.

The Spruce Lake Antiform (Pattee, 1989) occurs in the southern WCQ between Pillsbury Mountain and Spruce Lake, cored by unit BG. This asymmetric, W-plunging fold has a gently dipping north limb and a steep to vertical or slightly overturned south limb. Pattee's (1989) 1:24,000 map shows this fold adjoining the Amos Lake Synform (Glennie, 1973) along the southern edge of the map area. Our data suggest the presence of a nearly isoclinal, E–W-oriented synform/antiform pair between the Spruce Lake and Amos Lake structures.

Jessup River (JR) domain — This domain extends from the steep south limb of the Spruce Lake Antiform to the southern edge of the WCQ. It includes rocks of units BG, CG, and MU. Unit MU in this area is atypical in that it contains a large proportion of strongly foliated megacrystic gneisses similar to BG, interlayered with amphibolite, garnet amphibolite, calcsilicates, and metapelite. Compositional layering and foliation (Fig. 17P) strike nearly E–W. Steep to vertical dips in the northern part of the domain are replaced southward by moderate S dips. The northern half of the domain is characterized by predominantly strike-slip ductile shear. Outcrop-scale kinematic indicators are scarce and unreliable, but Pattee (1989) shows two map-scale, isocli-

nal S-folds with amplitudes on the order of 0.5 kilometers within the zone of most intense deformation, which indicate a sinistral sense of shear. Intensity of foliation is greatest in the eastern half of the domain. Lineations (Fig. 17Q) and a few minor fold axes (Fig. 17R) are subhorizontal and parallel to strike.

Honnedaga Lake (HL) domain — This small domain, wholly within the southern half of OFQ, consists of sheets of well-foliated granitic gneiss (unit CG, with some GA), with a consistent, shallow-to-moderate SSW dip. The foliations (Fig. 17S) are oblique to the regional ENE trends in the adjacent SE domain. The perimeter of the HL domain has been mapped as a thrust fault because it abruptly truncates structures north of the domain. The hypothetical thrust is marked by a zone of intense deformation that approximately follows the valley of Middle Branch of the Black River 1 to 2 kilometers north of and parallel to the northwestern arm of Honnedaga Lake. The north slope of the valley is a dip slope on strongly foliated granitic and charnockitic rocks with a few thin amphibolite layers. The foliation here strikes ESE and dips 10 to 30° SW, locally warped by open SW–NE cross-folds. WSW-plunging lineations (Fig. 17T) within the deformed zone are defined by quartz blades and mafic aggregates in the charnockite and by hornblende needles in the amphibolite. Similar lineations occur locally elsewhere in the Honnedaga Lake domain. No kinematic indicators were found.

Flatfish Pond (FP) domain — In the northeastern

corner of the RLQ, granitic and charnockitic gneisses of unit GA alternate with jotunite (unit JA) and thin, local layers of metasedimentary rocks. Steeply dipping, ESE-trending foliations (Fig. 17U) truncate the regional NE structural trend at a high angle. Despite the intensity of the foliation, no measurable lineations or shear sense indicators were observed. The FP domain may be part of a major shear zone and structural discontinuity (Fakundiny, 1986; Fakundiny et al., 1994).

Inlet and Stillwater zones — Two other zones of strong to intense deformation are noteworthy. One is exposed in sparse outcrops from Rocky Point on Fourth Lake north-northwest of the village of Inlet eastward to just south of Black Bear Mountain (SE BMQ); the other extends SW from the Stillwater Reservoir (EC NFQ), and is marked by a prominent linear valley containing Hitchcock Creek and Hitchcock Lake. In the Inlet zone, strongly foliated metapelites, calcsilicates, and quartzites are overlain by a thick layer of charnockite gneiss. The metasedimentary rocks contain a strong NNW-trending mineral lineation defined by high-temperature phases including sillimanite and enstatite, indicating deformation coincident with high-temperature metamorphism. Also present are fine-grained mylonites with a NW-oriented quartz stretching lineation. The quartz in the mylonites is strained and sutured, suggesting a late episode of lower-temperature shear. Marble melange exposed at Rocky Point may also have originated during this later movement. Other marbles in the Inlet zone contain large quartz and K-feldspar porphyroclasts that may represent tectonically disrupted pegmatites. Clear kinematic indicators are uniformly lacking. The Inlet zone crosses Route 28 north of the village of Inlet (Appendix A, Stop 9). To the west, it strikes into Fourth Lake, and it is not exposed in the low terrain northeast of Black Bear Mountain.

The Stillwater zone strikes approximately 230°, dips 40 to 60° NW, and is mappable within and parallel to unit BM for approximately 10 kilometers along strike. It is characterized by localized zones of intense shearing and grain size reduction (Figs. 18C, D) up to 10 meters thick, usually at or near contacts between leucogneiss and jotunite or gabbroic anorthosite. Kinematic indicators are scarce; in two outcrops S-C fabrics and asymmetric intrafolial folds

indicate NW-side-down movement with a sinistral strike-slip component. Mineral lineation is not well developed, although oriented sillimanite in a few outcrops plunges NW within the foliation plane. The Stillwater zone is unlike the other map-scale zones of ductile shear in that grain size in the most deformed rocks is fine to mylonitic, with little evidence of post-deformation annealing (Fig. 18D). This is consistent with relatively late movement postdating the thermal maximum. By contrast, rocks deformed at or before the thermal maximum, as indicated by cross-cutting leucosomes, typically exhibit coarser textures. The latter include both gneisses within the MRDZ (Fig. 18E) and charnockites and granites in less-deformed regions of the map area (Fig. 18F). The SW-NE orientation, NW-side-down movement, and textural similarities suggest that deformation in the Stillwater zone may be contemporaneous with that in the Carthage-Colton zone (Heyn, 1990), approximately 35 kilometers to the northwest.

Domical structures — The Snowy Mountain Dome (deWaard and Romey, 1963, 1969) in the Indian Lake 15' Quadrangle, east of the map area, is cored by anorthositic rocks. The dome appears to truncate foliation in the eastern WCQ, and to deflect the MRDZ northeastward along the Cedar River Valley (Weimer et al., 2001). Regional foliation wraps around the ovoid Ice Cave Mountain Dome in the southwestern OFQ, the Salmon Lake Dome in the northwestern RLQ, and the Gull Lake Dome in the southeastern MKQ, all of which are cored by granitic rocks (unit CG). The nearly 90° bend in Woodhull Lake (SW OFQ) appears to result from deflection of carbonate- and calcsilicate-rich metasedimentary rocks from the regional NE trend to NNW near Gull Lake Dome. The domical structures may result from solid-state diapiric rise of low-density core rocks through thermally weakened cover late in the Ottawan tectonometamorphic event (Whitney, 1983).

Structural synthesis — Folding throughout the map area involves all map units. With few exceptions, the folds are disharmonic at all scales, in keeping with deformation at high temperatures, relatively low viscosities, and high viscosity contrast. Major fold axes are subparallel and consistent throughout the region, gradually swinging from E-W at the eastern edge to NE-SW in the west. Distinct phases of

folding are hard to recognize due to the plastic nature of much of the deformation. Nevertheless, the overall picture is consistent with the presence of three essentially coaxial fold sets (F_1 – F_3 of McLelland and Isachsen, 1986). Minor fold axes are scattered and form several weak maxima, especially in the EC and WC domains. This scatter may be the result of distortion of small-scale structures during low viscosity ductile deformation. In the NW, SE, and Jessup River domains, numerous axes of tight-to-isoclinal minor folds are, however, subparallel to the major folds and to the principal lineation direction (Figs. 17C, L, R).

Stereonet plots of poles to foliation in each of the four large domains (NW, WC, EC, and SE) and the JR domain have the form of a broad girdle that defines a great circle (Figs. 17A, D, G, J, P). In each domain, the axis of the great circle lies within or close to the prominent maximum on the lineation diagram (Figs. 17B, E, H, K, Q). This coincidence of the dominant lineation direction with the axes of major folds has been previously noted in the southern and central Adirondack Highlands by McLelland and Isachsen (1986). The correlation, however, breaks down in large areas of the northwestern Highlands (Buddington and Leonard, 1962, their Fig. 15). In the EC and WC domains, a subordinate lineation maximum plunges NW at a high angle to the primary direction and to the major fold axes. The NW-plunging lineation may result from either (a) flexural slip on the major folds in areas of high ductility contrast, or (b) shearing not directly related to folding. Both the axial lineations and those at high angles to fold axes include mineral lineations defined by high-temperature phases such as sillimanite, consistent with syn-metamorphic deformation. Lineation submaxima at low angles to the primary trend may result from rotation of earlier lineations around late cross-folds (F_4 or F_5 of McLelland and Isachsen, 1986).

Pre-Ottawan deformation in the map area is difficult to recognize, although deformation during the Elzevirian orogenic cycle (ca. 1350–1180 Ma) has affected rocks elsewhere in the Adirondack Highlands (McLelland et al., 1996). In a few outcrops, xenoliths of foliated metasedimentary rock occur in granitic gneisses (Fig. 2A). Leucogneisses in unit KZa locally crosscut foliation in kinzigite and are themselves foliated and contain large garnets, suggesting two episodes of deformation and metamorphism. A

garnet-bearing metadiabase, mapped by Pattee (1989) in the southeastern quadrant of the WCQ near Whitney Lake, appears, on the basis of limited exposures, to be a dike crosscutting metasedimentary rocks. If correct, this would strongly support a pre-Ottawan tectonometamorphic event. Careful study of structures in metasedimentary rocks with unequivocal primary compositional layering, particularly in the SE domain where they are relatively abundant, is needed to establish the existence and nature of pre-Ottawan deformation.

Chiarenzelli et al. (1999) and Valentino and Chiarenzelli (1999) report evidence for large-scale sinistral transpression in the vicinity of the Snowy Mountain Dome, immediately east of the map area, as well as elsewhere in the central and southern Adirondacks. Several features within the map area are consistent with such a mechanism. Rocks in the MRDZ and Jessup River domains show evidence of intense strike-slip shearing and severe flattening. The majority of kinematic indicators within and near the MRDZ indicate sinistral displacement. S-folds mapped by Pattee (1989) within the JR domain, and apparent dragging of rocks in the Little Moose Mountain synform along the MRDZ, are also consistent with a sinistral movement sense. Farther north, in the Fulton Lakes synform, the structural basins near Nelson Lake (Central MKQ) and Bug Lake (SW RLQ) show a modified S-shape suggestive of map-scale sinistral rotation. The low-angle crosscutting of structural trends by the MRDZ indicates that shearing there postdates folding, at least in part. The coarse grain size of the sheared rocks within the MRDZ, and the local presence of undeformed crosscutting felsic segregations, indicate that high temperatures at the time of shearing probably persisted until after cessation of movement.

Brittle structures — Numerous brittle faults have been mapped, largely based on indirect evidence including photolinears and apparent offset of map units. It is difficult to establish the nature of the faulting or the amount of offset, because the fault zones are commonly occupied by alluvial valleys, wetlands, or bodies of water. In the few bedrock exposures within the fault zones brecciation, intense fracturing, and local development of mylonite are present, but no measurements of displacement were possible. Unmetamorphosed diabase dikes occur within or

near the fault zones in several locations. Some apparent faults may be "zero-displacement crackle zones" (Isachsen et al., 1981).

Most map-scale brittle faults and fracture zones are subvertical, and vary in orientation from ENE to NNE. They are most common in the southeastern part of the map area, and probably belong to same

NE to NNE trending set mapped throughout the central and eastern Highlands by Isachsen and McKendree (1977), where they displace rocks as young as Ordovician. A few WNW-trending faults or fracture zones are also present, notably the Independence River Fault in the southwestern NFQ.

Chapter 4

Metamorphism

Rocks throughout the region contain granulite facies mineral assemblages. Seal (1986) used the biotite-garnet and two-feldspar thermometers together with the garnet-rutile-sillimanite-ilmenite-quartz (GRAIL) assemblage in metapelitic rocks from the central part of the map area to estimate maximum metamorphic temperature and pressure of about 760°C and 7.6 ± 0.2 kbar, respectively. These conditions are consistent with projections of the isotherms and isobars of Bohlen et al. (1985) for Ottawa granulite facies metamorphism. Florence et al. (1995) determined metamorphic T and P of 710 to 730°C and 4 to 6 kbar with quartz-hercynite-garnet sillimanite equilibria and biotite breakdown reactions in metapelites in the Port Leyden Quadrangle, immediately west of the map area. Florence et al. (1995) interpret these data as evidence for anatexis at about 1150 Ma, roughly coeval with the regional AMCG magmatism and prior to the Ottawa granulite facies event. Pre-Ottawa contact metamorphism has been documented elsewhere in the Adirondack Highlands by Valley et al. (1990). McLelland et al. (1988, 1996) report evidence for still older (Elzevirian?) granulite facies metamorphism in the southern and eastern Adirondack Highlands.

Figure 19 summarizes the evidence from mineral assemblage in the map area. A pressure of 7 kbar, slightly less than Seal's (1986) value of 7.6 kbar, is assumed based on the common occurrence of fayalite plus quartz in granitic rocks, discussed in more detail below. The shaded area represents the most probable T-X_{CO₂} range during metamorphism, assuming the presence of a fluid phase. Temperatures of 780 to 830°C and intermediate H₂O-CO₂ mixtures are indicated, with local excursions to more water- or CO₂-rich compositions. These conclusions are tentative, since it is not clear which assemblages represent

Ottawa conditions and which may have been preserved from earlier events due to local absence of fluids (Valley et al., 1990). In the following discussion and in Figure 19, temperatures and pressures have been calculated using the program TWEEQU (Berman, 1991) unless otherwise noted.

Metagneous and metavolcanic rocks — In the eastern half of the map area, symplectic reaction rims of garnet and plagioclase around hypersthene and opaque oxides (Fig. 20A) occur locally in jotunite, gabbroic anorthosite, and, less commonly, charnockite. Similar garnet coronas in anorthosites and charnockites of the Adirondack High Peaks formed during cooling from granulite facies conditions. Several different geothermometers and geobarometers yield temperatures and pressures of formation in the range 580 to 650°C and 5 to 7 kbar (Spear and Markussen, 1997). These results are not directly applicable to the Fulton Lakes map area, where mineral compositions have not been determined, but they do suggest a common mode of origin on the cooling limb of a counterclockwise pressure-temperature-time path.

Reaction coronas, similar to those described by Whitney and McLelland (1973, 1983), occur in olivine metagabbros around both olivine and ilmenite in contact with plagioclase (Fig. 20B). Porphyroblastic garnet in the amphibolitic margins of olivine metagabbro bodies in the eastern third of the map area probably formed at the same time as the coronas, the growth of larger garnets facilitated by fluids infiltrating from surrounding rocks.

The outer garnet layer of the coronas is absent in the westernmost gabbro body at Cool Mountain (OFQ). The westward disappearance of garnet in both mafic rocks and charnockites suggests an E-W trend toward lower metamorphic pressures, consistent with the garnet "isograds" mapped by Budding-

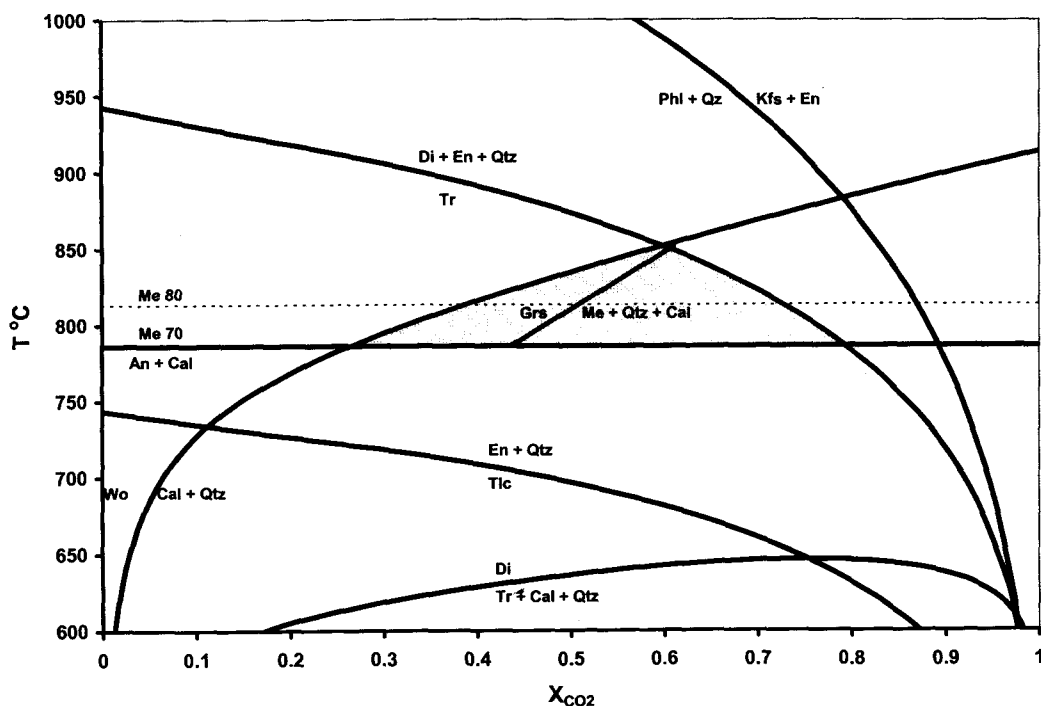


Figure 19. T - X_{CO_2} diagram for calcsilicate rocks. Location of some metamorphic reactions discussed in text as a function of temperature and fluid composition. Shaded area: Probable conditions at peak Ottawa metamorphism in the map area. All reactions, except those involving scapolite or garnet, were calculated with mineral composition data from a representative sample (RLJ26, Table 2) at 7 kbar pressure using the program TWEEQU (Berman, 1991). Presence of a fluid phase at $P_f = P_{\text{total}}$ is assumed. Reaction M5 is shown for two scapolite compositions (Me₇₀ and Me₈₀); reaction M6 is calculated for scapolite Me₇₀ and garnet Grs₈₅.

ton (1965, 1966) and deWaard (1965, 1967) and the petrologic studies of Florence et al. (1995) and Darling et al. (2000).

The presence of mesoperthitic alkali feldspar in granitic and charnockitic gneisses of units CG and GA, including anatectic leucosomes, suggests that metamorphism occurred at temperatures above the maximum of the feldspar solvus (ca. 750°C at 7 kbar; Luth, 1974). The hypersolvus feldspar either failed to recrystallize or did so at granulite facies conditions. The most common exceptions to this observation are in the most intensely deformed rocks such as those of the MRDZ (compare Figs. 18E and 18F). Nonperthitic or slightly perthitic alkali feldspars also occur where the rocks are relatively oxidized. Alkali feldspars in 276 thin sections of quartzofeldspathic rocks from the map area were classified as (a) perthite, (b) nonperthitic or weakly perthitic, com-

monly with well-developed microcline twinning, and (c) transitional or mixed. The corresponding hand specimens were tested with a magnet for the presence of magnetite. Where no response was obtained, the opaque oxides observed in thin section were assumed to be ilmenite. The results show a significant correlation of nonperthitic feldspar with magnetite. Strongly oxidized, ilmenohematite-bearing rocks of unit TH contain nonperthitic microcline almost exclusively.

	Alkali Feldspar		
	Perthite	Transitional	Nonperthitic
Magnetite absent	108	17	14
Magnetite present	45	28	64
Ilmeno-hematite	1	1	41

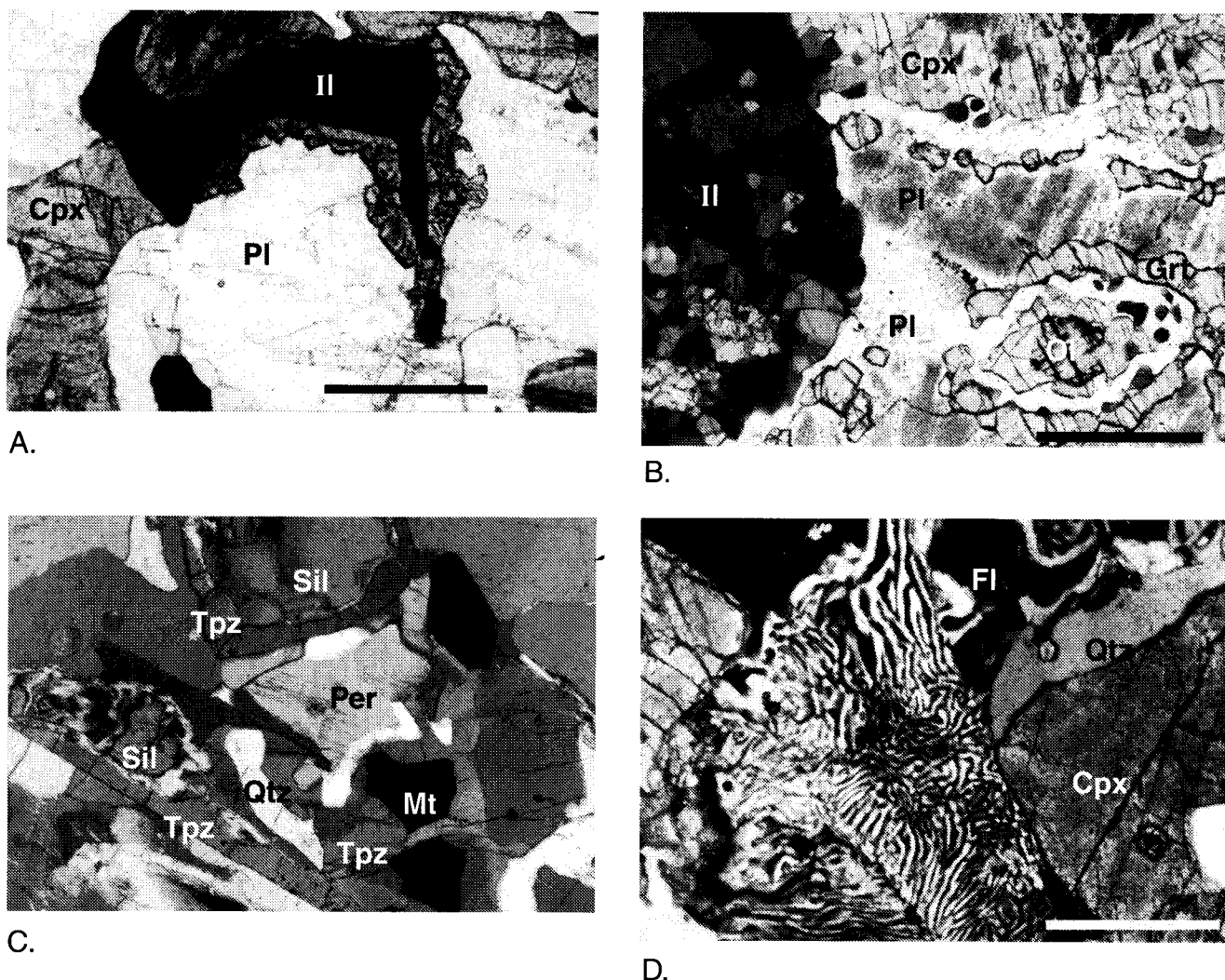
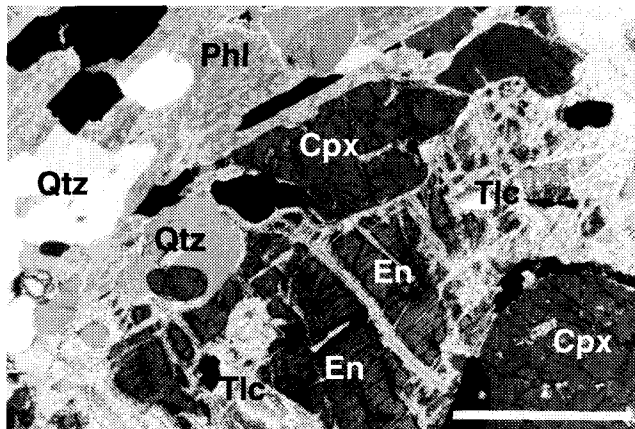
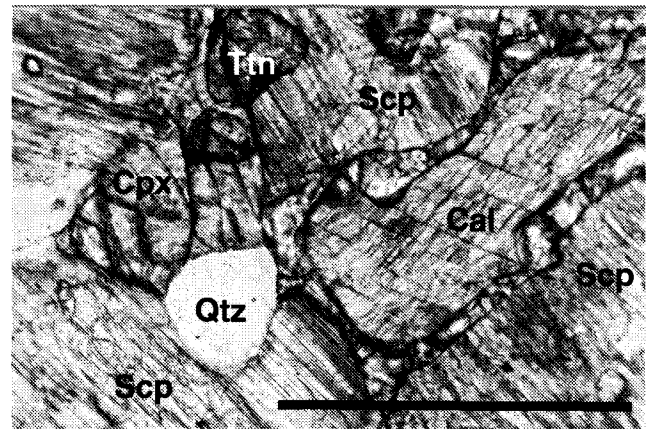


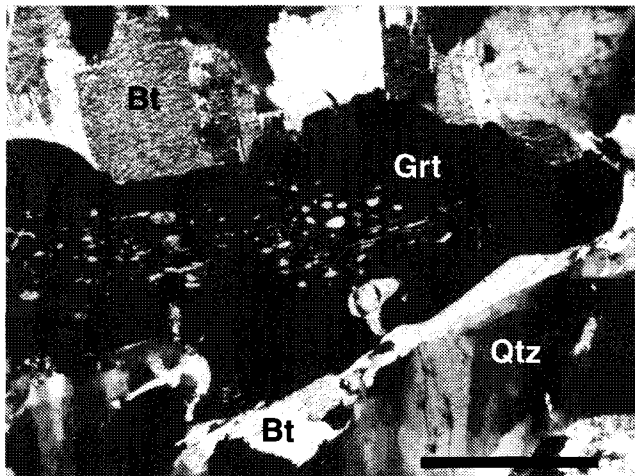
Figure 20. Photomicrographs of metamorphic features. (A) Symplectic reaction rim of garnet and plagioclase around ilmenite (Il) in jotunite. Similar rims are found on some orthopyroxene grains. Plagioclase (Pl), clinopyroxene (Cpx), hypersthene, and quartz are also present. Unit JA, hill 2060, SE corner of Brandreth Lake, RLQ; sample RLS77. Scale bar 1 mm, plane light. (B) Olivine metagabbro. Corona structure (lower R) consists of clinopyroxene, clear plagioclase, and garnet (Grt) around olivine (Ol). Dust in primary plagioclase (Pl) is spinel. At left, Ilmenite (Il) has thick reaction rim of hornblende (dark). Primary clinopyroxene (Cpx, upper R) is dusted with ilmenite. Unit OG, hill 2240 WSW of Mitchell Ponds, OFQ; sample OFH15. Scale bar 2 mm, plane light. (C) Topaz rims (Tpz) on sillimanite (Sil) and magnetite (Mt), Perthite (Per) and quartz (Qtz) also present. Leucogneiss, unit BM, roadcut on Q side of Rte 12, 2 mi. N of traffic signal in Port Leyden, Port Leyden 7.5' Quadrangle. Scale bar 1 mm, crossed polars. (D) Fluorite-quartz symplectite in calcsilicate quartzite, unit TH, Hill 2000, 0.7 mi. SSW of Gibbs Lake, MKQ; sample MKD48. Other phases include clinopyroxene (Cpx), quartz (Qtz), fluorite (Fl), and scapolite. Scale bar 1 mm, crossed polars. (E) Enstatite (En) partly altered to talc (Tlc); diopside (Cpx), phlogopite (Phl), quartz (Qtz), K feldspar, graphite, and pyrrhotite in Mg-rich calcsilicate rock. Retrograde tremolite is present locally in this thin section. Unit CM, roadcut on E side of Rte 28, 0.2 mi. S of entrance to Eighth Lake campsite, RLQ; sample RLJ26-2. Scale bar 2 mm, crossed polars. (F) Grossular (Gr₈₅) rims (high relief) on scapolite (Scp) and calcite (Cal) 0.9 mi. E of N end of Cedar Lakes, WCQ; sample WCH32. Scale bar 1 mm, plane light. (G) Garnet porphyroblast (Grt) with sillimanite inclusions, surrounded by biotite (Bt). Note outer layer of nearly inclusion-free garnet. (Crd)-Grt-Sil-Bt-Qtz-Pl metapelite, unit BL, roadcut on E side of Rte 28, 0.8 mi. N of entrance to Inlet town park, BMQ (Appendix A, Stop 9). Scale bar 2 mm, crossed polars. (H) Epidote-calcite-quartz symplectite surrounding garnet (Grt) in calcsilicate rock with microcline (Mc), quartz (Qtz), titanite, and calcite. Unit TH, 1.2 mi. SW of Thendara RR station, MKQ; sample MKC01. Scale bar 1 mm, crossed polars.



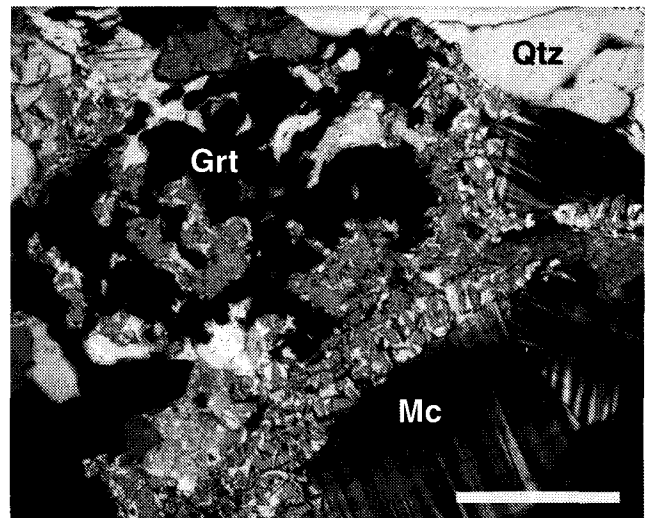
E.



F.



G.



H.

Figure 20. *continued*

The apparent coorelation of feldspar type with oxidation may indicate that perthitic textures are preserved under low fO_2 , fluid-absent metamorphic conditions (Valley et al., 1990), but recrystallize under more oxidizing conditions where fluids are present. Nonperthitic microcline is also present in metasedimentary or metasomatic rocks where $K_2O / Na_2O \gg 1$. Nonperthitic or micropertthitic alkali feldspar, ordinarily without microcline twinning, that occurs in intensely deformed gneisses such as those of the MRDZ (Fig. 18E), may result from recrystallization of perthitic feldspar during deformation at subsolvus temperatures.

The similarity of amphibole and pyroxene com-

positions to those in unmetamorphosed granitoids of comparable bulk composition (Fig. 6) suggests the absence of large-scale metamorphic reequilibration. This is not surprising in view of the overlap between the estimated ranges of metamorphic (ca. 750–820°C) and magmatic (800–900°C) temperatures.

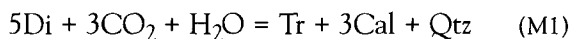
Fayalite occurs locally in both charnockites and granites, but has not been found together with orthopyroxene, precluding direct application of the fayalite-ferrosilite geobarometer (Bohlen and Boettcher, 1981). Fayalite (Fa_{95}) occurs with quartz in charnockite from near the center of the map area (Table 2, OFY01). Using Bohlen and Boettcher's (1981, Fig. 1) data, assuming $T = 800^\circ C$, and cor-

recting for Mn, this implies a maximum pressure around 7 kbar.

Sillimanite needles in the quartz-sillimanite nodular facies of unit BM commonly define a lineation, indicating a pre- or syndeformation origin of the sillimanite. Unfoliated quartz-feldspar veins and late pegmatites crosscut both sets of stringers. Buddington and Leonard (1962) attribute similar rocks in the northwestern Adirondack Highlands to metasomatic replacement of biotite-quartz-plagioclase gneiss, combined with metamorphic differentiation, and note a correlation of the sillimanite-nodular facies with intensity of deformation.

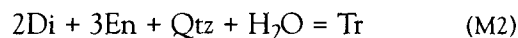
Nabelek (1997) interprets quartz-sillimanite segregations present in high-grade schists in the Black Hills of South Dakota as caused by partial melting in the presence of fluids with high a_{H^+} / a_{K^+} ratios and fluoride ion activities. Other observations suggest high fluoride activity in unit BM, consistent with this mechanism. Accessory fluorite is common in the sillimanite-nodular leucogneisses, and topaz rims on sillimanite occur locally in the Port Leyden 7.5' Quadrangle (Fig. 20C). Valley et al. (1983) report F-bearing garnet in calcsilicate rocks from the same area, and quartz-fluorite symplectites are present locally in both granitic and metasedimentary rocks (Fig. 20D). If the sillimanite-nodular facies was formed by the process proposed by Nabelek (1997), loss of alkalis may account for the presence of normative quartz well in excess of minimum-melt proportions in several analyzed leucogneiss samples (Fig. 4B).

Calcsilicates — Tremolite occurs in calcsilicates of units CM, MU, and BL throughout the map area. In some diopside-phlogopite-tremolite schists, it is clearly a primary metamorphic mineral, but more commonly it has grown at the expense of diopside and appears to be late. In the latter case, secondary calcite is usually present, suggesting the retrograde reaction



Diopside, however, appears to be stable in most thin sections; only a few contain both primary and retrograde tremolite. The assemblage $\text{Di} + \text{En} + \text{Qtz}$ occurs in three thin sections, with minor retrograde tremolite. This assemblage, on the high-temperature (left)

side of the reaction



(Fig. 19), probably indicates locally lower $a_{\text{H}_2\text{O}}$ during peak metamorphism. These samples are from carbonate-rich rocks, consistent with CO_2 dilution of the fluid phase.

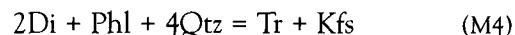
Phlogopite or magnesian biotite is commonly present in the calcsilicates, and conditions on the low-temperature (right) side of the reaction



are indicated in all but one thin section, where the univariant assemblage is present (Fig. 20E).

Electron microprobe analysis shows a primary tremolite (Table 2, MKB124) to be fluorine-rich (2.17% F; $X_F = 0.47$) and somewhat aluminous (3.57% Al_2O_3); coexisting phlogopite is also F-rich (4.86% F; $X_F = 0.54$). The fluorine content probably extends the stability of both minerals to higher temperatures (Valley et al., 1982). Less F is present in other analyzed tremolites (Table 2).

Univariant equilibrium for the reaction:



is near or below 600°C for pressures between 6 and 8 kbar. Lamb and Valley (1988) emphasize the uncertainties in the experimental calibrations of this reaction and the sensitivity of the calculation to small errors in the thermodynamic data. Moreover, impurities such as Fe, Al, and F in tremolite may affect the equilibrium temperature. In the map area, the high-temperature ($\text{Di} + \text{Phl} + \text{Qtz}$) assemblage is present in 23 of 34 thin sections studied; 5 have the low-T ($\text{Tr} + \text{Kfs}$) assemblage, and 6 are univariant (Fig. 20E). In some of the latter, textures suggest that tremolite is late and that reaction M4 occurred during cooling.

Wollastonite has been found at only three sites in or near the map area. Two are outcrops on the Moose River in the western half of the MKQ. One of these, a calcsilicate enclave in a thick amphibolite layer, may be a contact-metamorphosed xenolith. The other consists of sparse, local wollastonite that occurs with diopside and quartz in a layered metasedimentary sequence dominated by quartzite (Appendix A, Stop 3). The third wollastonite occurrence is



A.



C.



C.

Figure 21. Outcrops of migmatites. (A) Folded leucosomes in jotunite, unit JA, outcrop on W side of Rte 30, 0.8 mi. SE of Deerland, BMQ. (B) Folded leucosome in kinzigite, unit MU, 0.1 mi. S of Burnt Mtn, OFQ. (C) Migmatitic diopside-microcline calcsilicate rock, unit BM, 0.2 mi. SW of South Pond, W edge of RLQ.

a roadcut (Appendix A, Stop 12) in unit MU just outside the eastern boundary of the map area, where a meter-thick layer in diopside-rich calcsilicates contains the assemblage Cpx (Di_{66}) + Grt (Grs_{71}) + Wo + Kfs + Scp ($\sim\text{Me}_{75}$) + Cal. Elsewhere throughout the map, area quartz and calcite occur in unreacted contact. If the wollastonite is a product of Ottawan metamorphism, it indicates either localized dilution of the fluid phase by water, or fluid pressures much less than total pressure. It is more likely, however, that the wollastonite originated during the earlier AMCG magmatic event and persisted through granulite facies metamorphism due to fluid-absent conditions (Valley et al., 1990).

Scapolite is common in calcsilicate rocks throughout the area, ordinarily without coexisting plagioclase. X_{Me} of most analyzed scapolites is between 0.70 and

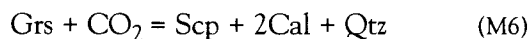
0.80, the relatively calcic composition indicative of temperatures on the high side ($> \sim 780^\circ\text{C}$) of the reaction



In the calculation for Figure 19, ideal solid solution is assumed ($a_{\text{Me}} = X_{\text{Me}}$). Actual meionite activities at these temperatures are probably higher (Moecher and Essene, 1990), in which case the temperature estimate is a minimum. Most scapolites appear to be in textural equilibrium, although in a few sections scapolite grains are rimmed by fine-grained mixtures of plagioclase and calcite that show incipient retrogression. In a few thin sections, scapolite occurs with plagioclase and quartz, also in apparent textural equilibrium. Scapolite in one of these is relatively sodic (Table 2, RLS126, $X_{\text{Me}} = 0.53$) consistent with an origin by partial metasomatic

replacement of plagioclase in the presence of Cl-bearing fluids, followed by recrystallization at higher temperatures.

Grossular-andradite garnet is common in the oxidized calcsilicates and quartzites of unit TH, but rare in less oxidized rocks. Pure grossular is stable at 7 kbar and 800°C only when $X_{\text{CO}_2} < \sim 0.32$, but increasing activity of trivalent iron with increasing f_{O_2} permits substitution of the andradite component, which extends the Ca-garnet stability field to lower temperatures and higher X_{CO_2} (Taylor and Liou, 1978). Andradite occurs locally with ilmenohematite in coarse-grained leucosomes in the microcline gneiss facies of TH. Rarely, grossular-rich garnet (e.g., Table 2, WCH32A, $X_{\text{Gr}} = 0.85$) occurs as thin rims around scapolite ($X_{\text{Me}} = 0.80$) and along grain boundaries between other phases in the vicinity of scapolite, in the assemblage Qtz + Cal + Kfs + Scp + Cpx + Grt (Fig. 20F). Textural evidence suggests the reaction



proceeding left with increasing temperature or decreasing X_{CO_2} . Reaction M6 can occur only over a restricted range of temperature and X_{CO_2} at 7 kbar (Fig. 19). Working with rocks of similar composition and using the data set of Holland and Powell (1990), Harley and Buick (1992) calculate a grid showing reaction M6 occurring at $X_{\text{CO}_2} = 0.30$ to 0.45 at 7.5 kbar, with the range decreasing to nil at about 6 kbar.

The summary in Figure 19 uses mineral composition data from sample RLJ26 (Table 2 and Fig. 20E). The calculated positions of the equilibria in the T- X_{CO_2} plane are only slightly displaced from those for pure endmembers, indicating that impurities such as Fe and F in tremolite and phlogopite, and Al in tremolite, have little net effect. The shaded area in Figure 19 shows the conditions indicated by most of the petrographic evidence; it becomes progressively smaller with decreasing pressure. Observed assemblages outside the shaded area are either texturally retrograde or consistent with local variations in water fugacity. Valley et al. (1990) and Edwards and Valley (1998) have shown that water fugacity in granulite facies rocks may vary significantly on a sub-meter scale, in response to buffering by hydrous mineral assemblages (Kohn, 1999).

Metapelites — Mineral assemblages in pelitic and semipelitic rocks commonly consist of biotite, quartz,

and plagioclase, with or without sillimanite and/or garnet. In a few locations, primarily in WCQ, biotite is sparse or absent and the assemblage is (Gr) + Sil + Grt + Qtz + Kfs. Here, as in similar rocks throughout the Adirondack Highlands, primary muscovite is absent. The absence of Al_2SiO_5 phases other than sillimanite restricts metamorphic pressures and temperatures to the high T, low P side of the kyanite-sillimanite transition. Kyanite and sillimanite pseudomorphs after kyanite are lacking, although kyanite is reported at one location in the Blue Mountain Lake Quadrangle east of the map area (Geraghty, 1978).

Pyralisite garnet in these metapelites is typically porphyroblastic and encloses grains of quartz, feldspar, sillimanite, and biotite. In most thin sections, these inclusions are concentrated toward the center of the porphyroblasts, surrounded by a zone of varying thickness containing few or no inclusions (Fig. 20G). Sillimanite inclusions in garnet consist chiefly of small needles with a distinct preferred orientation, whereas sillimanite exterior to garnet porphyroblasts is ordinarily coarser. Rarely, coarse sillimanite grains have thin rims of garnet. These textural relations suggest two periods of garnet growth that may correlate with the two tectonometamorphic events discussed above. Garnet porphyroblasts and reaction rims are commonly undeformed, although flattened and ovoid garnets are present in kinzigites within the MRDZ on the south face of Mitchell Ponds Mountain.

Cordierite occurs in scattered locations in biotite-rich metapelitic rocks of unit BL in the Raquette Lake, Big Moose, and McKeever Quadrangles, including Stops 3 and 9 of Appendix A. Buddington and Leonard (1962) and Stoddard (1988) describe cordierite from several locations in the northwestern Adirondack Highlands close to the Highlands-Lowlands boundary. It is rare in the eastern Highlands (Whitney and Olmsted, 1993), possibly due to the lack of appropriate Mg-rich bulk compositions rather than to unfavorable metamorphic pressure and temperature conditions.

Redox equilibria — A wide range of oxygen fugacities are represented. They vary from above the magnetite-hematite buffer reaction in oxidized rocks of the TH unit, to the fayalite-magnetite-quartz buffer in many granites and charnockites, and to the graphite- CO_2 buffer in graphite-rich metasedimentary rocks

and graphite-bearing charnockites (Fig. 2F). In quartzofeldspathic gneisses, fO_2 may affect both the appearance of the rock and its aeromagnetic signature. Oxidation of biotite to K feldspar and magnetite gives rise to aeromagnetic highs that follow the map trend of units LD and, to a lesser extent, BM. Higher fO_2 in much of unit TH stabilized ilmeno-hematite and produced strong local magnetic lows (Buddington and Lindsley, 1964; Balsley and Bromery, 1965a, b, c, d). In all three units, segregation of iron into oxide phases left mafic silicates Mg-rich and pale in color, and gave the rocks a deceptively leucocratic appearance.

Anatexis — Partial melting caused widespread migmatization in jotunite (Fig. 21A) and kinzigite (Fig. 21B), as well as in some calcsilicate rocks (Fig. 21C). Migmatization is also conspicuous in well-foliated granitic gneisses and charnockites (Figs. 2C, D and 18B). It is poorly developed or absent in less-deformed granitoids and in the interiors of thick granitic or charnockitic bodies. In many locations, quartzofeldspathic leucosomes occur both parallel to and crosscutting foliation. The alkali feldspar in most leucosomes is perthite, indicating that anatexis probably occurred at hypersolvus temperatures. The widespread occurrence of anatexis suggests that even where a separate fluid phase was absent during metamorphism, sufficient water or fluorine was present in hydrous minerals to facilitate melting.

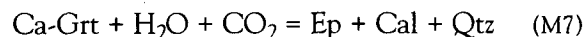
The timing of anatexis in the metasedimentary rocks is uncertain. Undeformed, crosscutting leucosomes are clearly Ottawan. Deformed leucosomes may be pre- or syntectonic Ottawan, or the product of an earlier tectonometamorphic event, or of contact anatexis in the vicinity of large granitic intrusions. With magmatic temperatures in the 800 to 900°C range, the heat from crystallizing charnockite and granite bodies would be likely to cause considerable partial melting, especially in metasedimentary rocks with abundant hydrous minerals such as biotite.

Relative timing of deformation and metamorphism — It is likely that the most recent (Ottawan) metamorphism outlasted deformation in most of the region, with the possible exception of the Stillwater and Inlet zones. Evidence for this includes: (a) a second generation of randomly oriented biotite in some well-foliated rocks; (b) undeformed garnet reaction rims on mafic minerals in well-foliated jotunite (Fig.

20A) and charnockite, and on scapolite in some calcsilicates; (c) skeletal poikiloblasts of magnesiohastingsite and clinopyroxene in unit TH and locally elsewhere; and (d) undeformed, crosscutting leucosomes in metapelites and granitic gneisses. The reaction rims in jotunite and charnockite suggest that a period of near-isobaric cooling followed peak metamorphism, consistent with a counterclockwise pressure-temperature-time path (Bohlen 1987; Spear and Markussen, 1997). There is little evidence for late-stage decompression associated with orogenic collapse.

Scattered occurrences of plagioclase-pyroxene symplectites, formed by breakdown of garnet, are found in the extreme southeastern part of the area in some of same rocks as the late garnet reaction rims (Pattee and Stoddard, 1988; Pattee, 1989). This suggests polycyclic metamorphism. Garnet porphyroblasts rimmed with or replaced by plagioclase-pyroxene symplectite may be relics of an early (Elzevirian?) tectonometamorphic event terminated by rapid uplift, whereas the more widespread garnet coronas are of later, probably Ottawan, origin.

Retrograde metamorphic effects — Some thin sections show evidence of retrogression. The common occurrence of retrograde tremolite in calcsilicate rocks probably originated by cooling from peak metamorphic conditions through reaction M1 (Fig. 19). Grossular-andradite garnet is surrounded or replaced by symplectic mixtures of epidote, calcite, and quartz in several thin sections of quartzites and calcsilicates from units TH and CM (Fig. 20H). This suggests the reaction



Epidote or clinozoisite may also partially replace plagioclase. Well-crystallized chlorite and, less commonly, muscovite occur locally in units TH, MU, and BL. In outcrops along the Moose River in the western MKQ, amphibolite near contacts with quartzite shows extensive development of coarsely crystalline chlorite; possibly the contacts were pathways for late aqueous fluids. Partial to complete replacement of enstatite by talc (Figs. 15A, 20E) and sillimanite by pyrophyllite is common. Complete replacement of scapolite by unidentified fine-grained sheet silicates occurs in some locations such as the Inlet zone where there is evidence of late deforma-

tion. Late hematitic alteration is common in parts of the NFQ, especially near brittle faults. In granites of that area, hematite as dust within alkali feldspar

grains and as flakes along grain boundaries and small fractures imparts a deep red color to otherwise fresh rock.

Chapter 5

Geochronology

Little geochronological work has been done with rocks from the Fulton Chain of Lakes area. A granitic gneiss sample from unit CG at the Beaver River spillway (Table 1A, NFA42) was dated by Chiarenzelli and McLelland (1991; their sample number NOFO-1). It yielded two populations of zircons. U / Pb data for four fractions of one population form a chord with a concordia intercept date of 1095 ± 5 Ma, while the other population gave scattered discordant points with a maximum $^{207}\text{Pb}/^{206}\text{Pb}$ age of 1154 Ma (Chiarenzelli and McLelland, 1991). A single fraction of zoned, prismatic zircons from sample BMS10B (unit CG), 1.2 km west northwest of Big Moose Station, gives a near-concordant date of 1153 ± 2 Ma (unpublished N.Y. State Geological Survey data). These results, together with the strong lithologic and geochemical similarity of the AMCG suite granites and charnockites to those elsewhere in the Adirondack Highlands (McLelland and Whitney, 1990; Whitney, 1992), make it probable that they are coeval with the latter, emplaced between roughly 1160 and 1090 Ma (Chiarenzelli and McLelland, 1991).

Other radiometric dates for rocks in and near the map area include scattered $^{207}\text{Pb} / ^{206}\text{Pb}$ ages up to 1406 Ma for small rounded pink zircons from a quartz-microcline-diopside-ilmenohematite gneiss of unit TH at Thendara (sample MKB07, unpublished N.Y. State Geological Survey data), consistent with a detrital origin. Florence et al. (1995) dated a nelsonite dike at Port Leyden (Port Leyden 7.5' minute Quadrangle, immediately west of MKQ), that yielded a minimum zircon age of 1104 ± 3 Ma. The metapelitic host rocks of the nelsonite, probably correlative with unit BM, gave a concordia intercept date of 1166 ± 53 Ma. Orrell and McLelland (1996) report single-grain U / Pb results for zircons from unit BM leucogneisses at Lyonsdale Bridge and Agers

Falls in the Port Leyden 7.5' Quadrangle. $^{207}\text{Pb} / ^{206}\text{Pb}$ ages range up to 1119 Ma, with one grain giving a concordant date of 1031 ± 8 Ma. The latter is within error of the 1034 ± 10 concordia intercept date for zircon from an undeformed pegmatite dike at the same location (McLelland et al., 2001). Orrell and McLelland (1996) interpret the 1031 Ma date as the emplacement age of the leucogneiss. However, since the majority of zircons in the rock record older ages, it is more likely that the 1031 Ma grain is a new or completely recrystallized zircon formed at the time of pegmatite emplacement. The intense deformation of unit BM and its involvement in the major F_2 and F_3 folds in the map area show clearly that it predates most Ottawa deformation.

The age of the Ottawa metamorphism in the Adirondack Highlands is not yet clearly established. McLelland et al. (1996, 2001) place it in the range 1090 to 1030 Ma, based on extensive U-Pb zircon studies of AMCG suite rocks. Florence et al. (1995) used U-Pb data from zircons and monazites from nelsonite and metapelites in the Port Leyden 7.5' Quadrangle to suggest a slightly younger age (1050–1000 Ma). The latter interval is in agreement with the 1026 to 996 Ma ages measured by Mezger et al. (1991, 1993) on metamorphic garnet and zircon in the central Highlands. Numerous other concordant or near-concordant zircon U-Pb ages in the 1040 to 990 Ma range indicate a high-temperature metamorphic event in the Adirondack Highlands after 1050 Ma (Silver, 1969; McLelland et al., 1988; unpublished N.Y. State Geological Survey data from zircons in anorthosite). A 995 ± 19 Ma Sm / Nd mineral isochron from a garnetiferous oxide-rich gabbro dike within the Marcy anorthosite massif (Ashwal and Wooden, 1983) also suggests a late date for Ottawa metamorphism. Davidson (1995) reports Ottawa high-grade metamorphism in the ca. 1060 to 1020

Ma range throughout much of the Grenville Province.

It is evident that additional geochronological work, using high-precision ion probe methods and well-characterized zircons, is necessary to elucidate the timing of the magmatic and metamorphic events in the west-central Highlands. Dating of rocks in the SE

domain, including the megacrystic biotite granite gneisses of unit BG, which are structurally the lowest rocks in the area, may help to determine whether traces of an Elzevirian tectonometamorphic event have been preserved.

Chapter 6

Geologic History and Tectonic Setting

Pre-1160 Ma — The sparse evidence cited above for multiple tectonomorphic events is the only clue to the geologic history of the map area prior to the AMCG magmatic event. Most of this evidence is from the SE domain, which is characterized by a suite of rocks substantially different from those in the northwestern two-thirds of the area. Units KZa and BG, apparently the most severely deformed rocks in the map area, have few counterparts north and west of the MRDZ. Indirect evidence of an older age for these rocks lies in the lithologic similarity of KZa to migmatitic biotite-quartz-plagioclase paragneisses associated with, and possibly intruded by, 1330 to 1300 Ma tonalitic gneisses in the southern and southeastern Adirondacks (McLelland and Chiarenzelli, 1990) and in the Mt. Holly Complex of Vermont (Ratcliffe et al., 1991). Megacrystic biotite granites of unit BG resemble the ca. 1250 Ma Tomantown granitic gneiss of the southern Highlands (Chiarenzelli and McLelland, 1991), which is also hosted by migmatitic paragneisses similar to KZa. KZa paragneisses also resemble the 1214 ± 21 Ma Popple Hill Gneiss of the northwestern Adirondack Lowlands (Carl, 1988; Carl and Sinha, 1992).

Little evidence exists regarding the depositional age of the carbonate-quartzite-metaevaporite suite, with minor metapelite, that occurs north of the MRDZ, save that it has been intruded by the AMCG suite. The overall character of these metasedimentary rocks is consistent with deposition in a shallow marine environment, in which restricted circulation led to local deposition of evaporites (units BL and MU, in part). The meta-arkoses of unit TH may be the immature siliciclastic filling of small grabens or half-graben associated with incipient rifting. This tectonic setting is consistent with the geochemical character of the AMCG granitoids. If the leucogneisses of unit BM are, as their chemistry suggests,

felsic metavolcanics of the AMCG suite, then the presence of interlayered metasedimentary rocks indicates that sedimentation overlapped in time with the early stages of AMCG magmatism.

1160 to 1050 Ma — The voluminous western Adirondack granitoids resemble, both in composition and mineralogy, Mesoproterozoic “anorogenic” and rapakivi-type granitoids throughout North America (e.g., Anderson, 1983; Emslie and Stirling, 1993; Frost and Frost, 1997; Frost et al., 1999), as well as worldwide (e.g., Haapala and Ramo, 1999). The similarities include: (a) consistent type A geochemical character; (b) common occurrence of fayalite, fluorite, and graphite that indicate reduced, relatively dry, iron- and halogen-enriched magmas; (c) ubiquitous presence of hypersolvus alkali feldspars that indicate relatively high solidus temperatures and low water activities; (d) the presence of minor associated mafic rocks of tholeiitic character, including anorthosite.

A-type granitic rocks, such as those of the AMCG suite, are commonly interpreted as “anorogenic,” a broad term that may encompass tectonic settings ranging from rift-related extension to post-collisional (Sylvester, 1989; Eby, 1992). Clearly, these settings are not mutually exclusive, and either rift- or plume-related extension, or delamination of subcrustal lithosphere, may have occurred following the Elzevirian Orogeny in the Adirondack Highlands. The geochemical evidence (Figs. 5A–D) is consistent with such a postcollisional setting.

Frost and Frost (1997) have proposed that large volumes of reduced, K- and Fe-enriched type A granitic magmas may be derived from partial melting of underplated tholeiitic basalts and their differentiates in an anorogenic or extensional intraplate setting. They cite the Wolf River Batholith of Wisconsin, the Pikes Peak Batholith of the Colorado Front Range,

and the Sherman Batholith of Wyoming as examples of granites that originated in this manner. Each has associated mafic and anorthositic rocks, consistent with the bimodal character of rapakivi and other A-type suites worldwide (Haapala and Ramo, 1999). The bimodal Adirondack AMCG suite may be the deformed and metamorphosed equivalent of such intraplate complexes. Subsidence associated with underplating may give rise to intracratonic basins (Stel et al., 1993), which suggests that at least part of the metasedimentary suite in the map area and elsewhere in the Adirondack Highlands may be coeval with AMCG magmatism.

Apart from variation largely attributable to differentiation (Whitney, 1992), the overall compositional uniformity of the granitoids is consistent with a uniform source region such as underplated mafic rocks. Lower crustal granulites would likely be less chemically uniform, and would yield more diverse partial melts. Neodymium model ages reported by Daly and McLelland (1991) for AMCG granitoids elsewhere in the Adirondack Highlands are also consistent with derivation of the bulk of the granitic magma from partial melting of recently underplated basalts, with, at most, minor contributions from crustal sources.

The dominantly tabular shape of the granitoid bodies, probably accentuated during subsequent deformation, and the scarcity of crosscutting relations with metasedimentary rocks, suggest emplacement as thick sills, laccoliths, or lopoliths under tectonically quiescent conditions, such as those described by Grocott et al. (1999) for Proterozoic granites and syenites in Greenland. Larger, domical unit CG bodies, such as those near Salmon Lake (NW RLQ), Ice Cave Mountain (SW OFQ), and Gull Lake (SE MKQ), may be thick, initially tabular, bodies that acquired their present shape at a later time by remobilization and buoyant ascent during Ottawaan metamorphism.

It is likely that granitic magmatism occurred in two or more separate pulses, with the earlier intrusions (now represented by the unit GA facies) originating prior to or coeval with the emplacement of mafic sills and dikes. The later pulse is now represented by the unit CG facies. The range of ages of these and similar granitoids throughout the Adiron-

dack Highlands indicates that AMCG-type magmatism may have continued sporadically for as much as 50 to 100 Ma (Chiarenzelli and McLelland, 1991).

Jotunites and anorthosite of unit JA appear to be sills emplaced in layered supracrustal rocks of unit BM. The anorthositic facies may have formed as concentrations of entrained plagioclase by flow differentiation or as in situ cumulates that have been subsequently disrupted by deformation. Valley et al. (1990), Florence et al. (1995), and Spear and Markussen (1997) have argued for a mid- to upper-crustal depth of emplacement for the Adirondack AMCG suite as a whole; if so, JA may be coeval, small-volume intrusives of the same suite emplaced at still shallower levels.

1050 to 990 Ma — Beginning about 1050 Ma, a collisional event caused crustal thickening by overthrusting, burying rocks presently exposed at the surface to depths on the order of 20 kilometers. AMCG intrusives and their host rocks were folded at this time. A relative SE-under-NW movement sense is suggested by the NE–E orientation and S–SE vergence of the major folds. Sinistral transpression occurred coeval with or subsequent to folding, with shearing concentrated within the Moose River, Jesup River, and, possibly, Flatfish Pond domains; SW-over-NE thrusting in the Honnedaga Lake domain may have accompanied the transpression. Vertical tectonic movement of large anorthosite and granite bodies then deflected the regional foliation (e.g., northeast of the Gull Lake Dome) and the MRDZ (west of the Snowy Mountain Dome).

Peak temperatures during the coeval granulite facies metamorphism were on the order of 800°C, perhaps due in part to residual heat from late stages of AMCG magmatism. Metamorphism and anatexis appear to have outlasted deformation, as indicated by undeformed, crosscutting anatectic leucosomes and pegmatites (Fig. 18B), annealing of highly strained rocks (Fig. 18E), and undeformed garnet reaction rims (Figs. 20A, B). Deformation after the metamorphic peak was more localized, notably within the Stillwater and Inlet zones. There is no evidence in the map area for large-scale synorogenic magmatism. Early stages of cooling may have been nearly isobaric (Spear and Markussen, 1997), and there is little evidence for sudden orogenic collapse.

Chapter 7

Glacial Geology

Glacial deposits in the map area consist principally of till of varying thickness, with local occurrences of kame and outwash deposits. Post-glacial alluvium is common in river valleys and other low-lying areas. The distribution of glacial materials is shown in the Adirondack Sheet of the *Surficial Geologic Map of New York* (Cadwell and Pair, 1991). In two sections of the Fulton Chain of Lakes region, glacial and/or alluvial overburden completely obscures the bedrock over large areas, rendering conjectural the bedrock geology. The largest of these areas, in the southwestern MKQ, south and west of White Lake, is entirely covered by kame and outwash deposits and is

nearly devoid of bedrock outcrops. Southwest of Cedar River Flow in the eastern WCQ, a substantial outcrop-free area of wetlands and alluvial inwash obscures critical bedrock relations at the junction of the Little Moose Mountain Syncline, the MRDZ, and the Snowy Mountain Dome.

Rare glacial striae and chattermarks indicate NE to SW ice flow, oblique to that in the eastern Adirondacks and the Black River Valley–Tug Hill area to the west. The NE–SW ice movement was subparallel to the dominant bedrock structural trends in most of the map area, suggesting that bedrock ridges may have controlled the direction of ice flow.

Chapter 8

Environmental Geology

The Adirondack region has been the focus of several studies of lake acidification due to acid precipitation. The Adirondack Lakes Survey Corporation (ALSC), under contract to the New York State Department of Environmental Conservation (DEC) and the Adirondack Park Agency (APA), measured pH, acid neutralizing capacity (ANC), and dissolved SiO_2 , Ca, Mg, Na, K, NH_4 , Al, SO_4 , NO_3 , Cl, F, organic carbon (DOC), and inorganic carbon (DIC) in 383 ponds and lakes in the map area. The measurements were made in the summer or early fall from 1984 to 1987.

The ALSC data (Kretser et al., 1989) were compared with the detailed geology. Ponds for which measurements are available were classified according to the dominant or exclusive bedrock unit in the watershed area. Table 5 shows the average values for ponds and lakes within each map unit. Averages and standard deviations for each unit are listed separately; they are also combined into three general categories: (a) GR comprises the dominantly granitic units (CG, GA, BM, LD, BG, and KZb); (b) MS includes those units that consist principally of metamorphosed sedimentary rocks (MU, CM, BL, TH, and KZa); and (c) MW (mixed watersheds) includes ponds and lakes with large watersheds underlain by substantial areas of both GR and MS. Only one watershed is underlain mainly by mafic rocks (AM). Watersheds where the surficial material is till (GRA, MSA) and those where outwash, kame, or alluvial overburden is dominant (GRB, MSB), are distinguished based on the mapping of Cadwell and Pair (1991).

Neutralization of acid precipitation in lake watersheds occurs principally by weathering and dissolution of mineral grains in the bedrock and overburden. Relatively soluble carbonate minerals such as calcite or dolomite are the most effective neutralizers. Where carbonates are absent, clay minerals

(scarce in Adirondack soils), mafic silicates such as olivine and pyroxenes (Johnson, 1984, Siegel and Pfannkuch, 1984) and amphiboles (April et al., 1986) may be the dominant influence, followed by plagioclase and alkali feldspars. In addition to the mineralogy, the extent to which acid precipitation is neutralized before reaching a pond or lake also depends on a complex of interrelated factors, including distance traveled, rate of flow, surface area of reactive mineral grains in the flow path, depth and permeability of overburden, depth of weathering, and ratio of runoff to groundwater input (e.g., Johnson et al., 1981; April et al., 1986; Staubitz and Zariello, 1989). Rapid runoff from heavy rain or snowmelt has little contact with bedrock or soil and consequently is unlikely to be significantly neutralized. On the other hand, groundwater in permeable glacial deposits or bedrock aquifers may retain little of the original acidity.

In most of the map area, the principal surficial material is glacial till of varying thickness. Smaller areas are covered by outwash, ice-contact, or alluvial deposits. Glacial deposits may contain substantial amounts of material of remote provenance (e.g., Kettles et al., 1991), especially in the finer grain-size fractions, and in ablation till more than in lodgement till. Permeability of surficial materials enhances their effect on water chemistry by allowing more extensive reaction between water and mineral grains in the soil. In general, tills are less permeable than well-sorted outwash and alluvium. Thus, the composition and acid buffering properties of the surficial material vary from place to place and may be significantly different from those of the bedrock.

Among the granitic units, ponds underlain by KZb, which consists chiefly of leucogneisses with sparse biotite, show consistently low pH values. With relatively few exceptions, lakes in uniformly granitic

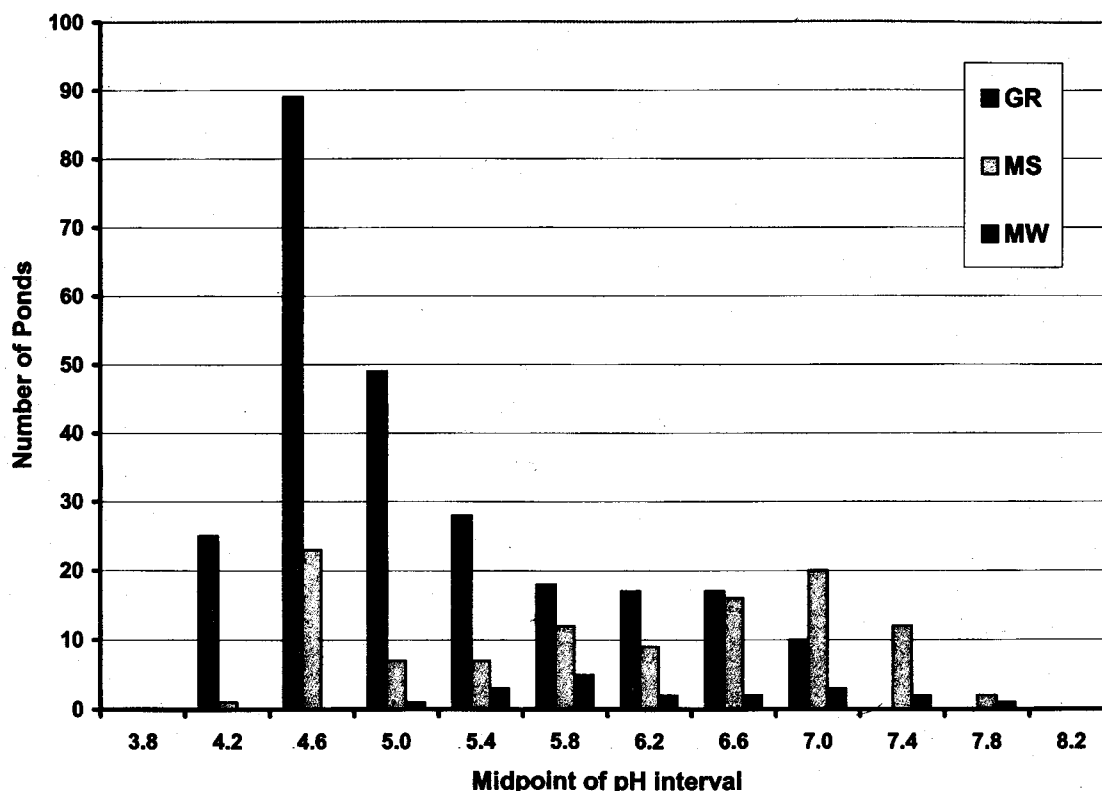


Figure 22. Effect of geology on lakewater pH. Histogram showing the distribution of average ALS pH values for watersheds with granitic (GR, dark gray), metasedimentary (MS, light gray), and mixed (MW, black) bedrock. Intervals of 0.4 pH units. The secondary maximum for MS in the pH 4.4–4.8 interval comprises ponds underlain by biotite-quartz-plagioclase gneisses of unit KZa.

and charnockitic gneisses of unit CG are also strongly acidic. Lakes underlain by heterogeneous granitic units (GA, BM, LD, and BG) generally have somewhat higher pH. With the partial exception of KZa, which contains considerable amounts of interlayered granitic gneisses, lakes underlain by metasedimentary rock units show higher average pH than those in granitic terrane. Although unit TH (meta-arkose) consists chiefly of quartzofeldspathic gneisses, lakes within it show unusually high average pH, probably due to the presence of interlayered calcareous rocks.

The distribution of average pH values for lakes with granitic (GR), metasedimentary (MS), and mixed (MW) bedrock are shown in Figure 22. The difference between the average pH for GR (5.15 ± 0.75) and MS (6.04 ± 1.03) is statistically significant at $p < .001$. In both categories, lakes in watersheds with permeable glacial deposits (GRb and MSb)

show significantly higher pH than those in watersheds with relatively impermeable tills (GRa and MSa, respectively). This may reflect the lower runoff-to-groundwater ratio and, consequently, increased exposure of the water to reactive minerals in areas with permeable overburden.

Within the study area, lakes in basins underlain by granitic rocks are in general more acidic and have lower ANC than those in areas underlain by metasedimentary rocks. This may be caused in part by the generally higher elevation, smaller size, thinner and/or less permeable overburden, and different vegetation in granitic watersheds compared to those underlain by metasedimentary rocks. Nevertheless, the effect of bedrock geology on water chemistry is not completely masked by the overburden, and bedrock mapping may be useful in predicting which lakes are at risk of acidification.

Tables

TABLE 1A
GEOCHEMISTRY OF GRANITOIDS (UNITS CG and GA)

MAJOR ELEMENTS

Sample	BMB44	BMB73A	BMG60	BMS10B	BMS11	BMS18	MKB133	MKB135	MKB153
Unit	CG	CG	CG	CG	CG	CG	CG	CG	CG
SiO ₂	74.58	71.17	67.93	68.82	67.34	72.77	75.12	72.12	72.47
TiO ₂	0.28	0.49	0.72	0.59	0.68	0.38	0.22	0.38	0.30
Al ₂ O ₃	12.25	13.08	13.43	13.69	14.24	13.34	12.37	13.48	13.58
Fe ₂ O ₃	0.60	1.19	3.46	1.01	1.47	0.99	0.94	0.94	0.92
FeO	2.05	3.05	3.12	3.96	3.61	2.31	1.18	2.04	2.01
MnO	0.04	0.05	0.09	0.08	0.08	0.06	0.02	0.04	0.04
MgO	0.03	0.23	0.35	0.26	0.26	0.17	0.06	0.06	0.10
CaO	1.01	1.68	1.46	2.00	2.26	1.33	0.84	1.20	1.39
Na ₂ O	2.84	3.22	3.01	3.41	3.53	2.79	3.05	3.15	3.28
K ₂ O	5.69	5.33	5.78	5.73	5.59	5.98	5.73	5.94	5.47
P ₂ O ₅	0.03	0.11	0.18	0.14	0.17	0.06	0.02	0.06	0.07
Total	99.40	99.60	99.53	99.69	99.23	100.18	99.55	99.41	99.63

TRACE ELEMENTS

Rb	195	175	131	167	115	170	328	175	224
Sr	104	140	107	139	170	119	71	140	132
Ba	559	664	957	770	955	773	202	634	460
Zr	366	435	563	631	753	524	394	521	299
Y	78	70	81	76	66	76	75	86	55
Nb	30	30	22	22	24	20	14	23	17
Ga	23	27	18	21	19	21	24	23	22
Ce	168	160	150	171	129	163	209	169	128
Li	18	16	18	12	5	8	13	8	12

MOLECULAR NORMS

qz	31.19	25.08	20.55	19.63	17.55	27.17	30.94	25.56	26.32
or	34.45	32.16	35.10	34.45	33.68	35.89	34.57	35.80	32.87
ab	26.14	29.53	27.78	31.16	32.33	25.45	27.97	28.85	29.96
an	3.97	5.61	6.23	5.22	6.63	6.31	3.21	5.20	6.28
hy	2.55	4.22	7.80	4.39	4.66	3.94	1.86	3.04	3.28
di	0.77	1.73	0.00	3.16	2.94	0.00	0.73	0.38	0.21
il	0.40	0.70	1.03	0.84	0.97	0.54	0.31	0.54	0.43
mt	0.46	0.73	1.12	0.86	0.88	0.57	0.36	0.51	0.50
co	0.00	0.00	0.00	0.00	0.00	0.00	0.00	0.00	0.00
ap	0.06	0.23	0.39	0.30	0.36	0.13	0.04	0.13	0.15

NA Not analyzed
ND Not detected

TABLE 1A (continued)
GEOCHEMISTRY OF GRANITOIDS (UNITS CG and GA)**MAJOR ELEMENTS**

Sample	MKB187	MKB201	MKB208	MKB212	MKB22	MKB268	MKC33	MKI15B	MKS30
Unit	CG	CG	CG	CG	CG	CG	CG	CG	CG
SiO ₂	76.98	68.74	72.97	68.98	69.92	71.48	66.61	71.05	65.93
TiO ₂	0.17	0.64	0.29	0.65	0.55	0.50	0.88	0.52	1.07
Al ₂ O ₃	11.89	14.31	14.02	14.15	13.77	12.93	13.74	13.41	14.97
Fe ₂ O ₃	0.41	1.99	0.39	1.50	1.97	1.81	2.53	1.59	0.82
FeO	1.18	2.08	1.22	3.30	2.31	2.58	4.54	2.40	4.47
MnO	0.02	0.08	0.02	0.08	0.07	0.06	0.10	0.06	0.08
MgO	0.05	0.47	0.34	0.46	0.27	0.22	0.53	0.38	1.50
CaO	0.69	1.88	1.37	2.05	1.12	1.71	2.27	1.64	3.12
Na ₂ O	2.90	3.42	3.84	3.46	2.67	2.87	2.91	3.30	3.49
K ₂ O	5.55	5.55	5.41	5.17	6.54	5.29	5.15	4.81	4.17
P ₂ O ₅	0.01	0.16	0.07	0.20	0.14	0.09	0.25	0.14	0.36
Total	99.85	99.32	99.94	100.00	99.33	99.54	99.51	99.30	99.98

TRACE ELEMENTS

Rb	318	163	156	213	273	184	131	216	69
Sr	36	185	202	135	100	138	205	156	158
Ba	100	756	625	553	682	735	1108	434	695
Zr	314	554	345	383	600	381	699	322	640
Y	133	76	73	87	163	77	64	71	68
Nb	18	24	21	25	50	23	18	23	18
Ga	24	22	21	26	23	23	21	21	20
Ce	193	142	207	156	177	147	132	143	136
Li	7	7	8	22	16	13	12	22	8

MOLECULAR NORMS

qz	34.54	20.24	24.34	20.84	23.42	27.22	20.28	26.18	19.38
or	33.43	33.41	32.12	30.98	39.63	32.07	31.32	29.09	25.21
ab	26.55	31.29	34.66	31.51	24.59	26.45	26.89	30.33	32.07
an	3.09	7.44	5.07	7.92	4.76	6.95	9.49	7.39	13.17
hy	1.58	4.88	1.94	5.73	5.12	4.73	8.66	5.14	6.73
di	0.26	0.80	1.04	0.85	0.00	0.92	0.34	0.00	0.21
il	0.24	0.91	0.41	0.92	0.79	0.71	1.26	0.74	1.53
mt	0.28	0.69	0.28	0.82	0.73	0.75	1.22	0.68	0.93
co	0.00	0.00	0.00	0.00	0.67	0.00	0.00	0.14	0.00
ap	0.02	0.34	0.15	0.42	0.30	0.19	0.54	0.30	0.77

NA Not analyzed
ND Not detected

TABLE 1A (continued)
GEOCHEMISTRY OF GRANITOIDS (UNITS CG and GA)

MAJOR ELEMENTS

Sample	MKS85	MKT15A	MKT46A	MKU01	MKU05	NFA42	NFB68	NFC27B	NFC31
Unit	CG	CG	CG	CG	CG	CG	CG	CG	CG
SiO ₂	71.74	72.97	73.85	71.10	64.54	71.75	66.54	68.40	70.32
TiO ₂	0.29	0.42	0.27	0.48	0.96	0.41	0.78	0.58	0.57
Al ₂ O ₃	13.11	12.60	12.97	13.68	13.86	13.49	13.73	14.06	13.24
Fe ₂ O ₃	3.64	1.40	0.68	1.33	2.16	1.12	4.30	1.29	1.49
FeO	NA	1.99	1.94	2.57	5.63	2.39	2.03	3.39	2.96
MnO	0.07	0.04	0.04	0.06	0.12	0.05	0.08	0.08	0.06
MgO	0.04	0.17	0.10	0.20	0.50	0.11	0.52	0.36	0.35
CaO	1.29	1.24	1.04	1.56	3.05	1.43	1.60	1.90	1.45
Na ₂ O	3.59	2.83	3.16	3.31	3.11	2.99	2.76	3.09	2.80
K ₂ O	5.42	5.31	5.26	5.49	5.08	5.79	6.48	5.87	5.96
P ₂ O ₅	0.03	0.11	0.05	0.09	0.26	0.07	0.21	0.14	0.11
Total	99.22	99.08	99.36	99.87	99.27	99.60	99.03	99.16	99.31

TRACE ELEMENTS

Rb	227	209	157	163	114	182	156	147	176
Sr	67	108	104	111	201	115	167	174	123
Ba	309	481	442	624	957	692	947	913	650
Zr	502	331	336	414	629	595	673	700	608
Y	121	52	57	72	94	72	78	81	70
Nb	25	17	17	17	24	25	24	25	25
Ga	27	20	21	22	21	21	21	21	21
Ce	216	120	106	138	144	134	157	177	171
Li	NA	25	16	24	5	14	13	14	14

MOLECULAR NORMS

qz	24.59	30.30	29.92	24.16	16.38	25.81	18.07	20.35	24.34
or	32.76	32.31	31.76	33.00	30.93	34.92	39.52	35.51	36.14
ab	32.97	26.17	29.00	30.24	28.78	27.40	25.58	28.41	25.80
an	3.73	5.60	4.94	6.37	9.13	6.42	6.13	7.33	6.11
hy	2.79	3.96	3.09	3.96	7.72	3.83	7.54	5.36	5.36
di	2.09	0.00	0.00	0.73	3.77	0.29	0.52	1.11	0.43
il	0.41	0.60	0.38	0.68	1.38	0.58	1.12	0.83	0.81
mt	0.58	0.58	0.45	0.67	1.36	0.60	1.06	0.81	0.77
co	0.00	0.23	0.34	0.00	0.00	0.00	0.00	0.00	0.00
ap	0.06	0.24	0.11	0.19	0.56	0.15	0.45	0.30	0.24

NA Not analyzed
 ND Not detected

TABLE 1A (continued)
GEOCHEMISTRY OF GRANITOIDS (UNITS CG and GA)**MAJOR ELEMENTS**

Sample	NFI57A	NFI79A	NFS12	NFS15	NFS20	NFS26	NFS27	NFS46	NFT67A
Unit	CG	CG	CG	CG	CG	CG	CG	CG	CG
SiO ₂	69.58	70.66	66.42	66.15	70.10	71.57	73.89	64.93	70.38
TiO ₂	0.48	0.43	0.81	0.87	0.26	0.38	0.28	0.53	0.40
Al ₂ O ₃	14.90	13.77	13.48	13.78	15.68	13.30	13.27	16.57	14.71
Fe ₂ O ₃	1.08	1.29	3.58	2.34	1.92	0.79	1.17	5.29	1.07
FeO	2.01	2.26	3.41	5.12	0.90	2.52	1.25	NA	1.36
MnO	0.05	0.05	0.12	0.10	0.02	0.05	0.04	0.08	0.04
MgO	0.60	0.18	0.54	0.48	0.40	0.27	0.06	0.32	0.39
CaO	2.09	1.45	2.36	2.71	0.96	1.56	0.94	1.72	1.57
Na ₂ O	3.67	3.17	3.01	3.44	3.95	2.84	3.73	6.89	3.79
K ₂ O	5.08	6.10	5.27	4.73	6.41	5.77	5.00	1.89	5.09
P ₂ O ₅	0.13	0.08	0.22	0.26	0.06	0.08	0.04	0.05	0.11
Total	99.67	99.44	99.22	99.98	100.66	99.13	99.67	98.27	98.91

TRACE ELEMENTS

Rb	186	179	117	105	163	166	153	35	109
Sr	285	156	175	191	122	118	122	124	223
Ba	739	719	935	849	519	835	596	94	763
Zr	295	439	558	579	355	509	326	975	253
Y	54	71	80	93	33	75	50	197	27
Nb	20	30	18	31	15	20	25	51	16
Ga	22	21	22	27	32	21	22	48	21
Ce	111	131	141	147	58	155	97	589	40
Li	14	15	10	7	NA	6	NA	NA	12

MOLECULAR NORMS

qz	20.81	22.73	19.36	17.88	17.12	26.36	27.95	10.41	22.58
or	30.32	36.73	32.12	28.54	37.68	34.96	29.96	11.26	30.57
ab	33.29	29.01	27.89	31.55	35.29	26.15	33.97	62.40	34.60
an	9.28	5.43	7.95	8.37	4.35	6.67	4.47	8.28	7.19
hy	4.56	3.61	7.72	7.68	3.91	3.99	2.64	5.48	3.43
di	0.27	1.09	2.12	2.91	0.00	0.59	0.00	0.00	0.00
il	0.68	0.61	1.16	1.24	0.36	0.54	0.40	0.74	0.57
mt	0.52	0.61	1.19	1.29	0.46	0.58	0.41	1.12	0.41
co	0.00	0.00	0.00	0.00	0.70	0.00	0.12	0.20	0.42
ap	0.27	0.17	0.47	0.56	0.12	0.17	0.08	0.11	0.23

NA Not analyzed

ND Not detected

TABLE 1A (continued)
GEOCHEMISTRY OF GRANITOIDS (UNITS CG and GA)

MAJOR ELEMENTS

Sample	OFA24	OFB92	OFC05	OFN14A	OFN18A	OFS17	OFS20	OFU01	OFU02
Unit	CG	CG	CG	CG	CG	CG	CG	CG	CG
SiO ₂	70.25	70.71	68.14	72.83	68.05	71.96	72.81	69.44	69.14
TiO ₂	0.57	0.55	0.63	0.34	0.63	0.36	0.37	0.68	0.66
Al ₂ O ₃	13.29	13.13	15.96	13.18	13.89	13.14	13.49	13.27	13.93
Fe ₂ O ₃	1.28	1.64	1.34	1.49	1.70	0.88	0.97	1.36	1.80
FeO	3.46	2.90	1.31	1.75	3.62	2.33	2.17	3.80	2.66
MnO	0.07	0.06	0.06	0.04	0.07	0.05	0.04	0.08	0.06
MgO	0.21	0.26	0.52	0.07	0.25	0.13	0.11	0.40	0.45
CaO	1.91	1.32	1.22	1.05	2.22	1.34	1.33	2.27	1.76
Na ₂ O	3.42	3.24	4.37	3.16	3.64	3.03	2.94	3.04	3.12
K ₂ O	5.60	5.47	6.26	5.89	5.15	5.88	6.00	5.14	5.82
P ₂ O ₅	0.14	0.06	0.10	0.04	0.12	0.03	0.05	0.16	0.18
Total	100.20	99.34	99.91	99.84	99.34	99.13	100.28	99.64	99.58

TRACE ELEMENTS

Rb	156	168	118	158	157	188	183	164	156
Sr	114	101	143	86	128	122	98	114	142
Ba	720	575	741	456	610	606	631	702	702
Zr	512	487	583	438	579	422	513	558	543
Y	64	70	72	82	93	58	56	92	73
Nb	18	22	18	19	22	23	16	26	22
Ga	19	21	18	21	26	18	21	25	24
Ce	137	141	188	162	165	132	111	143	163
Li	24	17	22	14	23	24	32	18	12

MOLECULAR NORMS

qz	21.73	24.31	13.35	26.49	19.19	26.20	26.49	23.58	21.36
or	33.52	33.10	36.90	35.43	31.07	35.65	35.92	31.09	35.07
ab	31.12	29.80	39.15	28.89	33.37	27.92	26.75	27.94	28.57
an	4.43	5.25	5.39	4.46	6.49	5.02	5.97	7.56	6.95
hy	3.89	5.01	3.66	3.16	4.65	2.80	3.40	5.30	5.36
di	3.40	0.84	0.00	0.46	3.17	1.28	0.31	2.32	0.60
il	0.80	0.78	0.88	0.48	0.90	0.51	0.52	0.97	0.94
mt	0.81	0.78	0.44	0.55	0.92	0.56	0.54	0.90	0.76
co	0.00	0.00	0.02	0.00	0.00	0.00	0.00	0.00	0.00
ap	0.30	0.13	0.21	0.09	0.26	0.06	0.11	0.34	0.38

NA Not analyzed
 ND Not detected

TABLE 1A (continued)
GEOCHEMISTRY OF GRANITOIDS (UNITS CG and GA)

MAJOR ELEMENTS

Sample	RLU95	WCB57	WCG41	WCH49	WCS31	WCS32	WCS33	BMC75	NFB130
Unit	CG	CG	CG	CG	CG	CG	CG	GA	GA
SiO ₂	70.51	75.70	74.63	66.69	69.39	68.08	68.62	70.64	66.79
TiO ₂	0.49	0.29	0.21	0.73	0.57	0.75	0.71	0.43	0.57
Al ₂ O ₃	13.70	11.59	12.44	14.30	13.56	13.81	14.05	13.67	15.67
Fe ₂ O ₃	0.63	1.20	0.85	2.11	1.15	1.98	1.47	1.99	0.96
FeO	3.58	1.47	1.75	3.46	3.53	3.37	3.23	2.12	2.62
MnO	0.07	0.05	0.05	0.10	0.07	0.10	0.07	0.06	0.07
MgO	0.17	0.07	0.08	0.34	0.22	0.41	0.46	0.33	0.39
CaO	1.62	0.65	0.98	2.25	1.96	1.98	1.93	1.79	1.98
Na ₂ O	2.93	2.67	3.21	3.61	3.51	3.57	3.50	3.33	4.20
K ₂ O	6.14	5.64	5.29	5.55	5.44	4.95	5.45	5.33	5.67
P ₂ O ₅	0.10	0.02	0.01	0.17	0.12	0.23	0.21	0.08	0.07
Total	99.94	99.35	99.50	99.31	99.52	99.23	99.70	99.77	98.99

TRACE ELEMENTS

Rb	173	210	274	109	181	120	130	171	152
Sr	156	41	45	177	112	140	147	118	199
Ba	727	299	322	999	614	680	725	784	614
Zr	489	483	369	849	623	608	639	476	600
Y	78	77	136	62	67	86	75	69	49
Nb	23	26	35	23	17	20	20	31	26
Ga	25	21	31	20	20	21	24	22	21
Ce	143	170	202	111	129	106	107	153	136
Li	14	NA	16	8	25	12	NA	12	12

MOLECULAR NORMS

qz	23.01	34.12	30.45	16.42	20.94	20.46	19.82	23.44	13.69
or	36.90	34.31	31.91	33.46	32.75	29.94	32.72	32.04	33.87
ab	26.76	24.69	29.43	33.08	32.12	32.81	31.94	30.42	38.13
an	6.20	3.07	3.99	6.56	5.28	7.21	6.64	6.73	7.24
hy	4.44	2.80	2.73	5.16	3.97	6.06	5.27	4.48	3.73
di	1.05	0.09	0.72	2.96	3.07	1.05	1.36	1.42	1.78
il	0.69	0.42	0.30	1.04	0.81	1.07	1.01	0.61	0.80
mt	0.74	0.46	0.45	0.95	0.81	0.92	0.81	0.69	0.61
co	0.00	0.00	0.00	0.00	0.00	0.00	0.00	0.00	0.00
ap	0.21	0.04	0.02	0.36	0.26	0.49	0.45	0.17	0.15

NA Not analyzed
 ND Not detected

TABLE 1A (continued)
GEOCHEMISTRY OF GRANITOIDS (UNITS CG and GA)**MAJOR ELEMENTS**

Sample	NFB75B	NFB84	NFB89A	NFI11A	NFS23	NFS24	NFS25	OFC52	OFS11
Unit	GA	GA	GA	GA	GA	GA	GA	GA	GA
SiO ₂	68.88	66.37	72.43	71.60	71.11	70.80	73.74	70.08	71.88
TiO ₂	0.71	0.64	0.38	0.36	0.39	0.49	0.30	0.52	0.51
Al ₂ O ₃	13.48	15.26	13.80	14.15	14.38	14.07	12.87	13.35	13.12
Fe ₂ O ₃	1.93	2.19	1.29	1.04	1.73	2.09	1.15	1.19	1.89
FeO	3.26	2.76	1.65	1.68	1.43	1.88	1.68	2.62	2.08
MnO	0.07	0.10	0.05	0.05	0.03	0.03	0.05	0.06	0.05
MgO	0.40	0.51	0.39	0.41	0.36	0.55	0.22	0.14	0.48
CaO	2.08	1.70	1.18	1.58	2.15	1.43	0.91	2.18	1.64
Na ₂ O	3.46	4.31	3.76	3.30	3.72	3.14	3.07	3.35	2.68
K ₂ O	5.20	5.69	4.36	5.48	4.21	5.60	5.73	5.41	5.42
P ₂ O ₅	0.16	0.12	0.07	0.07	0.08	0.10	0.02	0.08	0.10
Total	99.63	99.65	99.36	99.72	99.59	100.18	99.74	98.98	99.85

TRACE ELEMENTS

Rb	173	209	145	206	103	181	244	160	182
Sr	150	168	134	267	192	168	100	136	116
Ba	616	679	380	683	453	497	286	1109	589
Zr	388	726	347	238	313	442	400	540	434
Y	66	84	49	48	57	51	43	98	61
Nb	26	26	22	22	18	19	27	29	15
Ga	22	29	22	18	23	21	19	26	23
Ce	103	187	188	143	89	149	143	143	83
Li	10	8	16	8	NA	12	NA	12	NA

MOLECULAR NORMS

qz	20.99	12.37	27.68	24.56	25.18	23.83	28.82	23.00	27.92
or	31.34	33.87	26.21	32.81	25.25	33.51	34.57	32.76	32.74
ab	31.69	38.99	34.35	30.03	33.91	28.56	28.15	30.83	24.60
an	6.01	5.53	5.49	7.48	10.26	6.53	4.48	5.55	7.65
hy	4.97	5.53	4.07	3.90	4.13	5.47	3.01	2.29	5.35
di	2.76	1.74	0.00	0.00	0.03	0.00	0.00	4.00	0.00
il	1.01	0.90	0.54	0.51	0.55	0.69	0.43	0.74	0.73
mt	0.89	0.83	0.50	0.46	0.53	0.66	0.48	0.66	0.67
co	0.00	0.00	1.02	0.09	0.00	0.53	0.01	0.00	0.11
ap	0.34	0.25	0.15	0.15	0.17	0.21	0.04	0.17	0.21

NA Not analyzed
ND Not detected

TABLE 1A (continued)
GEOCHEMISTRY OF GRANITIODS
(UNITS CG and GA)

MAJOR ELEMENTS

Sample	RLS68	RLS82A	WCG40	WCS57A
Unit	GA	GA	GA	GA
SiO ₂	68.63	71.93	72.39	73.37
TiO ₂	0.60	0.39	0.37	0.33
Al ₂ O ₃	13.82	13.58	13.04	13.50
Fe ₂ O ₃	2.64	1.86	0.90	3.06
FeO	2.51	1.79	2.54	NA
MnO	0.05	0.05	0.06	0.03
MgO	0.64	0.25	0.21	0.32
CaO	1.15	1.28	1.35	2.45
Na ₂ O	2.87	2.72	2.62	3.12
K ₂ O	5.75	5.85	5.96	3.77
P ₂ O ₅	0.14	0.07	0.05	0.06
Total	98.80	99.77	99.49	100.01

TRACE ELEMENTS

Rb	145	157	176	101
Sr	191	141	100	200
Ba	906	770	768	613
Zr	560	446	418	411
Y	80	69	91	70
Nb	22	20	25	12
Ga	23	26	21	22
Ce	180	143	147	129
Li	29	14	20	NA

MOLECULAR NORMS

qz	23.06	27.25	27.86	31.98
or	35.03	35.30	36.08	22.72
ab	26.57	24.95	24.11	28.57
an	4.94	6.02	6.37	11.93
hy	7.09	4.48	4.22	3.50
di	0.00	0.00	0.12	0.05
il	0.86	0.55	0.53	0.47
mt	0.88	0.62	0.60	0.65
co	1.26	0.68	0.00	0.00
ap	0.30	0.15	0.11	0.13

NA Not analyzed
 ND Not detected

TABLE 1B
GEOCHEMISTRY OF GRANITOIDS (UNITS BM, LD, BG, and KZb)**MAJOR ELEMENTS**

Sample	BMB65A	BMC13A	BMC13B	BMC13C	BMS12	BMS15	BMS16	BMS17	MKB184
Unit	BM	BM	BM	BM	BM	BM	BM	BM	BM
SiO ₂	76.61	71.22	76.09	76.68	80.93	74.19	74.83	78.11	79.25
TiO ₂	0.22	0.43	0.18	0.19	0.16	0.25	0.17	0.14	0.10
Al ₂ O ₃	11.70	13.49	11.75	12.12	12.02	13.00	12.25	11.43	10.63
Fe ₂ O ₃	1.75	3.58	2.36	2.06	0.35	0.01	0.03	0.92	0.08
FeO	1.24	1.26	1.16	0.68	1.16	2.35	2.57	1.31	1.61
MnO	0.01	0.03	0.01	0.02	0.11	0.05	0.04	0.05	0.04
MgO	0.04	0.06	0.08	0.02	0.27	0.16	0.06	0.17	0.09
CaO	0.83	0.66	0.92	0.49	0.47	1.62	1.17	0.94	0.51
Na ₂ O	3.78	2.56	2.98	2.43	0.74	2.64	2.51	0.67	2.22
K ₂ O	3.15	6.14	4.03	5.28	3.98	5.56	5.65	6.52	4.85
P ₂ O ₅	0.02	0.05	0.03	0.01	0.01	0.05	0.01	0.01	0.01
Total	99.35	99.48	99.59	99.98	100.20	99.88	99.29	100.27	99.39

TRACE ELEMENTS

Rb	83	267	164	205	240	317	444	337	347
Sr	67	119	60	54	33	147	35	154	42
Ba	66	513	138	157	99	358	120	132	80
Zr	487	660	514	373	304	270	279	234	266
Y	83	73	86	52	33	34	224	62	65
Nb	23	30	19	19	15	27	42	18	30
Ga	23	24	22	21	24	22	29	20	21
Ce	265	200	334.5	200	81.47	196	341	219	136
Li	2	NA	16	NA	41	29	41	14	NA

MOLECULAR NORMS

qz	37.21	27.52	37.49	37.80	56.83	30.87	32.93	44.04	43.74
or	19.10	37.35	24.51	32.00	24.42	33.48	34.33	39.91	29.65
ab	34.83	23.67	27.55	22.39	6.90	24.16	23.18	6.23	20.62
an	4.09	3.04	4.50	2.43	2.35	7.34	5.63	4.76	2.55
hy	3.23	5.14	4.04	2.91	2.56	2.85	2.98	2.65	2.04
di	0.00	0.00	0.00	0.00	0.00	0.42	0.22	0.00	0.00
il	0.31	0.62	0.26	0.27	0.23	0.35	0.24	0.20	0.14
mt	0.50	0.80	0.59	0.45	0.27	0.42	0.47	0.39	0.30
co	0.68	1.75	0.99	1.73	6.42	0.00	0.00	1.79	0.93
ap	0.04	0.11	0.06	0.02	0.02	0.11	0.02	0.02	0.02

NA Not analyzed

ND Not detected

TABLE 1B (continued)
GEOCHEMISTRY OF GRANITOIDS (UNITS BM, LD, BG, and KZb)

MAJOR ELEMENTS

Sample	MKC26A	MKC26B	MKS24	NFA17B	PLS02	PLS04	PLS05	PLS06	RLS10
Unit	BM	BM	BM	BM	BM	BM	BM	BM	BM
SiO ₂	75.43	73.88	71.71	76.84	76.01	75.86	74.86	76.37	73.73
TiO ₂	0.12	0.28	0.48	0.20	0.15	0.19	0.10	0.30	0.30
Al ₂ O ₃	13.40	12.85	13.18	12.02	12.25	12.26	13.30	12.41	12.43
Fe ₂ O ₃	0.06	1.17	1.98	1.33	0.59	0.48	0.01	0.01	0.37
FeO	0.98	1.62	2.33	1.67	1.40	2.02	0.91	1.36	2.26
MnO	0.02	0.05	0.06	0.01	0.03	0.06	0.01	0.04	0.04
MgO	0.17	0.30	0.11	0.03	0.11	0.05	0.22	0.08	0.07
CaO	0.70	0.87	1.62	1.01	0.92	0.95	1.02	0.23	1.08
Na ₂ O	3.11	2.59	2.34	2.97	2.36	2.30	3.27	1.57	2.94
K ₂ O	5.72	5.97	5.07	4.04	5.43	5.97	5.39	6.85	5.81
P ₂ O ₅	0.12	0.05	0.09	0.02	0.02	0.01	0.03	0.02	0.05
Total	99.83	99.63	98.97	100.14	99.27	100.15	99.12	99.24	99.08

TRACE ELEMENTS

Rb	244	273	122	159	404	387	341	204	237
Sr	80	104	221	24	56	44	65	60	79
Ba	239	365	919	89	169	166	153	194	443
Zr	86	241	500	461	266	350	117	360	305
Y	29	38	48	72	70	154	109	41	80
Nb	12	21	15	11	27	18	10	20	25
Ga	16	20	19	25	23	24	22	14	23
Ce	38	139	119	311	170	294	89	127	160
Li	NA	NA	NA	16	17	12	10	16	22

MOLECULAR NORMS

qz	31.36	30.53	31.67	38.09	36.48	34.14	30.41	38.03	29.41
or	34.22	36.07	31.07	24.40	33.03	36.03	32.42	41.79	35.22
ab	28.28	23.78	21.80	27.26	21.82	21.10	29.89	14.56	27.09
an	2.72	4.08	7.73	4.99	4.57	4.75	4.95	1.04	3.65
hy	1.59	3.81	4.84	3.33	2.53	2.92	1.62	1.56	2.42
di	0.00	0.00	0.00	0.00	0.00	0.00	0.00	0.00	1.21
il	0.17	0.40	0.69	0.28	0.22	0.27	0.14	0.43	0.43
mt	0.18	0.48	0.74	0.51	0.35	0.44	0.16	0.25	0.46
co	1.22	0.74	1.26	1.09	0.97	0.35	0.34	2.30	0.00
ap	0.25	0.11	0.20	0.04	0.04	0.02	0.06	0.04	0.11

NA Not analyzed
 ND Not detected

TABLE 1B (continued)
GEOCHEMISTRY OF GRANITOIDS (UNITS BM, LD, BG, and KZb)**MAJOR ELEMENTS**

Sample	RLS111	RLS113	RLS75	RLU09	BMS19	BMS20	BLS01	RLA01B	RLB09B
Unit	BM	BM	BM	BM	BM	BM	LD	LD	LD
SiO ₂	71.84	74.73	83.39	77.39	77.42	73.49	77.94	70.47	69.81
TiO ₂	0.46	0.30	0.26	0.22	0.17	0.18	0.20	0.66	0.67
Al ₂ O ₃	15.62	13.14	11.85	11.97	12.72	12.25	11.45	13.45	13.78
Fe ₂ O ₃	3.38	1.47	0.30	1.45	0.01	0.14	0.55	3.34	3.37
FeO	NA	1.43	1.26	1.36	1.15	1.81	0.96	2.31	2.10
MnO	0.11	0.03	0.02	0.02	0.02	0.02	0.02	0.03	0.05
MgO	0.23	0.15	0.17	0.01	0.32	0.10	0.14	0.32	0.46
CaO	1.38	1.13	0.22	0.63	0.98	0.90	0.99	1.40	2.21
Na ₂ O	2.59	3.32	0.14	1.48	3.63	3.17	2.25	2.96	5.19
K ₂ O	4.10	4.95	2.81	5.17	4.08	5.12	5.39	4.84	2.31
P ₂ O ₅	0.08	0.04	0.06	0.02	0.02	0.02	0.04	0.15	0.16
Total	99.79	100.69	100.48	99.72	100.52	97.20	99.93	99.93	100.11

TRACE ELEMENTS

Rb	134	135	132	247	251	456	140	118	41
Sr	160	124	39	59	43	36	110	132	135
Ba	555	679	45	252	136	137	378	733	436
Zr	402	369	240	425	244	284	255	511	645
Y	71	82	5	66	118	110	62	57	71
Nb	19	21	22	26	22	17	16	15	18
Ga	27	25	26	29	25	25	17	19	22
Ce	NA	147	60	299	174	174	156	120.6	123.4
Li	NA	8	38	21	20	60	14	26	14

MOLECULAR NORMS

qz	34.44	30.24	68.26	44.30	34.97	31.26	39.10	27.25	21.92
or	24.82	29.51	17.36	31.69	24.25	31.55	32.63	29.32	13.76
ab	23.83	30.08	1.31	13.79	32.79	29.69	20.70	27.25	46.99
an	6.48	5.39	0.73	3.11	4.76	4.25	4.77	6.12	7.54
hy	3.91	3.38	2.04	3.06	2.08	2.38	1.93	6.55	5.65
di	0.00	0.00	0.00	0.00	0.00	0.22	0.00	0.00	1.97
il	0.66	0.42	0.38	0.32	0.24	0.26	0.29	0.94	0.94
mt	0.54	0.48	0.28	0.48	0.20	0.35	0.26	0.95	0.90
co	5.15	0.40	9.50	3.22	0.66	0.00	0.24	1.29	0.00
ap	0.17	0.08	0.13	0.04	0.04	0.04	0.09	0.32	0.34

NA Not analyzed
ND Not detected

TABLE 1B (continued)
GEOCHEMISTRY OF GRANITOIDS (UNITS BM, LD, BG, and KZb)

MAJOR ELEMENTS

Sample	RLU02	RLU105	RLU108	WCV04	WCV05	WCV17	OFC47	OFC61
Unit	LD	LD	LD	BG	BG	BG	KZB	KZB
SiO ₂	67.50	71.11	68.63	69.34	70.02	64.86	75.15	71.01
TiO ₂	0.73	0.64	0.73	0.43	0.56	0.87	0.28	0.58
Al ₂ O ₃	13.36	13.25	13.39	16.29	15.53	13.28	12.99	13.49
Fe ₂ O ₃	4.13	1.91	3.39	0.71	1.37	4.98	0.34	2.27
FeO	2.59	3.05	2.86	2.19	2.19	2.60	1.39	2.57
MnO	0.05	0.02	0.03	0.03	0.03	0.15	0.02	0.09
MgO	0.66	1.04	0.47	0.58	0.96	0.67	0.20	0.33
CaO	2.44	0.97	1.16	2.56	2.04	2.64	1.00	1.47
Na ₂ O	3.64	5.66	3.43	3.26	3.27	3.69	2.78	2.99
K ₂ O	4.47	1.73	4.48	3.96	3.64	3.73	5.20	4.63
P ₂ O ₅	0.21	0.18	0.18	0.16	0.22	0.27	0.05	0.09
Total	99.78	99.56	98.75	99.51	99.83	97.74	99.40	99.52

TRACE ELEMENTS

Rb	122	91	158	120	127	113	149	168
Sr	173	85	141	388	528	355	125	149
Ba	755	116	979	850	816	794	365	714
Zr	484	427	406	229	223	411	193	534
Y	83	46	58	18	22	41	15	66
Nb	20	16	23	10	11	16	10	23
Ga	19	20	21	22	18	19	16	19
Ce	113	67	125	78	127	135	136	123
Li	NA	NA	NA	NA	NA	34	NA	28

MOLECULAR NORMS

qz	19.73	24.09	24.47	26.12	28.25	19.13	28.42	28.16
or	26.99	10.30	27.38	23.75	21.82	23.06	28.09	32.07
ab	33.40	51.21	31.85	29.71	29.79	34.67	27.57	27.53
an	7.07	3.67	4.74	11.83	8.81	9.06	6.89	4.48
hy	7.08	7.81	7.68	4.51	6.11	8.69	5.94	4.60
di	3.12	0.00	0.00	0.00	0.00	2.24	0.00	0.00
il	1.04	0.90	1.05	0.61	0.79	1.27	0.83	0.68
mt	1.12	0.84	1.07	0.50	0.61	1.29	0.83	0.52
co	0.00	0.81	1.38	2.63	3.35	0.00	1.24	1.56
ap	0.45	0.38	0.39	0.34	0.47	0.59	0.19	0.38

NA Not analyzed
 ND Not detected

TABLE 1C
GEOCHEMISTRY OF GRANITOIDS WITHIN METASEDIMENTARY UNITS**MAJOR ELEMENTS**

Sample	BLS10	BMF43	MKB127	MKB277	OFB72	OFB108	RLS12
Unit	CM	MU	MU	MU	MU	MU	MU
SiO ₂	69.14	60.46	67.99	66.31	73.06	73.76	71.85
TiO ₂	0.70	1.26	0.67	0.82	0.32	0.29	0.48
Al ₂ O ₃	13.82	14.46	14.33	15.31	12.71	12.98	13.69
Fe ₂ O ₃	3.56	2.48	4.16	1.48	2.00	1.73	1.34
FeO	2.02	7.69	2.08	2.58	1.04	1.36	1.72
MnO	0.08	0.15	0.07	0.06	0.02	0.02	0.02
MgO	0.38	0.72	0.39	0.71	0.09	0.08	0.59
CaO	2.26	4.64	1.41	3.09	0.69	0.95	1.12
Na ₂ O	3.02	3.74	2.90	3.20	2.04	1.70	3.00
K ₂ O	4.93	3.47	5.70	5.11	6.62	6.50	5.31
P ₂ O ₅	0.15	0.37	0.15	0.12	0.05	0.04	0.18
Total	100.06	99.44	99.85	98.79	98.64	99.41	99.30

TRACE ELEMENTS

Rb	147	71	166	119	199	189	226
Sr	127	213	188	243	131	189	102
Ba	687	870	1139	1069	762	777	382
Zr	456	776	828	737	388	385	206
Y	84	70	85	39	31	28	47
Nb	18	24	23	17	14	5	15
Ga	22	22	23	15	20	22	20
Ce	154	143	141	80	159	185	112
Li	NA	10	NA	NA	14	NA	NA

MOLECULAR NORMS

qz	23.59	11.06	21.62	18.30	31.59	33.75	33.99
or	29.77	21.10	34.49	30.90	40.63	39.68	31.43
ab	27.71	34.56	26.67	29.41	19.03	15.77	25.54
an	9.81	12.78	6.16	12.61	3.22	4.60	4.74
hy	6.35	9.37	7.42	4.83	3.25	3.46	2.28
di	0.52	6.74	0.00	1.82	0.00	0.00	0.00
il	1.00	1.81	0.96	1.17	0.46	0.42	0.40
mt	0.93	1.78	1.04	0.70	0.51	0.53	0.30
co	0.00	0.00	1.33	0.00	1.20	1.71	1.22
ap	0.32	0.80	0.32	0.26	0.11	0.09	0.11

NA Not analyzed

ND Not detected

TABLE 1C (continued)
GEOCHEMISTRY OF GRANITOIDS WITHIN
METASEDIMENTARY UNITS

MAJOR ELEMENTS

Sample	WCH23	WCH26	WCS13
Unit	KZA	KZA	KZA
SiO ₂	73.31	69.96	72.52
TiO ₂	0.28	0.61	0.32
Al ₂ O ₃	13.64	12.71	13.46
Fe ₂ O ₃	0.85	1.59	0.87
FeO	1.25	3.96	1.94
MnO	0.03	0.07	0.04
MgO	0.18	0.13	0.19
CaO	1.08	2.07	1.28
Na ₂ O	2.80	2.63	2.94
K ₂ O	5.99	5.45	5.73
P ₂ O ₅	0.09	0.08	0.08
Total	99.50	99.26	99.37

TRACE ELEMENTS

Rb	192	127	253
Sr	175	101	128
Ba	670	1074	512
Zr	200	709	318
Y	26	82	45
Nb	15	24	17
Ga	16	21	23
Ce	135	173	158
Li	NA	8	NA

MOLECULAR NORMS

qz	28.94	25.78	27.57
or	36.09	33.27	34.59
ab	25.64	24.40	26.97
an	4.87	7.01	5.96
hy	2.62	5.07	3.48
di	0.00	2.45	0.00
il	0.40	0.88	0.46
mt	0.36	0.97	0.48
co	0.89	0.00	0.32
ap	0.19	0.17	0.17

NA Not analyzed
 ND Not detected

TABLE 1D
GEOCHEMISTRY OF UNIT TH GNEISSES
MAJOR ELEMENTS

Sample	BMC70	BMS23	BMS24K	BMS24P	BMS25	BMS27	avg BM	MKB07B	MKB70A
Quad	BM	BM	BM	BM	BM	BM	BM	MK	MK
SiO ₂	59.75	62.01	59.39	63.16	64.04	63.06	61.90	69.77	73.08
TiO ₂	1.73	1.33	1.42	1.41	1.12	1.14	1.36	0.65	0.65
Al ₂ O ₃	13.79	13.76	14.25	14.13	13.40	13.66	13.83	13.27	12.44
Fe ₂ O ₃	8.83	8.85	9.15	8.90	8.88	8.68	8.88	5.25	3.66
FeO	1.82	0.86	1.07	1.26	0.43	0.36	0.97	0.80	1.13
MnO	0.19	0.14	0.14	0.13	0.11	0.13	0.14	0.07	0.02
MgO	1.70	1.38	1.32	1.13	0.47	1.26	1.21	0.35	0.10
CaO	3.58	2.03	2.42	2.90	1.50	1.22	2.28	2.39	0.45
Na ₂ O	4.20	3.04	2.93	5.15	2.75	3.15	3.54	2.10	1.75
K ₂ O	3.16	5.66	6.55	1.29	6.96	6.60	5.04	5.33	6.03
P ₂ O ₅	0.51	0.37	0.41	0.39	0.28	0.29	0.38	0.15	0.08
Total	99.26	99.43	99.05	99.85	99.94	99.55	99.51	100.13	99.39

TRACE ELEMENTS

Rb	63	183	198	45	250	242	164	195	149
Sr	297	227	224	238	138	104	205	82	140
Ba	405	606	981	229	684	652	593	674	800
Zr	560	499	587	563	557	568	556	480	418
Y	95	100	92	88	111	104	98	61	37
Nb	25	21	23	27	24	25	24	15	16
Ga	21	32	34	34	27	30	30	20	16
Ce	149	144	136	145	152	162	148	120.8	75
Li	15	27	NA	NA	19	90	38	45	44

MOLECULAR NORMS

qz	9.89	12.04	6.57	15.60	13.38	10.83	11.39	27.50	35.22
or	19.27	34.59	40.14	7.80	42.46	40.13	30.69	32.49	37.08
ab	38.92	28.23	27.29	47.33	25.50	29.11	32.76	19.45	16.36
an	9.75	7.43	6.63	11.90	3.78	3.75	7.21	11.22	1.78
hy	12.71	13.01	12.32	12.69	9.54	12.04	12.05	7.02	4.91
di	4.12	0.39	2.44	0.17	1.61	0.43	1.52	0.00	0.00
il	2.49	1.92	2.05	2.01	1.61	1.63	1.95	0.93	0.94
mt	1.76	1.59	1.68	1.65	1.52	1.47	1.61	0.99	0.80
co	0.00	0.00	0.00	0.00	0.00	0.00	0.00	0.07	2.74
ap	1.10	0.80	0.89	0.83	0.60	0.62	0.81	0.32	0.17

NA Not analyzed
ND Not detected

TABLE 1D (continued)
GEOCHEMISTRY OF UNIT TH GNEISSES

MAJOR ELEMENTS

Sample	MKB70B	MKB190	MKB273	MKC021A	MKJ01	MKS36	MKS79A	MKS79C	MKS80
Quad	MK	MK	MK	MK	MK	MK	MK	MK	MK
SiO ₂	61.81	68.88	69.55	71.89	69.28	59.78	61.63	73.68	73.81
TiO ₂	0.92	0.69	0.72	0.67	0.64	0.82	0.90	0.74	0.85
Al ₂ O ₃	14.25	13.46	13.16	11.22	13.11	14.90	14.92	10.93	11.04
Fe ₂ O ₃	5.66	4.84	5.76	4.73	5.24	5.98	7.45	4.69	4.76
FeO	1.85	1.09	NA	NA	0.75	1.44	NA	NA	NA
MnO	0.12	0.04	0.07	0.06	0.06	0.11	0.08	0.05	0.02
MgO	2.67	0.29	0.47	0.48	0.27	3.18	1.56	0.46	0.31
CaO	4.54	0.95	0.95	2.82	1.44	4.23	1.02	1.53	0.44
Na ₂ O	2.30	2.35	3.69	1.80	4.40	2.24	1.64	1.59	1.91
K ₂ O	4.90	7.56	5.57	5.16	4.23	6.09	9.57	4.84	6.44
P ₂ O ₅	0.17	0.19	0.15	0.11	0.17	0.18	0.22	0.11	0.09
Total	99.19	100.34	100.09	98.94	99.59	98.95	98.99	98.62	99.67

TRACE ELEMENTS

Rb	183	230	173	177	122	255	325	151	226
Sr	162	121	95	106	150	210	161	139	66
Ba	599	903	577	678	513	538	1431	995	695
Zr	360	488	447	535	414	252	390	570	526
Y	52	55	51	75	76	59	53	69	61
Nb	17	14	17	25	27	15	17	21	29
Ga	18	19	24	21	21	24	26	20	17
Ce	107	111	NA	NA	123	121	NA	NA	NA
Li	106	18	NA	46	16	90	NA	NA	NA

MOLECULAR NORMS

qz	13.46	20.24	20.51	33.17	20.70	7.41	7.49	39.11	33.41
or	29.80	45.67	33.49	31.92	25.49	36.89	58.38	30.16	39.50
ab	21.26	21.58	33.72	16.92	40.30	20.63	15.21	15.06	17.81
an	14.50	3.55	2.95	7.64	3.60	12.94	3.74	7.25	1.66
hy	12.02	6.44	6.40	3.36	5.62	13.45	11.59	5.68	5.03
di	6.03	0.00	0.68	5.01	2.04	5.90	0.00	0.00	0.00
il	1.32	0.98	1.02	0.98	0.91	1.17	1.29	1.09	1.23
mt	1.25	0.97	0.92	0.78	0.97	1.22	1.21	0.78	0.78
co	0.00	0.16	0.00	0.00	0.00	0.00	0.60	0.64	0.39
ap	0.37	0.41	0.32	0.24	0.36	0.39	0.47	0.24	0.20

NA Not analyzed
 ND Not detected

TABLE 1D (continued)
GEOCHEMISTRY OF UNIT TH GNEISSES

MAJOR ELEMENTS

Sample OFB113	avg MK	
Quad	MK	MK
SiO ₂	75.17	69.03
TiO ₂	0.84	0.76
Al ₂ O ₃	10.32	12.75
Fe ₂ O ₃	3.51	5.13
FeO	0.54	1.09
MnO	0.10	0.07
MgO	0.59	0.89
CaO	3.75	2.04
Na ₂ O	2.56	2.36
K ₂ O	1.22	5.58
P ₂ O ₅	0.13	0.15
Total	98.73	99.84

TRACE ELEMENTS

Rb	24	199
Sr	107	130
Ba	534	764
Zr	361	444
Y	34	59
Nb	17	19
Ga	9	21
Ce	73	110
Li	28	52

MOLECULAR NORMS

qz	45.02	22.76
or	7.58	36.29
ab	24.17	21.63
an	13.74	7.44
hy	3.34	8.46
di	3.95	0.96
il	1.23	1.07
mt	0.68	1.06
co	0.00	0.00
ap	0.2	0.32

NA Not analyzed
 ND Not detected

TABLE 1E
GEOCHEMISTRY OF MAFIC ROCKS AND ANORTHOSITE

MAJOR ELEMENTS

Sample	NFS22	OFC69	RLS134	WCA30B	BES06*	BLS06C*	BMS40	BMT08B	NFI15A
Unit	AM	AM	BL	CM	GA	GA	GA	GA	GA
SiO ₂	51.67	49.09	43.08	46.59	50.44	47.75	50.45	48.05	46.61
TiO ₂	2.8	0.44	2.33	1.13	1.74	3.58	3.15	3.46	2.23
Al ₂ O ₃	14.38	15.71	13.27	13.76	15.18	12.16	13.35	13.16	17.96
Fe ₂ O ₃	14.72	10.7	17.34	10.67	12.61	1.08	16.63	16.65	13.3
FeO	NA	NA	NA	NA	NA	14.6	NA	NA	NA
MnO	0.21	0.15	0.2	0.19	0.2	0.23	0.34	0.24	0.19
MgO	2.83	9.76	8.78	7.8	6.49	4.03	4.07	4.18	4.5
CaO	6.09	10.71	10.22	13.87	9.75	8.24	5.62	7.92	8.25
Na ₂ O	3.64	2.44	0.44	1.84	2.83	2.63	3.98	3.46	3.46
K ₂ O	2.83	0.39	3.44	1.8	0.77	3.02	1.44	2.18	1.83
P ₂ O ₅	0.4	0.06	0.18	0.09	0.12	0.63	0.52	0.63	0.27
Total	99.57	99.45	99.28	97.74	100.13	97.95	99.55	99.93	98.6

TRACE ELEMENTS

Rb	83	3	111	86	15	97	26	82	34
Sr	264	200	304	519	289	201	128	239	396
Ba	566	62	266	341	161	446	361	354	335
Zr	386	41	101	72	90	299	259	248	145
Y	80	25	32	21	26	64	80	57	43
Nb	16	1.4	4	3	3	12	9	9	8
Ga	27	17	26	17	23	24	26	25	26
Ce	106	NA	19	NA	NA	74	62	NA	NA
Cr	ND	523	74	196	115	ND	64	ND	ND
Ni	ND	158	38	59	40	24	15	ND	23
V	115	125	434	266	226	307	265	267	202

MOLECULAR NORMS

qz	0.00	0.00	0.00	0.00	0.00	0.00	0.00	0.00	0.00
or	17.40	2.32	19.38	11.01	4.63	18.83	8.88	13.42	11.18
ab	34.02	22.02	0.00	6.86	25.89	24.92	37.30	32.14	25.62
an	15.14	30.93	25.21	24.83	26.94	13.15	14.94	14.53	29.02
hy	14.33	10.07	0.00	0.00	18.17	3.25	21.14	0.00	0.00
di	10.88	17.68	21.32	36.66	17.23	20.52	8.50	17.70	9.18
ol	0.90	14.56	23.44	10.93	2.39	9.81	0.80	12.96	15.15
ne	0.00	0.00	2.48	6.15	0.00	0.00	0.00	0.13	3.90
lc	0.00	0.00	1.52	0.00	0.00	0.00	0.00	0.00	0.00
il	4.06	0.62	3.40	1.63	2.47	5.26	4.58	5.02	3.21
mt	2.40	1.69	2.85	1.73	2.01	2.87	2.72	2.72	2.16
ap	0.87	0.13	0.39	0.19	0.26	1.39	1.13	1.37	0.58

NA Not analyzed

ND Not detected

TABLE 1E (continued)**GEOCHEMISTRY OF MAFIC ROCKS AND ANORTHOSITE****MAJOR ELEMENTS**

Sample	NFS35A	NFS35B	NFS38	NFS39	OFC89	RLD171	RLS82B	WCS57B	BLS09
Unit	GA	GA	GA	GA	GA	GA	GA	GA	JA
SiO ₂	45.38	53.15	48.28	50.79	47.49	44.86	52.30	47.27	57.43
TiO ₂	2.88	2.31	1.89	1.38	2.58	3.05	2.79	1.43	1.80
Al ₂ O ₃	14.26	14.21	14.63	17.03	14.24	15.10	14.41	13.64	14.24
Fe ₂ O ₃	17.63	13.90	14.21	12.29	15.25	16.94	13.44	14.60	2.12
FeO	NA	NA	NA	NA	NA	NA	NA	NA	8.57
MnO	0.26	0.26	0.21	0.17	0.23	0.23	0.19	0.21	0.13
MgO	5.82	4.02	6.07	6.99	5.63	5.83	3.23	8.05	1.39
CaO	8.53	6.39	8.22	9.34	9.52	9.71	7.16	8.85	5.39
Na ₂ O	3.32	4.17	4.11	3.96	3.38	3.15	4.10	2.69	3.07
K ₂ O	1.72	1.81	1.71	1.04	0.84	1.27	2.30	2.29	3.42
P ₂ O ₅	0.29	0.27	0.20	0.11	0.50	0.24	0.49	0.16	0.61
Total	100.09	100.49	99.53	103.10	99.66	100.38	100.41	99.19	98.17

TRACE ELEMENTS

Rb	54	37	51	13	8	12	50	122	70
Sr	303	278	249	310	219	235	249	134	278
Ba	320	402	184	114	138	139	449	139	694
Zr	157	251	123	92	170	134	330	202	426
Y	46	50	32	28	49	29	62	41	82
Nb	6	12	4	5	6	7	12	7	19
Ga	24	24	18	20	22	24	25	24	27
Ce	NA	NA	NA	32	NA	30	NA	37	95
Cr	ND	ND	45	82	95	130	50	383	ND
Ni	36	28	28	103	31	33	15	51	ND
V	257	167	222	201	266	398	216	282	91

MOLECULAR NORMS

qz	0.00	0.00	0.00	0.00	0.00	0.00	0.00	0.00	10.39
or	10.50	10.92	10.29	5.99	5.13	7.72	13.91	13.87	21.16
ab	20.84	38.22	26.32	29.87	31.35	19.16	37.70	18.06	28.86
an	19.55	15.02	16.73	24.97	21.91	24.00	14.46	18.84	15.68
hy	0.00	16.59	0.00	0.00	1.19	0.00	8.70	0.00	11.52
di	17.77	12.44	18.79	15.59	18.81	19.18	14.91	20.08	6.52
ol	17.75	0.73	15.72	16.75	14.35	16.35	3.13	20.40	0.00
ne	5.97	0.00	6.76	2.87	0.00	5.97	0.00	4.02	0.00
lc	0.00	0.00	0.00	0.00	0.00	0.00	0.00	0.00	0.00
il	4.14	3.28	2.68	1.87	3.71	4.37	3.98	2.04	2.63
mt	2.86	2.22	2.27	1.88	2.47	2.73	2.16	2.35	1.91
ap	0.63	0.58	0.43	0.22	1.08	0.52	1.05	0.34	1.34

NA Not analyzed

ND Not detected

TABLE 1E (continued)
GEOCHEMISTRY OF MAFIC ROCKS AND ANORTHOSITE

MAJOR ELEMENTS

Sample	BMC15	BMC25	BMS52	BMX304	BMX03	MKS27	NFC04	RLS53	RLS77B
Unit	JA	JA	JA	JA	JA	JA	JA	JA	JA
SiO ₂	54.02	53.59	54.29	53.99	51.54	52.64	57.82	59.03	55.77
TiO ₂	1.13	1.01	0.71	2.38	0.91	2.57	0.91	1.85	2.14
Al ₂ O ₃	20.43	23.34	24.45	16.97	22.94	16.02	20.16	14.24	15.05
Fe ₂ O ₃	1.76	1.05	3.15	1.08	5.09	4.84	1.54	3.45	2.50
FeO	4.85	3.55	NA	8.24	NA	7.64	3.63	6.68	8.96
MnO	0.10	0.06	0.03	0.13	0.07	0.18	0.11	0.13	0.16
MgO	2.25	0.96	1.34	2.73	2.22	2.11	1.77	1.69	2.02
CaO	8.61	10.25	8.30	7.43	9.73	8.09	7.33	5.88	6.61
Na ₂ O	3.62	4.27	4.87	3.29	4.37	2.86	3.61	2.81	3.14
K ₂ O	1.70	0.97	1.33	2.26	1.32	1.47	1.82	3.02	2.74
P ₂ O ₅	0.21	0.18	0.11	0.37	0.17	0.74	0.21	0.60	0.70
Total	98.68	99.23	98.58	98.87	98.36	99.15	98.91	99.36	99.76

TRACE ELEMENTS

Rb	44	5	13	35	24	20.5	29	67	48.5
Sr	550	609	674	444	538	387.5	402	302.5	336.5
Ba	231	216	230	674	198	413	222	664.5	628
Zr	156	129	66	291	83	415.5	124	398	442
Y	33	18	12	41	13	69	70	68	77
Nb	9	9	3	18	3	18.5	21	17	18.5
Ga	22	21	24	25	21	25	22	24.5	26
Ce	50	24	NA	52	16	93	103	94	117
Cr	62	ND	ND	ND	47	ND	ND	ND	ND
Ni	ND	ND	ND	ND	ND	ND	ND	ND	ND
V	108	80	31	144	63	157.5	90	101	124

MOLECULAR NORMS

qz	3.12	1.56	0.06	4.79	0.00	7.65	9.18	13.83	7.70
or	10.20	5.74	7.84	13.70	7.86	9.06	10.90	18.48	16.64
ab	33.00	38.42	43.65	30.32	36.59	26.75	32.85	26.12	28.99
an	35.01	41.75	40.39	25.52	39.37	27.71	33.88	18.01	19.47
hy	9.92	3.53	6.15	11.96	0.00	14.02	9.31	11.30	12.95
di	5.58	6.43	0.00	7.87	6.51	7.28	1.27	6.53	7.68
ol	0.00	0.00	0.00	0.00	5.47	0.00	0.00	0.00	0.00
ne	0.00	0.00	0.00	0.00	1.76	0.00	0.00	0.00	0.00
lc	0.00	0.00	0.00	0.00	0.00	0.00	0.00	0.00	0.00
il	1.60	1.41	0.99	3.40	1.28	3.74	1.28	2.67	3.06
mt	1.14	0.78	0.49	1.65	0.80	2.18	0.89	1.77	2.01
ap	0.45	0.38	0.23	0.79	0.36	1.61	0.44	1.30	1.50

NA Not analyzed

ND Not detected

TABLE 1E (continued)
GEOCHEMISTRY OF MAFIC ROCKS AND ANORTHOSITE

MAJOR ELEMENTS

Sample	RLS90	RLU48	OFS39	WCB83	OFF29C	MKB111	MKS96
Unit	JA	JA	KZA	KZA	LD	MU	MU
SiO ₂	54.84	56.41	48.00	47.87	45.39	44.60	42.88
TiO ₂	0.86	2.24	0.39	1.67	3.34	2.34	2.38
Al ₂ O ₃	19.95	14.02	23.52	16.39	14.67	13.78	13.85
Fe ₂ O ₃	5.29	4.85	6.95	13.47	15.54	16.41	17.08
FeO	NA	7.32	NA	NA	NA	NA	NA
MnO	0.09	0.16	0.08	0.19	0.39	0.18	0.13
MgO	2.71	1.74	6.98	8.14	5.47	7.15	9.19
CaO	9.41	6.10	11.10	10.37	8.18	9.56	7.70
Na ₂ O	4.90	2.78	2.17	1.51	3.98	2.95	2.06
K ₂ O	1.06	2.69	0.40	0.40	1.70	1.38	2.09
P ₂ O ₅	0.12	0.72	0.09	0.35	0.46	0.20	0.18
Total	99.23	99.03	99.68	100.36	99.12	98.55	97.54

TRACE ELEMENTS

Rb	11	61	10	4	40	23	79
Sr	480	276	370	202	112	381	261
Ba	157	585	81	68	78	130	454
Zr	70	424	24	59	217	117	92
Y	16	88	6	23	66	37	39
Nb	4	21	2	2	12	4	4
Ga	19	25	17	20	23	20	20
Ce	NA	124	6	NA	NA	NA	37
Cr	50	ND	51	63	63	88	77
Ni	ND	ND	91	69	59	35	30
V	78	152	27	258	195	427	441

MOLECULAR NORMS

qz	0.00	11.60	0.00	0.10	0.00	0.00	0.00
or	6.25	16.65	2.35	2.41	10.39	8.49	13.00
ab	43.93	26.15	19.41	13.85	23.04	17.26	14.55
an	29.27	18.68	53.05	37.55	17.73	21.13	23.53
hy	3.58	13.48	12.29	30.67	0.00	0.00	0.00
di	13.25	6.48	0.97	10.13	16.91	21.54	12.30
ol	1.44	0.00	10.11	0.00	15.26	18.87	26.07
ne	0.00	0.00	0.00	0.00	8.35	6.20	2.92
lc	0.00	0.00	0.00	0.00	0.00	0.00	0.00
il	1.20	3.27	0.54	2.38	4.81	3.40	3.49
mt	0.83	2.13	1.09	2.16	2.52	2.68	3.75
ap	0.25	1.58	0.19	0.75	0.99	0.44	0.40

NA Not analyzed

ND Not detected

TABLE 1F (continued)
GEOCHEMISTRY OF METASEDIMENTARY ROCKS

MAJOR ELEMENTS

Sample	RLC022	RLS135	WCH12	BMB81	BMS21	MKD23C	MKC23D	MKC01	MKC022
Unit	BL	BL	KZA	MU	MU	MU	MU	TH	TH
SiO ₂	68.52	64.77	66.95	80.36	73.64	57.54	84.24	75.49	77.62
TiO ₂	1.65	0.43	1.10	0.33	0.22	0.53	0.22	0.43	0.32
Al ₂ O ₃	16.26	4.46	15.05	7.73	14.13	9.88	7.72	7.89	7.34
Fe ₂ O ₃	6.47	3.41	5.09	2.79	0.01	0.54	0.88	2.90	2.59
FeO	NA	NA	NA	NA	1.57	2.69	NA	NA	NA
MnO	0.02	0.08	0.01	0.08	0.03	0.18	0.02	0.07	0.07
MgO	2.59	15.94	2.55	0.76	0.15	7.42	0.21	0.50	0.61
CaO	0.18	5.27	2.03	1.31	1.00	12.98	0.43	6.47	7.73
Na ₂ O	0.07	0.07	4.21	0.19	3.14	0.60	0.12	0.21	1.02
K ₂ O	3.74	2.07	2.28	6.04	5.51	6.87	5.80	3.97	0.32
P ₂ O ₅	0.17	0.08	0.06	0.07	0.14	0.09	0.07	0.06	0.06
Total	99.67	96.58	99.33	99.66	99.54	99.66	99.71	97.99	97.68

TRACE ELEMENTS

Rb	98	40	121	125	237	195	162	131	13
Sr	35	27	254	105	98	644	149	86	70
Ba	446	376	321	422	301	2643	997	484	75
Zr	268	76	292	197	141	167	128	228	227
Y	37	13	27	30	46	33	16	46	35
Nb	19	5	12	12	16	9	11	16	12
Ga	22	5	22	6	20	10	5	11	13
Ce	NA	17	NA	62	98	88	43	96	NA
Li	NA	NA	36	12	60	NA	10	30	NA

NA Not analyzed

ND Not detected

TABLE 1F (continued)
GEOCHEMISTRY OF METASEDIMENTARY
ROCKS

MAJOR ELEMENTS

Sample	MKD49	MKS82E
Unit	TH	TH
SiO ₂	68.29	75.35
TiO ₂	0.61	0.53
Al ₂ O ₃	8.02	9.00
Fe ₂ O ₃	2.82	3.98
FeO	1.08	NA
MnO	0.07	0.05
MgO	4.76	0.92
CaO	8.69	3.44
Na ₂ O	0.51	1.17
K ₂ O	4.48	4.74
P ₂ O ₅	0.10	0.08
Total	99.43	99.26

TRACE ELEMENTS

Rb	123	162
Sr	148	90
Ba	445	535
Zr	249	371
Y	32	59
Nb	13	20
Ga	13	16
Ce	56	NA
Li	NA	NA

NA Not analyzed
 ND Not detected

TABLE 2
ELECTRON MICROPROBE MINERAL ANALYSES

ORTHOPYROXENE			ORTHOPYROXENE			
Metasedimentary units			Metaigneous units			
Sample	RLJ26-2	WCE91	RLS45	WCS33	MKU05	MKS27
Unit	CM	CM	CG	CG	CG	JA
Spots	1	1	3	5	4	3
SiO ₂	58.66	58.66	46.54	46.99	46.88	48.17
TiO ₂	0.03	0.00	0.08	0.11	0.09	0.06
Al ₂ O ₃	0.61	0.88	0.37	0.22	0.29	0.73
FeO	5.68	3.91	45.76	46.01	46.43	37.48
MnO	0.29	0.27	1.31	1.41	1.30	0.98
MgO	35.19	36.24	4.13	4.90	4.49	11.87
CaO	0.42	0.33	0.84	0.80	0.96	0.91
Na ₂ O	0.00	0.00	0.00	0.00	0.00	0.01
Total	100.89	100.31	99.03	100.44	100.44	100.21

CLINOPYROXENE									
Metasedimentary units									
Sample	RLJ26-2	RLC01-2	WCE91	BLS10B	BLS10H	MKD23C	MKB124	PLS03	MKD48
Unit	CM	CM	CM	CM	CM	MU	MU	MU	TH
Spots	4	1	1	1	2	2	3	1	2
SiO ₂	55.89	55.11	54.87	50.90	52.86	52.13	56.16	52.53	52.95
TiO ₂	0.03	0.03	0.17	0.04	0.00	0.12	0.03	0.07	0.01
Al ₂ O ₃	0.79	0.63	2.26	2.00	1.24	1.55	0.61	1.04	1.54
FeO	1.46	5.29	1.06	11.15	9.79	5.87	2.34	10.48	3.34
MnO	0.12	0.10	0.14	0.33	0.41	0.38	0.24	0.15	0.24
MgO	17.88	14.80	17.44	10.53	12.15	14.48	17.01	11.68	16.07
CaO	24.34	24.95	24.07	24.30	23.94	24.73	24.82	24.69	25.36
Na ₂ O	0.27	0.17	0.22	0.56	0.10	0.35	0.16	0.37	0.27
Total	100.78	101.30	100.24	99.81	100.46	99.61	101.38	101.01	99.76

CLINOPYROXENE					FAYALITE	
Metaigneous units					Metaigneous units	
Sample	OFY01	WCS33	MKU05	MKS27	OFY01	
Unit	CG	CG	CG	JA	CG	
Spots	3	3	2	2	3	
SiO ₂	47.81	49.10	48.58	48.54	29.98	
TiO ₂	0.22	0.15	0.17	0.24	0.00	
Al ₂ O ₃	0.82	0.93	0.98	2.03	0.00	
FeO	29.25	24.86	25.31	17.86	68.49	
MnO	0.93	0.64	0.60	0.42	1.78	
MgO	1.48	4.27	3.91	9.16	0.94	
CaO	19.51	20.11	20.24	19.93	0.02	
Na ₂ O	0.54	0.64	0.39	0.34	0.00	
Total	100.56	100.70	100.18	98.52	101.21	

TABLE 2 (continued)
ELECTRON MICROPROBE MINERAL ANALYSES

PHLOGOPITE				GARNET			
Sample	RLJ26-2	MKB124	WCE91	WCH32	BLS10H	MKB48	MKB48
Unit	CM	MU	CM	CM	CM	TH	TH
spots	3	2	2	1	4	1	1
SiO ₂	43.52	44.53	41.01	38.55	38.23	37.59	35.77
TiO ₂	1.78	0.39	2.31	0.29	0.65	0.22	0.88
Al ₂ O ₃	14.44	12.21	14.21	19.32	17.01	18.59	9.67
FeO	2.45	2.71	1.70	4.32	8.10	5.16	15.43
MnO	0.02	0.02	0.05	0.22	0.38	0.39	0.15
MgO	25.02	26.16	25.28	0.22	0.24	0.18	0.34
CaO	0.02	0.00	0.03	35.49	33.93	36.65	34.23
Na ₂ O	0.16	0.17	0.03	0.00	0.00	0.00	0.00
K ₂ O	9.58	9.83	10.03	0.00	0.00	0.00	0.00
F	1.20	4.86	1.27				
Total	98.19	100.86	95.92	98.41	98.52	98.78	96.47
				Rim on Scapolite		Rim on Scapolite	Porphy- roblast
SCAPOLITE							
Sample	BLS10B	BLS10F	RLC01-2	PLS03	RLS126	MKD48	
Unit	CM	CM	CM	MU	MU	TH	
spots	2	3	2	3	6	2	
SiO ₂	43.89	44.94	46.03	46.03	50.96	43.22	
Al ₂ O ₃	27.91	27.71	27.09	27.17	25.36	28.53	
FeO	0.10	0.12	0.03	0.07	0.10	0.08	
CaO	19.41	18.82	18.08	17.93	14.03	20.26	
Na ₂ O	2.64	2.93	3.09	3.58	5.10	1.88	
K ₂ O	0.13	0.16	0.15	0.17	0.90	0.15	
SO ₃	0.00	0.07	0.00	0.67	0.09	0.00	
Cl	0.02	0.07	0.08	0.18	1.46	0.00	
Total	94.10	94.81	94.54	95.80	98.01	94.12	
EqAn	0.68	0.71	0.64	0.64	0.48	0.75	
FELDSPARS							
Sample	MKD23	RLS126	RLC01-2				
Unit	MU	MU	CM				
spots	3	6	1				
SiO ₂	63.55	59.52	65.79				
Al ₂ O ₃	19.14	26.20	19.05				
FeO	0.02	0.13	0.01				
CaO	0.00	8.56	0.26				
Na ₂ O	0.84	6.69	0.69				
K ₂ O	15.25	0.28	14.39				
BaO	0.89	NA	NA				
Total	99.68	101.38	100.19				
	Kfs	Pl	Kfs				

TABLE 3
VARIMAX ROTATED Q-MODE FACTORS (UNITS CG and GA)

MJOR ELEMENTS				MOLECULAR NORMS			
	Q1	Q2	Q3		Q1	Q2	Q3
SiO ₂	55.11	74.71	72.19	qz	1.88	30.54	22.16
TiO ₂	1.80	0.26	0.22	or	30.06	35.41	30.97
Al ₂ O ₃	14.89	12.51	15.52	ab	29.24	25.85	37.83
FeO _{Tot}	13.21	2.70	0.75	an	12.22	4.16	5.89
MnO	0.21	0.04	0.01	hy	13.45	2.85	1.83
MgO	1.01	0.00	0.44	di	7.05	0.28	0.00
CaO	4.81	0.92	1.24	il	2.58	0.38	0.31
Na ₂ O	3.16	2.82	4.22	mt	2.37	0.48	0.13
K ₂ O	4.94	5.88	5.25	co	0.00	0.00	0.79
P ₂ O ₅	0.53	0.02	0.04	ap	1.15	0.05	0.08
TRACE ELEMENTS							
Rb	0	238	136				
Sr	232	73	232				
Ba	1657	450	527				
Zr	1264	406	164				
Y	132	90	0				
Nb	37	25	10				
Ga	24	23	20				

TABLE 3. Results of Q-mode factor analysis using the program G-QFAC (Miesch, 1976); data from units CG and GA. Major element oxides in weight percentage, trace elements in ppm, normative minerals in mole percentage.

TABLE 4
COMPARATIVE GEOCHEMISTRY OF MAFIC SUITES

	Suite Averages				
	Map Area n = 27	Adk. HP n = 78	KEW n = 20	SUO n = 30	CSR n = 31
SiO ₂	49.71	48.28	50.00	49.02	51.16
TiO ₂	2.28	2.68	1.79	2.55	2.41
Al ₂ O ₃	14.71	14.85	15.26	15.17	14.83
Fe ₂ O ₃	14.11	14.78	12.35	14.96	14.04
MnO	0.21	0.20	0.17	0.19	0.20
MgO	5.20	6.04	5.57	4.29	5.40
CaO	8.29	9.09	8.45	7.41	9.06
Na ₂ O	3.06	2.73	3.02	2.62	2.74
K ₂ O	1.87	1.07	1.10	1.62	1.04
P ₂ O ₅	0.38	0.63	0.26	0.65	0.51
Rb	47	20	33	52	22
Sr	278	323	316	344	301
Ba	329	336	356	624	557
Zr	224	188	201	255	280
Y	50	44		55	
Nb	10	11	16	22	
Ga	23	22			
Cr	82	90	184	40	
Ni	43	60	107	29	
V	222	195			

MOLECULAR NORMS

	Map Area	Adk. HP	KEW	SUO	CSR
qz	0.00	0.00	0.00	1.82	2.14
or	11.01	7.46	6.77	10.08	6.24
ab	28.14	25.21	28.25	24.80	25.03
an	22.80	24.50	25.88	26.28	25.58
hy	9.92	17.47	20.71	22.89	20.80
di	14.14	13.09	12.83	6.48	13.46
ol	7.97	3.77	0.37	0.00	0.00
il	3.08	4.27	2.59	3.75	3.42
mt	2.21	2.55	2.02	2.48	2.24
co	0.00	0.00	0.00	0.00	0.00
ap	0.75	1.69	0.57	1.42	1.08
mg	0.422	0.447	0.457	0.360	0.428

KEW Keweenawan mafics; Basaltic Volcanism Study Project (1981)
 SUO Suomenniemi Dikes; Ramo (1991)
 CSR Columbia-Snake River Lavas; Carlson and Hart (1988)

TABLE 4. Comparison of average major- and trace-element contents of mafic rocks from the map area (W Adks.) with those from the High Peaks region (Adk. HP); the Keweenawan (KEW, from Basaltic Volcanism Study Project, 1981) and Columbia River–Snake River Plain (CSR, from Carlson and Hart, 1988) tholeiitic flood basalts; and the Suomenniemi Dike Swarm (SUO, from Ramo, 1991).

TABLE 5
LAKEWATER pH AND CHEMISTRY BY BEDROCK MAP UNIT

Unit	BG		BM		CG		GA		KZB		LD	
N	3		29		148		53		10		10	
	Mean	S.D.	Mean	S.D.	Mean	S.D.	Mean	S.D.	Mean	S.D.	Mean	S.D.
pH	5.98	0.41	5.28	0.71	5.08	0.74	5.48	0.87	4.37	0.15	5.61	0.90
ANC	32	35	8	50	2	55	28	71	-49	20	17	45
DIC	1.17	0.65	0.90	1.25	1.04	1.17	1.26	1.34	0.86	0.64	1.14	1.12
DOC	5.47	3.35	5.43	3.47	6.24	3.99	7.95	4.68	7.79	3.15	8.58	3.77
SiO ₂	4.27	1.10	1.84	1.96	1.76	2.21	2.44	2.06	0.95	0.86	2.51	2.58
Ca	1.63	0.59	1.57	0.60	1.33	0.77	1.96	1.26	0.82	0.15	1.96	0.85
Mg	0.44	0.12	0.32	0.15	0.27	0.17	0.35	0.16	0.21	0.05	0.43	0.20
Na	0.63	0.13	0.54	0.27	0.47	0.32	0.52	0.21	0.28	0.05	0.60	0.30
K	0.24	0.02	0.31	0.12	0.26	0.16	0.27	0.12	0.16	0.18	0.21	0.09
NH ₄	0.02	0.02	0.03	0.04	0.05	0.11	0.04	0.16	0.01	0.03	0.01	0.02
ALIM	30	14	82	51	96	57	66	49	145	68	52	34
SO ₄	4.96	0.50	5.43	0.98	5.04	1.13	4.91	1.44	5.47	0.73	5.75	1.32
NO ₃	0.17	0.19	0.08	0.14	0.07	0.14	0.03	0.05	0.01	0.03	0.03	0.08
Cl	0.33	0.05	0.26	0.10	0.27	0.33	0.27	0.14	0.31	0.33	0.27	0.13
F	0.05	0.00	0.09	0.04	0.07	0.04	0.08	0.04	0.04	0.01	0.06	0.02

Unit	BL		CM		KZA		MU		TH		AM	
N	5		8		24		67		5		1	
	Mean	S.D.	Mean	S.D.	Mean	S.D.	Mean	S.D.	Mean	S.D.		
pH	6.39	1.27	6.73	0.85	5.39	0.97	6.11	0.98	6.72	0.49		5.84
ANC	105	115	143	117	18	74	69	97	90	33		13
DIC	2.35	0.78	2.23	1.12	0.82	0.70	1.24	1.29	1.45	0.25		0.54
DOC	7.79	3.82	5.58	2.80	5.82	2.24	5.60	3.14	6.87	3.11		4.00
SiO ₂	2.47	2.43	2.65	1.49	1.34	1.09	2.56	2.31	2.80	1.89		1.00
Ca	3.58	2.51	4.11	1.97	1.66	1.22	2.62	1.99	2.81	1.26		1.61
Mg	0.54	0.30	0.52	0.12	0.36	0.20	0.47	0.28	0.53	0.23		0.26
Na	1.48	1.88	0.54	0.20	0.43	0.17	1.65	5.30	1.50	1.37		0.42
K	0.38	0.28	0.29	0.09	0.25	0.34	0.35	0.13	0.35	0.12		0.17
NH ₄	0.02	0.02	0.03	0.06	0.06	0.10	0.03	0.05	0.05	0.06		0.00
ALIM	16	15	39	55	101	81	34	42	62	57		3
SO ₄	4.07	1.97	5.34	0.72	5.49	0.95	5.03	1.20	4.32	1.57		4.60
NO ₃	0.14	0.28	0.02	0.04	0.03	0.06	0.11	0.18	0.05	0.07		0.14
Cl	2.71	4.93	0.30	0.08	0.51	1.26	2.37	11.07	2.26	4.50		0.20
F	0.08	0.05	0.09	0.04	0.04	0.02	0.08	0.04	0.10	0.03		0.08

TABLE 5. Comparison of means and standard deviations for water chemistry data in ponds and lakes from the map area. Data from the ALSC (1984-1986) study are classified according to the predominant or exclusive map unit in the watershed area. Composite units: GR, includes granitic units CG, GA, BG, BM, KZB, and LD. GRA, GR with till soils. GRB, GR with kame, outwash, or alluvial soils. MS includes metasedimentary units CM, MU, BL, KZA, and TH. MSA, MS with till soils. MSB, MS with kame, outwash, or alluvial soils. MW, lakes with substantial amounts of two or more map units in the watershed.

TABLE 5 (continued)
LAKEWATER pH AND CHEMISTRY BY BEDROCK MAP UNIT

Composite units (see text for explanation)

Unit	GR		GRA		GRB		MS		MSA		MSB	
N	253		212		41		109		80		29	
	Mean	S.D.	Mean	S.D.	Mean	S.D.	Mean	S.D.	Mean	S.D.	Mean	S.D.
pH	5.15	0.75	5.07	0.76	5.45	0.93	6.04	1.03	5.88	1.04	6.48	0.88
ANC	3	52	0	47	24	67	66	97	56	99	92	86
DIC	1.04	1.18	0.98	1.14	1.35	1.34	1.28	1.18	1.22	1.17	1.43	1.23
DOC	6.74	4.18	6.38	4.05	8.44	4.35	5.81	2.96	5.92	3.16	5.49	2.32
SiO ₂	1.93	2.16	1.69	1.89	3.19	2.91	2.30	2.06	2.12	1.94	2.81	2.33
Ca	1.43	0.75	1.38	0.69	1.68	0.98	2.57	1.92	2.54	2.10	2.66	1.33
Mg	0.29	0.17	0.28	0.15	0.36	0.22	0.46	0.26	0.43	0.22	0.54	0.32
Na	0.49	0.29	0.47	0.28	0.55	0.33	1.28	4.20	1.31	4.70	1.22	2.44
K	0.26	0.15	0.26	0.15	0.27	0.12	0.32	0.20	0.31	0.22	0.35	0.13
NH ₄	0.04	0.12	0.05	0.13	0.02	0.03	0.04	0.06	0.04	0.06	0.03	0.06
ALIM	88	57	94	57	59	46	48	59	61	63	21	34
SO ₄	5.09	1.21	5.22	1.19	4.34	1.20	5.08	1.21	5.26	1.15	4.57	1.24
NO ₃	0.06	0.12	0.07	0.13	0.04	0.07	0.08	0.16	0.08	0.14	0.10	0.21
Cl	0.27	0.27	0.27	0.29	0.25	0.10	1.82	8.81	1.96	9.89	1.43	4.82
F	0.07	0.04	0.07	0.03	0.09	0.05	0.07	0.04	0.07	0.04	0.08	0.04

Unit	MW		All	
N	19		382	
	Mean	S.D.	Mean	S.D.
pH	6.31	0.78	5.47	0.95
ANC	59	74	24	74
DIC	0.92	0.76	1.10	1.17
DOC	3.93	1.19	6.32	3.81
SiO ₂	3.45	1.14	2.10	2.12
Ca	2.73	1.41	1.82	1.35
Mg	0.49	0.21	0.35	0.21
Na	0.98	0.63	0.74	2.28
K	0.37	0.10	0.28	0.17
NH ₄	0.02	0.02	0.04	0.10
ALIM	34	28	74	59
SO ₄	5.53	0.88	5.10	1.19
NO ₃	0.27	0.29	0.08	0.15
Cl	0.89	1.02	0.74	4.75
F	0.07	0.02	0.07	0.04

ANC = Acid Neutralizing Capacity

ALIM = Inorganic Monomeric Aluminum

DIC = Dissolved Inorganic Carbon

DOC = Dissolved Organic Carbon

UNITS

pH	pH units
ANC	microequivalents / liter
ALIM	micrograms / liter
all others	milligrams / liter

Data from Kretser et al. (1989)

References

- ANDERSON, J.L. 1983. Proterozoic anorogenic granite plutonism of North America, p. 133-164. In Medaris, L.G. et al. (eds.), *Proterozoic Geology: Selected papers from an international symposium*. Geological Society of America Memoir 161.
- , and R.L. CULLERS. 1978. Geochemistry and evolution of the Wolf River Batholith, a Late Precambrian rapakivi massif in north Wisconsin, U.S.A. *Precambrian Research*, 7:287-324.
- , and D.R. SMITH. 1995. The effects of temperature and fO_2 on the Al-in-hornblende barometer. *American Mineralogist*, 80:549-559.
- APRIL, R.A., R.M. NEWTON, and L.T. COLES. 1986. Chemical weathering in two Adirondack watersheds: past and present-day rates. *Geological Society of America Bulletin*, 97:1232-1238.
- ASHWAL, L.D., and J.L. WOODEN. 1983. Sr and Nd isotope geochronology, geologic history and origin of the Adirondack anorthosite. *Geochimica et Cosmochimica Acta*, 47:1975-1986.
- BALSLEY, J.R., and R.W. BROMERY. 1965a. Aeromagnetic map of the Old Forge Quadrangle and part of the West Canada Lakes Quadrangle, Herkimer and Hamilton Counties, New York. U.S. Geological Survey Geophysical Investigations, Map GP-501.
- , and ———. 1965b. Aeromagnetic map of the Number Four Quadrangle, Herkimer and Lewis Counties, New York. U.S. Geological Survey Geophysical Investigations, Map GP-502.
- , and ———. 1965c. Aeromagnetic map of the Raquette Lake Quadrangle, Hamilton County, New York. U.S. Geological Survey Geophysical Investigations, Map GP-503.
- , and ———. 1965d. Aeromagnetic map of the Big Moose Quadrangle, Herkimer and Hamilton Counties, New York. U.S. Geological Survey Geophysical Investigations, Map GP-504.
- , and ———. 1965e. Aeromagnetic map of the McKeever Quadrangle and part of the Port Leyden Quadrangle, North-central New York. U.S. Geological Survey Geophysical Investigations, Map GP-510.
- BASALTIC VOLCANISM STUDY PROJECT. 1981. Basaltic volcanism on the terrestrial planets. Pergamon Press, New York. Section 1.2.2.5, p. 60-77.
- BERMAN, R.G. 1991. Thermobarometry using multi-equilibrium calculations: a new technique with petrologic applications. *Canadian Mineralogist*, 29:833-855.
- BOHLEN, S.R. 1987. Pressure-temperature-time paths and a tectonic model for the evolution of granulites. *Journal of Geology*, 95:617-632.
- , and A.L. BOETTCHER. 1981. Experimental investigations and geological applications of orthopyroxene geobarometry. *American Mineralogist*, 66:951-964.
- , J.W. VALLEY, and E.J. ESSENE. 1985. Metamorphism in the Adirondacks: I. Petrology, Pressure and Temperature. *Journal of Petrology*, 26:971-992.
- BROWN, C.E., and R.A. AYUSO. 1985. Significance of tourmaline-rich rocks in the Grenville Complex of St. Lawrence County, New York. U.S. Geological Survey Bulletin 1626-C, 33 p.
- BUDDINGTON, A.F. 1965. The origin of three garnet isograds in Adirondack gneisses. *Mineralogical Magazine*, 34:71-81.
- . 1966. The occurrence of garnet in the granulite facies terrane of the Adirondack Highlands: a discussion. *Journal of Petrology*, 7:331-335.
- , and B.F. LEONARD. 1962. Regional geology of the St. Lawrence County magnetite district, Northwest Adirondacks. U.S. Geological Survey Professional Paper 376, 145 p.

- , and D. LINDSLEY. 1964. Iron-titanium oxide minerals and synthetic equivalents. *Journal of Petrology*, 5:310-357.
- , and R. RUEDEMANN. 1934. Geology and mineral resources of the Hammond, Antwerp, and Lowville Quadrangles. New York State Museum Bulletin 296, 251 p.
- CADWELL, D.H., and D. PAIR. 1991. Surficial geologic map of New York, Adirondack Sheet. New York State Museum Map and Chart Series 40.
- CARL, J.D. 1988. Popple Hill Gneiss as dacitic volcanics: a geochemical study of mesosome and leucosome, Northwest Adirondacks, New York. *Geological Society of America Bulletin*, 100:841-849.
- , W.F. deLORRAINE, D.G. MOSE, and Y.N. SHIEH. 1990. Geochemical evidence for a revised Precambrian sequence in the northwest Adirondacks, New York. *Geological Society of America Bulletin*, 102:182-192.
- , and A.K. SINHA. 1992. Zircon U-Pb age of Popple Hill Gneiss and a Hermon-type granite gneiss, northwest Adirondack Lowlands, New York. *Geological Society of America Abstracts with Programs*, 24:11.
- CARLSON, R.W., and W.K. HART. 1988. Flood basalt volcanism in the northwestern United States, p. 35-61. In J.D. Macdougall (ed.), *Continental flood basalts*. Kluwer Academic Publishers.
- CHIARENZELLI, J.R., and J.M. McLELLAND. 1991. Age and regional relationships of granitoid rocks of the Adirondack Highlands. *Journal of Geology*, 99:571-590.
- , D.W. VALENTINO, and J.M. McLELLAND. 1999. Large-scale evidence for transpressional deformation in the central and southern Adirondacks? *Geological Society of America Abstracts with Programs*, 31:A10.
- CANNON, R.S. 1937. Geology of the Piseco Lake Quadrangle. New York State Museum Bulletin 312, 107 p.
- COISH, R.A., and C.W. SINTON. 1991. Geochemistry of mafic dikes in the Adirondack Mountains: implications for late Proterozoic continental rifting. *Contributions to Mineralogy and Petrology*, 110:500-514.
- DALE, N.C. 1935. Geology of the Oswegatchie Quadrangle. New York State Museum Bulletin 302, 101 p.
- DALY, J.S., and J.M. McLELLAND. 1991. Juvenile Middle Proterozoic crust in the Adirondack Highlands, Grenville Province, northeastern North America. *Geology*, 19:119-122.
- DARLING, R.S., and F.P. FLORENCE. 1995. Apatite light rare earth element chemistry of the Port Leyden nelsonite, Adirondack Highlands, New York: implications for the origin of nelsonite in anorthosite-suite rocks. *Economic Geology*, 90:964-968.
- , F.P. FLORENCE, G.W. LESTER, and P.R. WHITNEY. 2000. Petrogenesis of prismatine-bearing, cordierite+garnet metapelites in the western Adirondack Highlands. *Geological Society of America Abstracts with Programs*, NE32:13.
- DAVIDSON, A. 1995. A review of the Grenville Orogen in its North American type area. *AGSO Journal of Australian Geology and Geophysics*, 16:3-24.
- de la ROCHE, H., J. LETERRIER, P. GRANDCLAUDE, and M. MARCHAL. 1980. A classification of volcanic and plutonic rocks using R1-R2 diagram and major-element analyses — its relationships with current nomenclature. *Chemical Geology*, 29:183-210.
- deLORRAINE, W.F., and J. JOHNSON. 1997. Geologic field guide to the Balmat zinc mine, St. Lawrence County, New York. New York State Geological Association Field Trip Guide, 69:85-116.
- deWAARD, D. 1961. Tectonics of a metagabbro laccolith in the Adirondack Mountains, and its significance in determining top and bottom of a metamorphic series. *Proceedings Koninkl. Nederl. Akademie van Wetenschappen, Amsterdam*, B64:335-342.
- . 1962. Structural analysis of a Precambrian fold: the Little Moose Mountain Syncline in the southwestern Adirondacks. *Proceedings Koninkl. Nederl. Akademie van Wetenschappen, Amsterdam*, B65:404-417.
- . 1964. Mineral assemblages and metamorphic subfacies in the granulite-facies terrane of the Little Moose Mountain Syncline, south-central Adirondack Highlands. *Proceedings Koninkl. Nederl. Akademie van Wetenschappen, Amsterdam*, B67:344-362.
- . 1965. The occurrence of garnet in the granulite-facies terrane of the Adirondack Highlands. *Journal of Petrology*, 6:165-191.

- . 1967. The occurrence of garnet in the granulite-facies terrane of the Adirondack Highlands and elsewhere, an amplification and reply. *Journal of Petrology*, 8:210-232.
- , and W.D. ROMNEY. 1963. Boundary relationships of the Snowy Mountain anorthosite in the Adirondack Mountains: Proceedings Koninkl. Nederl. Akademie van Wetenschappen, Amsterdam, B66:251-264.
- , and ———. 1969. Chemical and petrologic trends in the anorthosite-charnockite series of the Snowy Mountain massif, Adirondack Highlands. *American Mineralogist*, 54:529-537.
- , and M. WALTON. 1967. Precambrian geology of the Adirondack Highlands, a reinterpretation. *Geologische Rundschau*, 56:596-629.
- EBY, G.N. 1992. Chemical subdivision of the A-type granitoids: petrogenetic and tectonic implications. *Geology*, 20:641-644.
- EDWARDS, K.J., and J.W. VALLEY. 1998. Oxygen isotope diffusion and zoning in diopside: the importance of water fugacity during cooling. *geochimica et Cosmochimica Acta*, 62:2265-2277.
- EKSTROM, H. 1989. Petrologic investigations of the Tomantown Batholith, southern Adirondack Mountains, New York. *Colgate Journal of Science*, 21:41-52.
- EMSLIE, R.F., and J.A.R. STIRLING. 1993. Rapakivi and related granitoids of the Nain plutonic suite: geochemistry, mineral assemblages, and fluid equilibria. *Canadian Mineralogist*, 31:821-847.
- FAKUNDINY, R.H. 1986. Trans-Adirondack structural discontinuities, p. 64-75. In Aldrich, M.J., and A.W. Laughlin (eds.), *Proceedings of the Sixth International Conference on Basement Tectonics*.
- , J. YANG, and N.K. GRANT. 1994. Tectonic subdivisions of the mid-Proterozoic Adirondack Highlands in northeastern New York. *Northeastern Geology*, 16:82-93.
- FALLON, S.P. 1990. Stratigraphy and structural geology of the Long Lake area, Adirondack Mountains, New York. Ph.D. thesis, University of Massachusetts (Amherst), 313 p. plus map.
- FLORENCE, F.P., and R.S. DARLING. 1997. Timing of intrusion, anatexis, and metamorphism in the Port Leyden area of the western Adirondacks. *New York State Geological Association Field Trip Guide*, 69:41-49.
- , R.S. DARLING, and S.E. ORRELL. 1995. Moderate pressure metamorphism and anatexis due to anorthosite intrusion, western Adirondack Highlands, New York. *Contributions to Mineralogy and Petrology*, 21:424-436.
- FROST, C.D., and B.R. FROST. 1997. Reduced rapakivi-type granites: the tholeiite connection. *Geology*, 25:647-650.
- , B.R. FROST, K.R. CHAMBERLAIN, and B.R. EDWARDS. 1999. Petrogenesis of the 1.43 Ga Sherman Batholith, SE Wyoming, USA: a reduced, rapakivi-type anorogenic granite. *Journal of Petrology*, 40:1771-1802.
- GERAGHTY, E.P. 1978. Structure, stratigraphy, and petrology of part of the Blue Mountain Lake 15' Quadrangle, central Adirondack Mountains, New York. Ph.D. thesis, Syracuse University, 186 p.
- GLENNIE, J.S. 1973. Precambrian geology of the Piseco Lake area, south-central Adirondack Mountains, New York. Ph.D. thesis, Syracuse University, 45 p.
- GREW, E.S., M.G. YATES, G.H. SWIHART, P.B. MOORE, and N. MARQUEZ. 1991. The paragenesis of serendibite at Johnsburg, New York, USA: an example of boron enrichment in the granulite facies, p. 247-285. In Perchuk, L.L. (ed.), *Progress in metamorphic and magmatic petrology*, Cambridge University Press.
- GROCOTT, J., A.A. GARDE, B. CHADWICK, A.R. CRUDEN, and C. SWAGER. 1999. Emplacement of rapakivi granite and syenite by floor depression and roof uplift in the Paleoproterozoic Ketilidian Orogen, South Greenland. *Journal of the Geological Society, London*, 156:15-24.
- HAAPALA, I., and O.T. RAMO. 1999. Rapakivi granites and related rocks: an introduction. *Precambrian Research*, 95:1-7.
- HARLEY, S.L., and I.S. BUICK. 1992. Wollastonite-scapolite assemblages as indicators of granulite pressure-temperature-fluid histories: The Rauer Group, East Antarctica. *Journal of Petrology*, 33:693-728.
- HAUER, K.L. 1995. Protoliths, diagenesis, and depositional history of the Upper Marble, Adirondack Lowlands, New York. Ph.D. thesis, Miami (Ohio) University, 281 p.
- HAWTHORNE, F.C. 1981. Crystal chemistry of the amphiboles, p. 1-95. In Veblen, D.R. (ed.), *Amphiboles and other hydrous pyriboles-mineralogy*. Mineralogical Society of America Reviews in Mineralogy, 9A.

- HENDERSON, P. 1984. Rare earth element geochemistry. Elsevier, New York.
- HEYIN, T. 1990. Tectonites of the northwest Adirondack Mountains, New York: structural and metamorphic evolution. Ph.D. thesis, Cornell University, 203 p.
- HOLLAND, T.J.B., and R. POWELL. 1990. An enlarged and updated internally consistent thermodynamic data set with uncertainties and correlations: The system $K_2O-Na_2O-CaO-MgO-MnO-FeO-Fe_2O_3-Al_2O_3-TiO_2-SiO_2-C-H-O$. *Journal of Metamorphic Geology*, 8:89-124.
- IRVINE, T.N., and W.R.A. BARAGAR. 1971. A guide to the chemical classification of the common volcanic rocks. *Canadian Journal of Earth Science*, 8:523-548.
- ISACHSEN, Y.W., E.P. GERAGHTY, and R.W. WIENER. 1981. Fracture domains associated with a basement-cored dome – The Adirondack Mountains, New York, p. 287-305. In Gabrielsen, R.H., I.B. Ramberg, D. Roberts, and O.A. Steinlein (eds.), *Proceedings of the Fourth International Conference on Basement Tectonics*. International Basement Tectonics Association.
- , and D.W. FISHER. 1970. Geologic map of New York, Adirondack sheet: New York State Museum Map and Chart Series, 15.
- , and E. LANDING. 1983. First Proterozoic stromatolites from the Adirondack Massif: stratigraphic, structural, and depositional implications. *Geological Society of America Abstracts with Programs*, 15:601.
- , and W. MCKENDREE. 1977. Preliminary brittle structures map of New York. New York State Museum Map and Chart Series, 31.
- , W.M. KELLY, C. SINTON, R.A. COISH, and M.T. HEIZLER. 1988. Dikes of the northeast Adirondack region: introduction to their distribution, orientation, mineralogy, chronology, magnetism, chemistry, and mystery. New York State Geological Association Field Trip Guide, 60:215-243.
- JOHNSON, N.M. 1984. Acid rain neutralization by geological materials, p. 37-53. In Bricker, O.P. (ed.), *Geological aspects of acid deposition*. Butterworth, Boston.
- , N.M., C.T. DRISCOLL, J.S. EATON, G.E. LIKENS, and W.H. McDOWELL. 1981. 'Acid Rain', dissolved aluminum, and chemical weathering at the Hubbard Brook Experimental Forest, New Hampshire. *Geochimica et Cosmochimica Acta*, 45:1421-1438.
- KETTLES, I.M., W.W. SHILTS, and W.B. COKER. 1991. Surficial geochemistry, south-central Canadian Shield: implications for environmental assessment. *Journal of Geochemical Exploration*, 41:29-57.
- KOHN, M.J. 1999. Why most "dry" rocks should cool "wet." *American Mineralogist*, 84:570-580.
- KRETZER, W., J. GALLAGHER, and J. NICOLETTE. 1989. Adirondack Lakes Survey, 1984-1987. An evaluation of fish communities and water chemistry. Adirondack Lakes Survey Corporation, Ray Brook, New York.
- LAMB, W.M., and J.W. VALLEY. 1988. Granulite facies amphibole and biotite equilibria, and calculated peak-metamorphic water activities. *Contributions to Mineralogy and Petrology*, 100:349-360.
- LONG, P.E. 1978. Experimental determination of partition coefficients for Rb, Sr, and Ba between alkali feldspars and silicate liquids: *Geochimica et Cosmochimica Acta*, 42:833-848.
- LUTH, W.C. 1974. Analysis of experimental data on alkali feldspars; unit cell parameters and solvi, p. 297-312. In MacKenzie, W.S., and J. Zussman (eds.), *The Feldspars*. Manchester University Press.
- MANIAR, P.D., and P.M. PICCOLI. 1989. Tectonic discrimination of granitoids: *Geological Society of America Bulletin*, 101:635-643.
- McLELLAND, J.M., L.D. ASHWAL, AND L. MOORE. 1994. Composition and petrogenesis of oxide-rich, apatite-rich gabbro-norites associated with Proterozoic anorthosite massifs: examples from the Adirondack Mountains, New York. *Contributions to Mineralogy and Petrology*, 116:225-238.
- , and J. CHIARENZELLI. 1990. Geochronological studies in the Adirondack Mountains and the implications of a Middle Proterozoic tonalite suite, p. 175-194. In Gower, C., T. Rivers, and C. Ryan (eds.), *Mid-Proterozoic Laurentia-Baltica*. Geological Association of Canada Special Paper 38.

- _____, _____, P.R. WHITNEY, and Y.W. ISACHSEN. 1988. U-Pb zircon geochronology of the Adirondack Mountains and implications for their geologic evolution: *Geology*, 16:920-924.
- _____, J.S. DALY, and J. McLELLAND. 1996. The Grenville orogenic cycle (ca. 1350-1000 Ma): an Adirondack perspective. *Tectonophysics*, 265:1-28.
- _____, M. HAMILTON, B. SELLECK, J. McLELLAND, D. WALKER, and S. ORRELL. 2001. Zircon U-Pb geochronology of the Ottawa Orogeny, Adirondack Highlands, New York: regional and tectonic implications. *Precambrian Research*, 109:39-72.
- _____, and J. HUSAIN. 1986. Nature and timing of anatexis in the eastern and southern Adirondack Highlands. *Journal of Geology*, 94:17-25.
- _____, and Y.W. ISACHSEN. 1986. Synthesis of geology of the Adirondack Mountains, New York, and their tectonic setting within the southwestern Grenville Province, p. 75-94. In Moore, J.M., A. Davidson, and A. Baer (eds.), *The Grenville Province*. Geological Association of Canada, Special Paper 31.
- _____, A. LOCHHEAD, and C. VYHNAL. 1988. Evidence for multiple metamorphic events in the Adirondack Mountains, New York. *Journal of Geology*, 96:279-298.
- _____, and P.R. WHITNEY. 1977. The origin of garnet in the anorthosite-charnockite suite of the Adirondacks. *Contributions to Mineralogy and Petrology*, 60:161-181.
- _____, and _____. 1990. Anorogenic, bimodal emplacement of anorthositic, charnockitic, and related rocks in the Adirondack Mountains, New York, p. 301-315. In Stein, H.J., and J.L. Hannah (eds.), *Ore-bearing granite systems: Petrogenesis and mineralizing processes*. Geological Society of America Special Paper 246.
- MEZGER, K., E.J. ESSENE, B.A. van der PLUIJM, and A.N. HALLIDAY. 1991. U-Pb garnet, sphene, monazite, and rutile ages: implications for the duration of high-grade metamorphism and cooling histories, Adirondack Mountains, New York. *Journal of Geology*, 99:415-428.
- _____, _____, _____, and _____. 1993. U-Pb geochronology of the Grenville Orogen of Ontario and New York: constraints on ancient crustal tectonics. *Contributions to Mineralogy and Petrology*, 114:13-26.
- MIESCH, A.T. 1976. Interactive computer programs for petrologic modeling with extended Q-mode factor analysis. *Computers and Geosciences*, 2:439-492.
- MILLER, W.J. 1909. Geology of the Remsen Quadrangle, including Trenton Falls and vicinity in Oneida and Herkimer Counties. New York State Museum Bulletin 126, 51 p.
- _____. 1910. Geology of the Port Leyden Quadrangle, Lewis County, New York. New York State Museum Bulletin 135, 61 p.
- MOECHER, D.P., and E.J. ESSENE. 1990. Phase equilibria for calcic scapolite, and implications of variable Al-Si disorder for P-T, T-X_{CO₂}, and a-X relations. *Journal of Petrology*, 31:997-1024.
- MOINE, B., P. SAUVAN, and J. JAROUSSE. 1981. Geochemistry of evaporite-bearing series: a tentative guide for the identification of metaevaporites. *Contributions to Mineralogy and Petrology*, 76:401-412.
- NABELEK, P.I. 1997. Quartz-sillimanite leucosomes in high-grade schists, Black Hill, South Dakota: a perspective on the mobility of Al in high-grade metamorphic rocks. *Geology*, 25:995-998.
- NELSON, A.E. 1968. Geology of the Ohio Quadrangle, southwestern part of the Adirondack Mountains, New York. U.S. Geological Survey Bulletin 1251, p. F1-F46.
- ORRELL, S.E., and J.M. McLELLAND. 1996. New single grain zircon and monazite U-Pb ages for Lyon Mt. gneiss, western Adirondack Highlands, and the end of the Ottawa Orogeny. *Geological Society of America Abstracts with Programs*, 28:A88.
- OWENS, B.E., M.W. ROCKOW, and R.F. DYMEK. 1993. Jotunites from the Grenville Province, Quebec: petrological characteristics and implications for massif anorthosite petrogenesis. *Lithos*, 30:57-80.
- PATTEE, J. 1989. The geology of the West Canada Lakes 7.5' Quadrangle, south-central Adirondack Mountains, New York. M.S. thesis, North Carolina State University, 204 p. with maps.
- _____, and E.F. STODDARD. 1988. Reaction textures in mafic and calc-silicate granulites, south-central Adirondacks. *Geological Society of America Abstracts with Programs*, 20:61.
- PEARCE, J.A., N.B.W. HARRIS, and A.G. TINDLE. 1984. Trace element discrimination diagrams for the tectonic interpretation of granitic rocks. *Journal of Petrology*, 25:956-983.

- POTTER, D.B. JR. 1985. The stratigraphy and structure of the Loon Pond Syncline, Adirondack Mountains, New York State. Ph.D. thesis, University of Massachusetts (Amherst), 139 p.
- RAMO, O.T. 1991. Petrogenesis of the Proterozoic rapakivi granites and related rocks of southeastern Fennoscandia: Nd and Pb isotopic and general geochemical constraints. Geological Survey of Finland, Bulletin 355, 161 p.
- RATCLIFFE, N.M., J.N. ALEINIKOFF, W.C. BURTON, and P. KARABINOS. 1991. Trondhjemitic, 1.35-1.31 Ga gneisses of the Mount Holly Complex of Vermont: evidence for an Elzevirian event in the Grenville basement of the United States Appalachians. Canadian Journal of Earth Sciences, 28:77-93.
- REVETTA, F.A., and W.H. DIMENT. 1973. Simple Bouguer gravity anomaly maps of New York, Adirondack sheet. New York State Museum Map and Chart Series, 17b.
- RIVERS, T., J. MARTIGNOLE, C.F. GOWER, and A. DAVIDSON. 1989. New tectonic divisions of the Grenville Province, southeast Canadian Shield. Tectonics 8:63-84.
- SEAL, T.L. 1986. Pre-Grenville dehydration metamorphism in the Adirondack Mountains, New York: evidence from pelitic and semi-pelitic metasediments. M.S. thesis, State University of New York at Stony Brook, 64 p.
- SIEGEL, D.I., and H.O. PFANNKUTCH. 1984. Silicate dissolution influence on Filson Creek chemistry, northeastern Minnesota. Geological Society of America Bulletin, 95:1446-1453.
- SIEVER, R. 1992. The Silica Cycle in the Precambrian. *Geochimica et Cosmochimica Acta*, 56:3265-3272.
- SILVER, L.T. 1969. A geochronologic investigation of the Adirondack Complex, Adirondack Mountains, New York, p. 233-252. In Isachsen, Y.W. (ed.), *Origin of anorthosite and related rocks*. New York State Museum Memoir 18.
- SPEAR, F.S., and J.C. MARKUSSEN. 1997. Mineral zoning, P-T-X-M phase relations, and metamorphic evolution of some Adirondack granulites, New York. *Journal of Petrology*, 38:757-783.
- STAUBITZ, W.W., and P.J. ZARIELLO. 1989. Hydrology of two headwater lakes in the Adirondack Mountains of New York. *Canadian Journal of Fisheries and Aquatic Science*, 46:268-276.
- STEL, H., S. CLOETINGH, M. HEEREMANS, and P. van der BEEK. 1993. Anorogenic granites, magmatic underplating, and the origin of intracratonic basins in a non-extensional setting. *Tectonophysics*, 95:285-299.
- STODDARD, E.F. 1988. Distribution and significance of cordierite in the northwest Adirondacks. *Geological Society of America Abstracts with Programs*, 20:73.
- SYLVESTER, P.J. 1989. Post-collisional alkaline granites. *Journal of Geology*, 97:261-280.
- TAYLOR, B.E., and J.G. LIOU. 1978. The low-temperature stability of andradite in C-O-H fluids. *American Mineralogist*, 63:378-393.
- VALENTINO, D.W., and J.R. CHIARENZELLI. 1999. Snowy Mountain Dome, Adirondacks, New York: evidence for Proterozoic sinistral transpression (?). *Geological Society of America Abstracts with Programs*, 31:A75.
- VALLEY, J.W., S.R. BOHLEN, E.J. ESSENE, and W. LAMB. 1990. Metamorphism in the Adirondacks: II. The role of fluids. *Journal of Petrology*, 31:555-596.
- , and E.J. ESSENE. 1980. Calc-silicate reactions in Adirondack marbles: the role of fluids and solid solutions. *Geological Society of America Bulletin*, 91, Part I:114-117; Part II:720-815.
- , E.U. PETERSEN, E.J. ESSENE, and J.R. BOWMAN. 1982. Fluorophlogopite and fluor tremolite in Adirondack marbles and calculated C-O-H-F fluid compositions. *American Mineralogist*, 67:545-557.
- , E.J. ESSENE, and D.R. PEACOR. 1983. Fluorine-bearing garnets in Adirondack calc-silicates. *American Mineralogist*, 68:444-448.
- WALTON, M.S., and D. deWAARD. 1963. Orogenic evolution of the Precambrian in the Adirondack Highlands, a new synthesis. *Proceedings Koninkl. Nederl. Akademie van Wetenschappen, Amsterdam*, B66:98-106.
- WATSON, E.B., and T.M. HARRISON. 1983. Zircon saturation revisited: temperature and composition effects in a variety of crustal magma types. *Earth and Planetary Science Letters*, 64:295-304.

- , and ———. 1984. Accessory minerals and the geochemical evolution of crustal magmatic systems: a summary and prospectus of experimental approaches. *Physics of the Earth and Planetary Interiors*, 35:19-30.
- WEIMER, E., D. VALENTINO, J. CHIARENZELLI, and W. ORNDORFF. 2001. The Moose River Plain shear zone, central Adirondacks, New York. *Geological Society of America Abstracts with Programs*, 33:A11.
- WHALEN, J.B., K.L. CURRIE, and B.W. CHAPPELL. 1987. A-type granites: geochemical characteristics, discrimination, and petrogenesis. *Contributions to Mineralogy and Petrology*, 95:407-419.
- WHELAN, J.F., R.O. RYE, W. deLORRAINE, and H. OHMOTO. 1990. Isotopic geochemistry of a Mid-Proterozoic evaporite basin: Balmat, New York. *American Journal of Science*, 290:396-424.
- WHITNEY, P.R. 1983. A three-stage model for the tectonic history of the Adirondack region, New York. *Northeastern Geology*, 5:61-72.
- . 1992. Charnockites and granites of the western Adirondacks, New York, USA: a differentiated A-type suite. *Precambrian Research*, 57:1-19.
- , and J.M. McLELLAND. 1973. Origin of coronas in metagabbros of the Adirondack Mountains, New York. *Contributions to Mineralogy and Petrology*, 39:81-98.
- , and ———. 1983. Origin of biotite-hornblende-garnet coronas between oxides and plagioclase in olivine metagabbros, Adirondack region, New York. *Contributions to Mineralogy and Petrology*, 82:34-41.
- , and J.F. OLMSTED. 1993. Bedrock geology of the Au Sable Forks Quadrangle, northeastern Adirondack Mountains, New York. *New York State Museum Map and Chart Series*, 43.
- WIENER, R.W., J.M. McLELLAND, Y.W. ISACHSEN, and L.M. HALL. 1984. Stratigraphy and structural geology of the Adirondack Mountains, New York: review and synthesis, p. 1-57. In Bartholemew, M.J. (ed.), *The Grenville Event in the Appalachians and related topics*. Geological Society of America Special Paper 194.
- WYNNE-EDWARDS, H.R. 1972. The Grenville Province, p. 263-334. In Price, R.A., and R.J.W. Douglas (eds.), *Variations in tectonic styles in Canada*. Geological Association of Canada Special Paper 11.
- YOUNG, D.A. 1995. Kornerupine-group minerals in Grenville granulite-facies paragneiss, Reading Prong, New Jersey. *Canadian Mineralogist*, 33:1255-1262.

Appendix A

Suggested Field Trip

Much of the map area, including many of the best examples of its geologic features, is accessible only with difficulty. The following roadlog is designed to illustrate most of the common (and a few uncommon) rock types in the area, together with some of the structural features. Note that Stops 1, 2, 12, and 13 are outside, although adjacent to, the Fulton Chain-of-Lakes map area. Stops 3, 5, and 8 involve considerable walking and are not recommended in inclement weather. In the early spring, Stop 3 may be inaccessible due to high water, and Stop 10 due to impassable roads. The trip begins in Port Leyden, on Route 12 north of Utica, and ends on Route 30 north of Long Lake. The entire trip should take 1.5 to 2 days at a reasonable pace.

Miles

- 0.0 Start at the intersection of Route 12 and East Main Street in Port Leyden; go E on East Main Street.
- 0.1 Turn L (N) onto Lincoln Street.
- 0.3 Turn R (E) onto North Street (unpaved); proceed 0.1 miles and park in front of Cataldo Electric Barn on L.

Stop 1. Port Leyden Nelsonite

(condensed from manuscript by Robert Darling and Frank Florence)

Across the road from the lot, near the power pole, is a large, rounded outcrop. Walk over the top of it (you are now facing south) and down to the left. Go into the woods about 40 meters to the southeast. There are some small outcrops of pelitic gneiss (light colored) containing some weathered exposures of nelsonite (dark). The nelsonite is in the form of a dike about 3 to 4 meters wide. Farther to the south, at the bottom of the hill, is a water-filled mine shaft. Good nelsonite specimens can be found in the waste pile (if you dig).

The nelsonite is relatively homogeneous, equigranular and fine-grained (0.1–0.5 mm). It contains 32–43% magnetite, 30–45% apatite; 8–15% ilmenite; 5–11% pyrite (or pyrrhotite); and 4–6% chlorite, garnet, zircon, and monazite (Darling and Florence, 1995). The magnetite and apatite occur as separate, equant grains, whereas ilmenite typically occurs as interstitial, poikilitic, coarser (0.5–1.5 cm) but optically continuous grains (as observed in reflected light). These textures are inferred to be primarily of igneous origin and indicate cotectic crystallization of magnetite and apatite later joined by eutectic ilmenite.

The nelsonite is hosted by metapelitic gneisses, on strike with unit BM in the map area, that contain quartz-sillimanite nodules similar to those in the leucogranitic facies of unit BM. These gneisses record metamorphic conditions of 710–730° C and 4–6 kbar, based on quartz-hercynite-garnet-sillimanite equilibria and biotite breakdown reactions (Florence et al., 1995). This is the first described occurrence of Ti-bearing nelsonite that does not occur within or in proximity to anorthosite-suite rocks. Darling and Florence (1995) infer that anorthosite-suite rocks were once present in this area; they generated the nelsonite and were primarily responsible for causing metamorphism at the conditions described above. Note that anorthosite suite rocks of unit JA are commonly found in the map area within or adjacent to unit BM.

Return to vehicles and retrace route to East Main Street.

Miles

- 0.6 Corner of Lincoln and East Main. Turn L onto East Main.
- 1.1 Intersection of East Main Street and River Road. Turn L (N) on River Road.
- 1.9 River Road forks L; continue straight ahead on Marmon Road. The road climbs through

- a terrace of lacustrine and deltaic sand; outcrop in this area is very scarce, found only where streams have cut to bedrock.
- 2.5 Penny Settlement Road on R; continue on Marmon Road.
 - 4.0 Junction with Hunkins Road; continue (L) on Marmon Road.
 - 4.3 Lyonsdale; turn R on Lowdale Road, and cross three short one-lane bridges over the Moose River.
 - 4.5 Just beyond the third bridge, park on either side of road (beware of deep sand) and cautiously climb down to the streamworn outcrops to the L (W) of the road.

Stop 2. Leucogneiss with Quartz-Willimanite Stringers

These large outcrops consist of biotite-sillimanite leucogranitic gneiss of unit BM, containing minor magnetite, fluorite, and spinel. Abundant quartz-sillimanite stringers, veins, and lenses stand out as ribs on weathered surfaces. These are ordinarily subparallel to foliation in the leucogneisses, but locally cross-cut it. In some parts of the exposure, two or more intersecting sets of stringers are present; in others they are isoclinally folded. Pegmatites are also present, some parallel to foliation and others crosscutting, late, and undeformed. Orrell and McLelland (1996) have dated single-crystal zircons from similar rocks at Agers Falls, about 1 kilometer downstream from here. One yielded a concordant age of 1031 ± 8 Ma; several others gave scattered Pb / Pb ages up to 1119 Ma, confirming the complex history of these rocks.

Similar rocks are also present in scattered occurrences of unit BM throughout much of the northern half of the map area, although the sillimanite stringers and nodules are rarely as well developed as they are here. Northeastward from Lyonsdale these rocks are covered for nearly 10 kilometers, but reappear, together with jotunite, along strike in and near Otter Creek, and again with stratiform anorthosite in the area southwest of Stillwater Reservoir, where they exhibit mylonitic fabrics.

More detailed descriptions of Stops 1 and 2 may be found in Florence and Darling (1997).

Turn around and retrace route to Port Leyden.

- 7.9 Intersection of River Road and East Main Street. Continue on River Road.
- 8.0 Turn L (E) on Moose River Road.
- 17.7 Red schoolhouse (dated 1875) on right; small outcrop on left is a clinopyroxene quartzite.
- 18.0 Pullout on L (N) overlooks the Moose River. Park here; beware of soft sand and mud. Follow the rough trail to the river and walk downstream along the south bank. CAUTION: The rocks here may be partially or wholly submerged at times of high water, especially during spring runoff. If this is the case, omit this stop because currents are swift and dangerous.

Stop 3. Quartzite, Calcsilicates, and Mg-Rich Paragneiss

Rapids in the Moose River expose a section of metasedimentary rocks that are assigned to unit BL based on the preponderance of quartzite. However, they differ from BL exposures farther east in that they contain greater proportions of calcsilicates and an unusual magnesium- and boron-rich facies.

To the west (downstream) the first large outcrop is of diopside-quartz calcsilicate rock that grades into quartzite; sparse wollastonite is present here but may be difficult to find. A short distance beyond, a prominent ledge of diopside-phlogopite-tremolite quartzite extends more than halfway across the river. The rocks here strike NNE to NE across the river; the downstream side of the ledge is a dip slope. Ribbing on dip surfaces of quartzite and oriented needles of tremolite define a SW-plunging lineation. From here downstream to a sharp northward bend in the river, numerous outcrops expose quartzite with layers and lenses of diopside-rich calcsilicates, and local concentrations of pyrite and pyrrhotite. Some of the quartzite shows prominent centimeter-scale laminations. Near the bend, quartzite is overlain by strongly foliated amphibolite, followed by diopside-calcite marble. The first exposures beyond the bend are of

biotite-quartz-plagioclase gneiss which also contains tourmaline, rutile, and locally abundant prismatic [ideally $\text{Mg}_3\text{Al}_6(\text{Si,Al,B})_5\text{O}_{21}(\text{OH,F})$], cordierite, and garnet (Darling et al., 2000). The prismatic occurs as prismatic crystals up to a decimeter long, oriented in the plane of foliation and locally forming radiating clusters on foliation surfaces. This exceptionally Mg- and B-rich assemblage suggests the presence of evaporites in the protolith. **NO HAMMERS, PLEASE**; sample only from loose material. From here, return to the vehicles; there is a well-worn fishermen's path through the woods at the top of the bank.

Continue E on Moose River Road.

- 21.9 Intersection of Moose River Road with Route 28; turn R (S) on Route 28.
- 26.2 Park in paved pullouts on either side of the road. Walk about 0.1 mile south to roadcut on the L (E) side.

Stop 4. Fayalite Granite

Fayalite, commonly partially or wholly altered to iddingsite or chlorite, is present locally in rocks of unit CG throughout the area. At some locations, e.g., Stop 7, fayalite occurs in mafic charnockite. More commonly, the fayalite-bearing rocks are felsic granites or leucogranites, despite their dark olive-green color. This exposure, on the west flank of the Gull Lake Dome, is representative of the latter type. In thin section, these rocks consist principally of coarse perthite and quartz, with minor biotite, fayalite, hornblende, and fluorite. Perthite grains locally have albite rims. The felsic nature of the rock is evident from the chemical analysis (Table 1A, MKS85). These rocks differ from the well-known fayalite granites at Au Sable Forks and Wanakena in that they lack iron-rich clinopyroxenes and abundant zircon.

Although foliation at this location is faint to absent even on weathered surfaces, similar rocks elsewhere in the map area are well foliated; thus it is unlikely that these fayalite granites are post-tectonic. More probably, they are late differentiates of the region-wide charnockite-granite suite, and have a similar deformation history.

Return to vehicles, turn around and head N on Route 28 toward Old Forge.

- 30.5 Moose River Road on L. Continue N on Route 28.
- 30.6 Bridge over Moose River.
- 38.9 Sharp L turn onto Jones Road.
- 39.05 Turn R on Okara Lakes Road.
- 39.3 Sharp L turn with trail signs. Park on either side of the road.

Stop 4. Unit TH (Quartz-Lump Facies)

Follow the marked trail east approximately 0.6 kilometers, then bushwhack N45°E up a steep slope. Exposures on the slope are mainly fine-grained, equigranular (phlogopite)-plagioclase-quartz-microcline gneiss with ilmenohematite, but lacking the diopside and magnesiohastingsite present in this unit at Stop 6. At ca. 73% SiO_2 (Table 1D, MKS80), this is among the most felsic examples of gneiss in unit TH. Slabs on the south face of the hill show cryptic compositional layering on weathered surfaces; alternating, centimeter-scale layers of plagioclase- and microcline-rich rock are revealed by cobaltinitrite staining. One thin section shows millimeter-scale streaks rich in oxides, titanite, and zircon parallel to foliation. These could be paleoblacksands or concentrations resulting from metamorphic differentiation during deformation.

In an outcrop extending over much of the open hilltop, these rocks are overlain by a layer of impure quartzite at least 20 meters thick. Scattered lumps of nearly pure quartz up to 30 centimeters in longest dimension, somewhat flattened in the plane of foliation and locally elongated parallel to the N20°E lineation. Foliation in the host quartzite wraps around these lumps. Possible interpretations include (a) quartz-cobble conglomerate in which only the largest clasts have survived deformation, or (b) tectonically dismembered quartz veins or layers of nearly pure quartzite. Crosscutting pegmatite veins with salmon-pink microcline are common, especially near the east end of the outcrop.

In addition to quartz, the minerals include microcline, plagioclase, scapolite, grossular-andradite garnet, phlogopite, calcite, epidote, and sphene in varying proportions, as well as a few large, euhedral zircons. Epidote, intergrown with quartz and calcite, locally forms retrograde symplectic rims around garnet. Sample MKS82E, Table 1F, is an analysis of typical "matrix" material. A bizarre quartz-fluorite symplectite occurs in a thin section of similar rock along strike to the northeast.

On the west shoulder of this hill, the granitic facies of unit TH reappears overlying the quartzite. The quartzite layer can be traced northeastward in scattered outcrops for a distance of roughly 6 kilometers to Gibbs Lake, where it wraps around the nose of an overturned anticline. Additional quartzite outcrops (lacking the quartz lumps) are present along the trail southwest of the hilltop exposure.

Return to vehicles. As you approach the road, please stay on the trail. Avoid the private driveway which parallels it to the south. Retrace route to intersection of Jones Road and Route 28.

- 39.7 Junction of Jones Road and Route 28; Turn L (E) on 28 toward Old Forge. Immediately after the turn, there is a large boulder of quartz-lump "conglomerate" in the ditch on the L (N) side of the road. This can serve as a substitute for Stop 5 in case of bad weather.
- 40.2 Park on right shoulder of road (well out of traffic) and cautiously cross Route 28 to outcrops on the steep bank N of the road.

Stop 6. Unit TH (Granitic Facies)

These small, glacially smoothed outcrops show alternating, centimeter-scale, salmon-pink (quartz-microcline) and pale green (magnesianhastingsite-diopside-quartz-microcline) layers. The pink layers appear to be leucosomes from partial melting; similar material also forms crosscutting veins. These rocks are strongly oxidized granitoids of unit TH. Opaque minerals, where present, are almost exclusively steel-gray ilmenohematite. In outcrops where compositional layering is less prominent, the pale color of the

mafic minerals and lack of grain-shape fabric cause this rock to resemble massive leucogranite. Diopside and magnesianhastingsite are poikiloblastic in thin section. In the upper left of the exposure, a string of small pyroxene grains defines a 4-centimeter Z fold.

Continue E on Route 28.

- 40.5 On the left are low roadcuts of massive quartz-microcline gneiss with coarser quartz-microcline segregations containing megascopic ilmenohematite and a few large andraditic garnets.
- 40.8 Rocks in the roadcut on the L are strongly laminated and clearly metasedimentary, but have the typical unit TH mineralogy.
- 41.4 Thendara railroad station on R.
- 42.3 The roadcut on the left is phlogopite-diopside-plagioclase-quartz-microcline gneiss of unit TH, superficially massive but with cryptic layers consisting of alternating plagioclase- and microcline-rich rocks.
- 42.4 Railroad underpass.
- 44.6 In the village of Old Forge. Enchanted Forest/Water Safari tourist trap on L.
- 46.6 A recent rockfall is visible on the L (N), where cliff-forming charnockite overlies a thin layer of marble and calcsilicates.
- 47.6 Obscure intersection with Hollywood Road on R. Park on the R in pullout just beyond the intersection. Walk back (W) on Route 28, and cautiously cross road to roadcuts on the N side.

Stop 7. Charnockite

This long roadcut exposes relatively mafic charnockite of unit CG. This hornblende-hypersthene-clinopyroxene-quartz-plagioclase-mesoperthite gneiss is dark olive green to gray on fresh blasted surfaces, but shows the typical "maple-sugar" brown rind on weathered surfaces. The unusually dark variety near the east end of the exposures contains minor olivine (Fa₉₅). Fayalite and hypersthene have not been observed together in the same thin section. Whole-rock and fayalite analyses (numbered

OFY01) are given in Tables 1A and 2, respectively.

At first glance, the blasted face appears nearly structureless, but weathered surfaces reveal strong foliation and thin coarse-grained layers (partial melts?). Compositional layering becomes evident toward the west end of the cut. Note the fine-grained layer and associated quartz vein. This exposure, like much of unit CG elsewhere, contains a few small lenses and shreds of amphibolite but lacks the continuous amphibolite layers typical of unit GA.

Return to vehicles and proceed E on Route 28.

51.5-52.0 Outcrops on the L are calcsilicates that dip under a thick, ridge-forming layer of charnockite.

53.5 Village of Eagle Bay. Turn L on Big Moose Road.

56.5 On R (east) at a sharp bend, new roadcuts expose biotite leucogneiss (sample BMS19, Table 1B).

59.2 Intersection of North Shore Road on R; bear L on Big Moose Road.

60.3 Wayback Inn on R.

60.5 Railroad tracks visible on L (south). Park on either side of the road, wherever safe. Bushwhack to the tracks.

Stop 8. Leucogneiss and Anorthosite

This is a walking traverse of about 2 kilometers along a railroad. **HAMMERS ARE A NECESSITY**; many outcrops are coated with railroad soot. Turn left and walk along either side of the tracks. Along most of the route, the rocks are leucogneisses of unit BM with a few layers of metasedimentary rocks and hornblende granitic gneiss. The traverse ends at a long, high cut on the right (W) side that exposes rocks of the anorthosite suite (unit JA). These anorthositic and jotunitic gneisses, with a maximum thickness on the order of a few hundred meters, can be traced in intermittent outcrop around an irregular loop, 40 kilometers long, outlining the tight to overturned, doubly plunging Big Moose anticline. This traverse crosses part of the south limb of

the structure near its western end.

The leucogneisses (Table 1B, BMS15, 16, and 17) contain quartz, minor plagioclase, perthite and/or microcline, with variable amounts and combinations of biotite, magnetite, garnet, sillimanite, fluorite, sphene, and pyrite. A specimen from these cuts in the New York State Museum collection contains megascopic topaz. The sillimanite-nodular facies (see Stop 2) is exposed two kilometers west along strike.

Retrace route along the tracks to the vehicles and continue W along Big Moose Road.

61.1 Big Moose Road turns sharply L and crosses railroad tracks. Park on shoulder, or along driveway to L just beyond the tracks.

Stop 8A. Hornblende Granitic Gneiss

Strongly foliated hornblende granitic gneiss of unit CG, typical of the core rocks of the Big Moose anticline, is exposed in a freshly blasted cut on the north side of the road just before it turns left and crosses the railroad tracks.

Turn around and return to Route 28 via Big Moose Road.

68.7 Junction of Big Moose Road and Route 28. Turn L (E) on 28.

70.2 Park on R shoulder well out of traffic and cautiously cross road. This stop consists of two small cuts on the E side of the road. Beware of the ditch in front of outcrops, which usually contains water.

Stop 9. Biotite Gneiss with Cordierite; Quartzite; Tectonized Calcsilicates (Units BL and CM)

The southern cut consists of intensely deformed calcite-quartz-untwinned microcline-diopside rocks with variable amounts of tremolite, sphene, sericitized scapolite, epidote, pyrite, and graphite. Sharply

defined centimeter-scale layering, probably of tectonic origin, is present throughout. Lenses of quartz suggest tectonically disrupted quartz veins or pegmatite. One or two of these have asymmetric shapes but they are not convincing as kinematic indicators. A spectacular marble tectonic breccia occurs on Rocky Point, a few hundred meters along strike to the northwest. These rocks are within the Inlet deformation zone.

The northern cut is dark gray or blue-gray quartzite with interlayered (cordierite)-(garnet)-sillimanite-biotite-quartz-plagioclase gneisses (unit BL; compare to Stop 3). White quartz veins and quartz-microcline pegmatite occur parallel to foliation. Ptygmatically folded leucosomes are also present. Cordierite, first reported here by Seal (1986), occurs locally as irregular gray to black grains up to 1 centimeter in size that resemble dark, dull quartz. It is difficult to find; look in the vicinity of the quartz-feldspar pods. The pale lavender garnets show, in thin section, clear rims surrounding cores packed with oriented sillimanite needles and other inclusions. Coarser grains and bundles of sillimanite occur outside the garnets, and locally define a N20–30W lineation parallel to quartz lineation in the calcsilicates of the southern cut.

Proceed E on Route 28.

- 70.9 Village of Inlet; entrance to town park (with public restrooms) on R.
- 71.8 Turn right onto Limekiln Road.
- 73.8 Road forks; take L fork to enter Moose River Plains Recreation Area. Sign in at the gate and proceed on gravel road. This is a public camping and recreation area which may be closed in the winter and early spring; in the fall, beware of hunters. **DRIVE SLOWLY!**
- 78.6 Intersection, turn L.
- 80.7 Outcrops on L are marble overlain by granitic gneiss and amphibolite. The road at this point follows one of several nearly E-W belts of metasedimentary rocks.
- 81.3 **CAUTION!** Sharp R bend in road.
- 82.4 Intersection with Rock Dam Road on R, bear L.

- 84.4 Trail to Lost Ponds on L.
- 86.4 Trail to Sly Pond on R.
- 86.5 Park in campsite on N side of road (if unoccupied), and walk NW about 100 m to outcrops on the S side of a small ridge.

Stop 10. Granitic Gneiss with Thin Amphibolite Layers (Unit GA); Moose River Deformation Zone

These strongly foliated granitic gneisses are within the Moose River deformation zone (MRDZ). The straight foliation in uniformly medium-to coarse-grained rocks is typical. Coarser aggregates of quartz and feldspar occur both as thin layers parallel to foliation and as irregular crosscutting patches. Some of the patches occupy the spaces between ghost boudins that are defined by curving foliation but lack any evident lithologic contrast with the surrounding gneisses. The eastward tilt of these segregations suggests sinistral movement. Note the apparent lack of grain-size reduction despite the intense deformation; this may be due to post-deformation annealing.

A few thin biotite amphibolite layers are present here. Elsewhere within the MRDZ, similar thin amphibolites outline isoclinal intrafolial folds, while thicker amphibolite layers are commonly boudinaged. Lineation, although weakly developed in these outcrops, is nearly ubiquitous and locally strong within the MRDZ. The lineation is subparallel to the strike of the foliation and layering throughout the zone and is defined by quartz blades and streaks of mafic minerals in the gneisses, and by oriented hornblende crystals in the amphibolite.

Turn around and retrace route through Moose River Plains.

- 101.2 Junction of Limekiln Road and Route 28; turn R and proceed E on 28.
- 103.5 Outcrops on R are calcsilicate-rich metasedimentary rocks of unit CM.
- 103.7 Pullout on L with view of Seventh Lake.
- 111.0 Intersection of Route 28 with Sagamore Road (R) and Antlers Road (L). Turn L (N)

onto Antlers Road. The road crosses a narrow bridge over muskeg and turns sharply R, then L, in Raquette Lake village.

- 111.7 Intersection with Mick Road on R. Park in the open area at the intersection, and walk down Mick Road about 0.2 miles, examining the outcrops along the N side of the road.

Stop 11. Quartzite, Biotite Schist, and Mafic Gneisses (Unit BL)

These outcrops are representative of the structurally highest rocks in the Fulton Lakes Synform. They include garnet-biotite quartzites, biotite-sillimanite schists, and mafic garnet-hypersthene-clinopyroxene-biotite-plagioclase gneisses. Elsewhere in the map area, similar quartzites contain tourmaline. Near the base of the outcrops at the western end, several small quartzite "anticlines" surrounded by biotite-sillimanite schist show grooved upper surfaces that define a N30°–45°E lineation. It is not clear whether these are folds or the tops of large quartzite boudins. Near the east end of the series of outcrops, a lens of calcsilicates is present.

Retrace route along Antlers Road.

- 112.4 Intersection with Route 28. Turn L (E). The road skirts the S end of Raquette Lake.
- 116.7 Entrance to Golden Beach State Campsite on L.
- 119.4 View of Utowana Lake to N. This elongate lake follows marbles and calcsilicate rocks, as do the Fulton Lakes to the W.
- 121.3 Crossing Loon Brook, at the eastern edge of the Raquette Lake Quadrangle.
- 121.9 Park on shoulder well out of traffic.

Stop 12. Calcsilicates and Amphibolite (Unit CM)

These four roadcuts, two on each side, are just outside the eastern edge of the map area on the south limb of the Fulton Lakes Synform. The ENE-striking

rocks cross the road at a slight angle. A thick layer of biotite amphibolite (northwest and southeast outcrops) is enclosed within diopside-rich calcsilicate rocks, and cut by (microcline)-(quartz)-sphene-pyroxene-plagioclase pegmatites that superficially resemble gabbroic anorthosite. The northeast outcrop contains a layer of granitic gneiss, with composition close to the average for the CG suite (Table 1F, BLS10).

The calcsilicates are equigranular, predominantly fine-grained, layered rocks that range from dark green clinopyroxenite to mixtures of clinopyroxene with plagioclase, microcline, scapolite, calcite, or grossular-andradite garnet. It is unclear whether the layering, best seen near the west end of the northwest outcrop, is relict sedimentary layering or the result of tectonically induced metamorphic differentiation. In the southwest roadcut, a deeply weathered layer near the west end contains the assemblage calcite-wollastonite-clinopyroxene-grandite garnet-microcline. Two microprobe analyses of scapolite from the northwest outcrop yield compositions (EqAn 71 and 68) close to mizzonite, indicative of metamorphic temperatures near 800° C.

At least two lineations are present in these outcrops, one oriented about N20°W and one close to N30°E. The latter appears to parallel the axes of small isoclinal folds in the northeast outcrop. Both are at a high angle to the dominant regional E-W lineation.

END OF MILEAGE LOG.

To get to Stop 13, drive east on Route 28 to Blue Mountain Lake, and turn L (N) on Route 30 to Long Lake village. At the bridge over Long Lake, continue N on 30, 4.25 miles to roadcuts on both sides of the road on a slight uphill grade. Just ahead on the L are several cottages and an unmarked gate to Whitney Park, a large area of timberland owned by Whitney Industries which includes much of the northern half of the Raquette Lake, and the southern half of the Tupper Lake 15' Quadrangles. New York State has recently purchased the tract near Little Tupper Lake.

Stop 13. Jotunite, Anorthosite, and Granitic Gneiss (Units JA and GA)

These outcrops in the Long Lake 15' Quadrangle just outside the northeast corner of the map area are similar in lithology and structure to the rocks in the northeastern Raquette Lake Quadrangle (Flatfish Pond Domain). Interlayered granitic gneisses, anorthosite suite rocks, and amphibolite strike east-southeast with steep dips, truncating the northeast-trending structures prevalent in most of the map area. The anorthositic and jotunitic rocks here are interlayered in unit GA, in contrast to the rest of the area where they occur within or adjacent to unit BM.

Rocks on the left (W) side of the road and at the south end of the cut on the east side are heteroge-

neous, strongly foliated hornblende granitic gneisses and charnockites of unit GA. The remainder of the cut on the east is in unit JA and consists of heterogeneous hornblende-pyroxene-plagioclase gneiss with minor, variable amounts of biotite, quartz, perthite, and plagioclase megacrysts up to 20 centimeters across. Also present are layers and pods of anorthosite and gabbroic anorthosite, and numerous flattened enclaves of biotite schist, marble, and fine-grained calcsilicate rocks. The abundance of metasedimentary xenoliths is noteworthy, in that many occurrences of jotunite in the High Peaks region are also rich in such xenoliths. The transition between the mafic and granitic gneisses is marked by locally pegmatitic textures and euhedral garnets up to 3 centimeters.

END OF TRIP

Appendix B

Notes on Mapping Units

Units from published mapping in adjacent areas that are equivalent or similar, in whole or in part, to units used on this map are listed below. I&F refers to the units used by Isachsen and Fisher (1970); B&L refers to those of Buddington and Leonard (1962); references to other work are written out.

Unit CG: B&L: gha, ghs, ghgn; I&F: hbg, phgs, phqs.

Unit GA: B&L: hg, sphg; I&F: hbg, phgs, phqs; Nelson (1968): pCsg.

Unit BG: B&L: gpb; I&F: hbg, mu, mug. BG closely resembles Unit 2 of the Piseco Lake sequence mapped by Glennie (1973) in the Piseco Lake Quadrangle south of the West Canada Lakes Quadrangle. It may be equivalent to the Tomantown granitic gneiss of the southern Adirondacks (Ekstrom 1989; Chiarenzelli and McLelland, 1991), or to the Rooster Hill Megacrystic Gneiss (Wiener et al., 1984).

Unit JA: B&L: di, gba, am; I&F: not separately mapped.

Unit OG: B&L: gb, am; I&F: gb, am.

Unit AM: B&L: am; I&F: am.

Unit BL: B&L: ms, msq; I&F: mu.

Unit KZa: B&L: msg, ms; I&F: garb, mug.

Unit KZb: B&L: ga, gagn, ms; I&F: mug, mu, lg.

Unit TH: (Thendara gneiss) B&L: gm, ms; I&F: mu, mug.

Unit CM: B&L: msp, mspq, msl, mslq; I&F: mu, mb.

Unit MU: B&L: ms; I&F: mu, mug; Nelson (1968): pCgr, pCgn.

Unit BM: B&L: gaa, gagn, gm; I&F: lg, mu, mug. Stratiform bodies of jotunite, gabbroic anorthosite gneiss, and metanorthosite occur within BM in addition to those mapped separately as JA. The separate body of BM between Lake Rondaxe and Queer Lake (SC BMQ) consists almost entirely of leucogneiss.

Unit LD: B&L: gaa, gagn, gao; I&F: mug. The name "Lake Durant Sequence" is used by Walton and deWaard (1963) and Geraghty (1978) for similar rocks in the Blue Mountain Lake Quadrangle and elsewhere; the type locality just north of Lake Durant in the Blue Mountain Lake quadrangle (Walton and deWaard, 1963) is on strike with LD in the Raquette Lake Quadrangle.

Appendix C

Lithology and Location of Analyzed Samples

Granitoids (units CG and GA)

Sample	Unit	Lithology #	N LAT	W LONG
BMB44	CG	Bt-Hbl granite gneiss	43.8206	74.8703
BMB73A	CG	Hbl granite gneiss	43.9806	74.8547
BMG60	CG	Mt-Hbl granite gneiss	43.8425	74.9586
BMS10B	CG	Hbl granite gneiss	43.8200	74.9269
BMS11	CG	Charnockite	43.7780	74.8250
BMS18	CG	Bt-Hbl granite gneiss	43.8172	74.8466
MKB133	CG	Bt leucogranite gneiss (Fa, Fl)	43.6775	75.1481
MKB135	CG	Hbl granite gneiss	43.6539	75.1508
MKB153	CG	Hbl granite gneiss	43.6744	75.1764
MKB187	CG	Bt leucogranite gneiss (Fa, Fl)	43.6944	75.1797
MKB201	CG	Hbl granite gneiss	43.6883	75.2219
MKB208	CG	Cpx granite gneiss	43.6072	75.2450
MKB212	CG	Bt charnockite	43.7010	75.0500
MKB22	CG	Hbl granite gneiss	43.6894	75.0919
MKB268	CG	Bt-Hbl granite gneiss	43.7416	75.0113
MKC33	CG	Charnockite	43.7300	75.1169
MKI15B	CG	Hbl granite gneiss	43.5717	75.2472
MKS30	CG	Charnockite	43.7406	75.1419
MKS85	CG	Hbl granite gneiss (Fa, Fl)	43.5564	75.1419
MKT15A	CG	Bt-Hbl granite gneiss (Fa)	43.5978	75.0736
MKT46A	CG	Hbl granite gneiss	43.5300	75.0477
MKU01	CG	Hbl granite gneiss (Fa)	43.5438	75.0913
MKU05	CG	Charnockite	43.7200	75.1358
NFA42	CG	Hbl granite gneiss	43.8867	75.1092
NFB68	CG	Charnockite	43.7847	75.0108
NFC27B	CG	Hbl granite gneiss	43.9208	75.1264
NFC31	CG	Hbl granite gneiss	43.9289	75.1260
NFI57A	CG	Charnockite	43.8356	75.2439
NFI79A	CG	Bt-Hbl granite gneiss	43.9775	75.1442
NFS12	CG	Charnockite	43.7797	75.0786
NFS15	CG	Charnockite	43.7761	75.0875
NFS20	CG	Hbl quartz syenite gneiss	43.7669	75.2386

* Samples from adjacent quadrangles

Significant minor constituents shown in parentheses

See Appendix D for mineral name abbreviations.

Granitoids (units CG and GA) *continued*

Sample	Unit	Lithology #	N LAT	W LONG
NFS26	CG	Hbl granite gneiss	43.8561	75.0025
NFS27	CG	Hbl granite gneiss	43.7519	75.1558
NFS46	CG	Bt-Mt-Chl granite gneiss	43.8969	75.0506
NFT67A	CG	Hbl granite gneiss	43.8467	75.2417
NWS01	CG*	Bt-Hbl granite gneiss	43.4797	75.0150
OFA24	CG	Hbl granite gneiss	43.5356	74.8314
OFB92	CG	Hbl granite gneiss	43.5556	74.9361
OFC05	CG	Bt-Hbl quartz syenite gneiss	43.6672	74.9542
OFN14A	CG	Hbl granite gneiss (Fa)	43.5703	74.9092
OFN18A	CG	Charnockite (Fa)	43.5769	74.9083
OFS17	CG	Hbl granite gneiss	43.5769	74.8833
OFS20	CG	Hbl granite gneiss (Fa)	43.5874	74.8691
OFU01	CG	Bt-Hbl granite gneiss	43.5197	74.9366
OFU02	CG	Hbl granite gneiss	43.5211	74.7527
OFU03	CG	Charnockite	43.5105	74.7544
OFY01	CG	Charnockite (Fa)	43.7200	74.9467
PLS01	CG*	Hbl quartz syenite gneiss	43.5325	75.3117
RLA11A	CG	Bt-Hbl granite gneiss (Grt)	43.7533	74.6389
RLS11	CG	Charnockite	43.8781	74.5689
RLS13	CG	Charnockite	43.8128	74.6839
RLS19	CG	Bt-Hbl granite gneiss	43.9625	74.5833
RLS45	CG	Charnockite (Grt)	43.9514	74.5200
RLU19	CG	Hbl granite gneiss	43.9628	74.6469
RLU88	CG	Charnockite	43.9814	74.7072
RLU95	CG	Hbl granite gneiss	43.9017	74.6494
WCB57	CG	Hbl granite gneiss	43.6922	74.7406
WCG41	CG	Bt-Hbl granite gneiss (Fa, Fl)	43.7152	74.5383
WCH49	CG	Charnockite	43.5888	74.5233
WCS31	CG	Charnockite	43.6989	74.5619
WCS32	CG	Charnockite	43.5155	74.7347
WCS33	CG	Charnockite	43.5222	74.7250
BMC75	GA	Bt-Hbl granite gneiss	43.9167	74.7519
NFB130	GA	Charnockite	43.9033	75.2000
NFB75B	GA	Charnockite	43.9092	75.2022
NFB84	GA	Charnockite	43.8814	75.1500
NFB89A	GA	Hbl-Bt granite gneiss	43.8197	75.2311
NFI11A	GA	Bt-Hbl granite gneiss	43.7975	75.1983
NFS23	GA	Cpx granite gneiss	43.7761	75.2014
NFS24	GA	Bt-Hbl granite gneiss	43.7750	75.2058
NFS25	GA	Hbl granite gneiss	43.8616	75.1275
OFC52	GA	Charnockite	43.6383	74.7847

* Samples from adjacent quadrangles

Significant minor constituents shown in parentheses

See Appendix D for mineral name abbreviations.

Granitoids (units CG and GA) *continued*

Sample	Unit	Lithology #	N LAT	W LONG
OFS11	GA	Bt-Hbl granite gneiss	43.5528	74.9072
RLS68	GA	Hbl granite gneiss	43.9306	74.5706
RLS82A	GA	Hbl granite gneiss	43.9281	74.7156
WCG40	GA	Bt-Hbl granite gneiss	43.7175	74.5383
WCS57A	GA	Hbl granite gneiss	43.6889	74.6222

Granitoids (units BM, LD, and BG)

BMB65A	BM	Mt-Bt leucogneiss	43.9756	74.8900
BMC13A	BM	Mt-Bt granite gneiss	43.8153	74.9558
BMC13B	BM	Mt-Bt leucogneiss	43.8153	74.9558
BMC13C	BM	Mt-Bt leucogneiss	43.8153	74.9558
BMS12	BM	Mt-Bt leucogneiss (Sil, Grt)	43.8119	74.9378
BMS15	BM	Bt granite gneiss (Grt, Fl)	43.8058	74.9166
BMS16	BM	Bt granite gneiss (Grt, Fl)	43.8072	74.9111
BMS17	BM	Leucogneiss (Sil, Grt)	43.8133	74.9080
MKB184	BM	Bt leucogneiss (Grt)	43.7516	75.2381
MKC26A	BM	Bt granite gneiss (Grt)	43.6964	75.1150
MKC26B	BM	Bt granite gneiss (Fl)	43.6969	75.1128
MKS24	BM	Hbl granite gneiss	43.7278	75.1886
NFA17B	BM	Bt leucogneiss	43.7700	75.1336
PLS02	BM*	Mt-Bt leucogneiss (Sil, Tpz)	43.6058	75.3592
PLS04	BM*	Leucogneiss (Grt, Fl)	43.6242	75.2772
PLS05	BM*	Leucogneiss (Fl)	43.6236	75.2728
PLS06	BM*	Leucogneiss (Sil, Grt)	43.6192	75.3031
RLS10	BM	Bt-Hbl granite gneiss (Fl)	43.8864	74.5883
RLS111	BM	Bt leucogneiss (Sil, Grt)	43.9386	74.6758
RLS113	BM	Bt-Hbl granite gneiss	43.9244	74.6614
RLS75	BM	Bt leucogneiss (Sil)	43.8725	74.7442
RLU09	BM	Bt leucogneiss (Sil)	43.9481	74.6356
BMS19	BM	Bt leucogneiss	43.7991	74.8508
BMS20	BM	Bt granite gneiss (Grt, Fl)	43.7836	74.8383
BLS01	LD*	Bt leucogneiss (Fa)	43.8450	74.4050
RLA01B	LD	Mt-Bt granite gneiss	43.7514	74.7017
RLB09B	LD	Mt-Hbl-Bt granite gneiss	43.7531	74.6778
RLU02	LD	Mt-Cpx granite gneiss (Ttn)	43.7794	74.6414
RLU105	LD	Mt-Bt granite gneiss	43.8100	74.5603
RLU108	LD	Mt-Bt granite gneiss	43.8189	74.5528
WCV04	BG	Hbl-Bt granite gneiss (Kfs meg)	43.5278	74.5786
WCV05	BG	Bt granite gneiss (Kfs meg)	43.5264	74.5781
WCV17	BG	Hbl-Bt granite gneiss (Kfs meg)	43.5264	74.5219

* Samples from adjacent quadrangles

Significant minor constituents shown in parentheses

See Appendix D for mineral name abbreviations.

Granitoids within Metasedimentary Units

Sample	Unit	Lithology #	N LAT	W LONG
BLS10	MU*	Hbl granite gneiss	43.8350	74.4917
BMF43	MU	Bt Charnockite	43.7717	74.9425
MKB127	MU	Mt-Bt granite gneiss	43.6081	75.1569
MKB277	MU	Bt-Cpx granite gneiss	43.6540	75.0470
OFB72	MU	Mt-Bt granite gneiss	43.6847	74.9967
OFB108	MU	Bt granite gneiss	43.7444	74.9806
RLS12	MU	Bt granite gneiss	43.8158	74.6711
OFC47	KZb	Bt granite gneiss	43.5914	74.7986
OFC61	KZb	Mt-Bt granite gneiss	43.5397	74.8000
WCH23	KZa	Bt granite gneiss	43.6350	74.6789
WCH26	KZa	Hbl granite gneiss	43.6227	74.6700
WCS13	KZa	Bt-Hbl granite gneiss (Grt)	43.6194	74.6419

Unit TH Gneisses

BMC70	TH	Ilh-Cpx-Mhg granite gneiss	43.9133	74.8550
BMS23	TH	Ilh-Bt-Mhg granite gneiss (Ttn)	43.9083	74.8064
BMS24K	TH	Ilh-Cpx-granite gneiss (Ttn)	43.9061	74.8142
BMS24P	TH	Ilh-Cpx-Qtz-Pl gneiss	43.9061	74.8142
BMS25	TH	Ilh-Bt-Cpx granite gneiss (Ttn)	43.9036	74.8222
BMS27	TH	Ilh-Phl-granite gneiss (Ttn)	43.9072	74.8281
MKB07B	TH	Ilh-Phl-Mhg-Cpx granite gneiss	43.7000	75.0136
MKB70A	TH	Mt-Bt-Sil granite gneiss	43.6653	75.0750
MKB70B	TH	Ilh-Phl-Cpx granite gneiss (Ttn)	43.6653	75.0750
MKB190	TH	Ilh-Cpx-granite gneiss (Ttn)	43.6339	75.0827
MKB273	TH	Ilh-Phl-Cpx granite gneiss (Ttn)	43.6520	75.0730
MKC021A	TH	Ilh-Phl-granite gneiss (Grt, Ttn)	43.6922	75.0283
MKJ01	TH	Ilh-Cpx granite gneiss (Ttn)	43.6519	75.0772
MKS36	TH	Ilh-Mhg-Cpx granite gneiss (Ttn)	43.6681	75.0678
MKS79A	TH	Bt Quartz Syenite Gneiss	43.6156	75.1022
MKS79C	TH	Bt granite gneiss (Ttn)	43.6156	75.1022
MKS80	TH	Phl granite gneiss	43.6906	75.0283

Mafic Metaigneous Rocks and Metanorthosite

NFS22	AM	Mt-Qtz-Kfs-Opx-Cpx amphibolite	43.7628	75.2242
OFC69	AM	Opx-Cpx amphibolite	43.5343	74.7860
RLS134	BL	Grt-Opx-Cpx-Bt schist	43.8158	74.6433
WCA30B	CM	Cpx-Scp amphibolite (Ttn)	43.6867	74.6675
BES06	GA*	Bt-Cpx-Hbl gabbro	43.8839	75.3656
BLS06C	GA*	Kfs-Opx-Cpx amphibolite	43.8939	74.4192
BMS40	GA	Opx-Cpx amphibolite	43.9767	74.7992

* Samples from adjacent quadrangles

Significant minor constituents shown in parentheses

See Appendix D for mineral name abbreviations.

Mafic Metaigneous Rocks and Metanorthosite *continued*

Sample	Unit	Lithology #	N LAT	W LONG
BMT08B	GA	Kfs-Opx-Cpx amphibolite	43.9525	74.8811
NFI15A	GA	Bt amphibolite	43.8097	75.2111
NFS35A	GA	Bt-Cpx amphibolite	43.8753	75.1369
NFS35B	GA	Kfs-Opx-Cpx amphibolite	43.8753	75.1369
NFS38	GA	Bt amphibolite	43.8911	75.1817
NFS39	GA	Opx-Cpx amphibolite	43.9156	75.1950
OFC89	GA	Bt-Opx-Cpx amphibolite	43.5619	74.9508
RLD171	GA	amphibolite	43.8744	74.5044
RLS82B	GA	Kfs-Opx-Cpx amphibolite	43.9244	74.7169
WCS57B	GA	Opx-Cpx-Bt amphibolite	43.6889	74.6222
BLS09	JA	Hbl jotunite	43.9739	74.4281
BMC15	JA	Qtz-Hbl gabbroic anorthosite	43.8136	74.9503
BMC25	JA	Bt-Hbl anorthosite	43.8269	74.9053
BMS52	JA	Hbl anorthosite	43.7981	74.9211
BMX304	JA	Hbl jotunite	43.8144	74.9086
BMX03	JA	Bt-Hbl anorthosite	43.9944	74.7692
MKS27	JA	jotunite	43.7200	75.1892
NFC04	JA	Bt-Hbl gabbroic anorthosite	43.8647	75.0156
RLS53	JA	Grt-Qtz-Kfs jotunite	43.9747	74.5736
RLS77B	JA	Grt-Qtz-Kfs jotunite	43.9114	74.6831
RLS90	JA	Bt-Hbl gabbroic anorthosite	43.8778	74.6531
RLU48	JA	Qtz-Kfs jotunite	43.9936	74.6003
OFS39	KZA	Bt-Hbl leuconorite	43.6125	74.7525
WCB83	KZA	Opx-Cpx amphibolite	43.6278	74.6322
OFF29C	LD	Kfs-Bt amphibolite (Ttn)	43.7175	74.7703
MKB111	MU	Cpx amphibolite	43.6053	75.1958
MKS96	MU	Chl-Cpx amphibolite	43.6100	75.0275
OFH15	OG	Olivine metagabbro	43.6608	74.7611
WCC25	OG	Opx-Cpx-Hbl anorthosite	43.5744	74.6547
WCC26	OG	Hbl leuconorite	43.5772	74.6992

Mafic Rocks in Unit CG

MKS28	CG	Hbl-Cpx quartz diorite	43.7292	75.1394
BMP40X	CG	Hbl-Cpx leucodiorite	43.7703	74.8467

Metasedimentary Rocks

BLS10A	CM*	Kfs-Di granulite	43.8350	74.4917
MKB183	BM	Grt-Sil-Bt-Kfs-Qtz gneiss	43.7156	75.2367
PL-MRT	BM*	Mt-Sil-Bt-Qtz-Pl-Kfs gneiss	43.6139	75.3167
RLN15A	BM	Bt-Pl granulite	43.8847	74.7494

* Samples from adjacent quadrangles

Significant minor constituents shown in parentheses

See Appendix D for mineral name abbreviations.

Metasedimentary Rocks *continued*

Sample	Unit	Lithology #	N LAT	W LONG
RLS125	BM	Di-Scp-Pl-Kfs-Qtz granulite	43.9381	74.7178
MKB274	BL	Bt-Qtz-Di-Pl gneiss	43.6542	75.0794
MKC16	BL	Sil-Grt-Bt-Qtz-Kfs-Pl gneiss	43.6606	75.0275
MKS102	BL	Ru-Sil-Bt-Pl-Crd-Pmn gneiss	43.6108	75.1672
RLC021	BL	Tur-Grt-Pl-Bt quartzite	43.7653	74.7489
RLC022	BL	Sil-Bt-Qtz schist	43.7653	74.7489
RLS135	BL	Di-Phl-Tr schist	43.8311	74.6486
WCH12	KZa	Grt-Bt-Qtz-Pl gneiss	43.7052	74.7108
BMB81	MU	Kfs-Di quartzite	43.7640	74.9790
BMS21	MU	Grt-Bt-Kfs-Pl-Qtz gneiss	43.7639	74.7986
MKD23C	MU	Ttn-Kfs-Di granulite	43.7464	75.0328
MKC23D	MU	Di-Kfs quartzite	43.7464	75.0328
MKC01	TH	Ep-Grt-Scp-Kfs-Qtz-Cal marble	43.6908	75.0253
MKC022	TH	Cal-Ttn-Grt-Di-Scp-Pl quartzite	43.6922	75.0283
MKD49	TH	Ep-Grt-Scp-Kfs-Qtz granulite	43.7217	75.0019
MKS82E	TH	Ttn-Ep-Grt-Di-Scp-Kfs quartzite	43.6917	75.0283
OFB113	TH	Di-Qtz-Pl gneiss	43.7306	74.9850

* Samples from adjacent quadrangles

Significant minor constituents shown in parentheses

See Appendix D for mineral name abbreviations.

Appendix D

Abbreviations Used in Text, Figures, Equations, and Tables

Minerals and endmembers (uppercase first letter)

Ab	Albite	Mhg	Magnesiohastingsite
An	Anorthite	Me	Meionite
Amp	Amphibole	Mt	Magnetite
Ap	Apatite	Opx	Orthopyroxene
Bt	Biotite	Or	Orthoclase
Cal	Calcite	Per	Perthite
Crd	Cordierite	Phl	Phlogopite
Chl	Chlorite	Pl	Plagioclase feldspar
Cpx	Clinopyroxene	Pmn	Prismatine
Di	Diopside	Qtz	Quartz
En	Enstatite	Ru	Rutile
Ep	Epidote	Scp	Scapolite
Fa	Fayalite	Sil	Sillimanite
Fl	Fluorite	Spl	Spinel
Gr	Graphite	Tlc	Talc
Grs	Grossular	Ttn	Titanite (sphene)
Grt	Garnet	Tr	Tremolite
Hbl	Hornblende	Tur	Tourmaline
Il	Ilmenite	Tpz	Topaz
Ilh	Ilmenohematite	Wo	Wollastonite
Kfs	K-feldspar	Zr	Zircon
Mc	Microcline		

Normative minerals (Tables 1A–E, 3, and 4; lowercase first letter)

qz	quartz	di	diopside	mt	magnetite
or	orthoclase	ol	olivine	co	corundum
ab	albite	ne	nepheline	ap	apatite
an	anorthite	lc	leucite		
hy	hypersthene	il	ilmenite		

Quadrangles

The first two characters in a sample number designate the quadrangle of origin. Quadrangles are designated in text by 3-letter abbreviations ending in "Q", e.g., BMQ stands for Big Moose Quadrangle.

Quadrangles within map area

BM Big Moose 15'
MK McKeever 15'
NF Number Four 15'
OF Old Forge 15'
RL Raquette Lake 15'
WC West Canada Lakes 15'

Adjoining quadrangles

BE Belfort 7.5'
BL Blue Mountain Lake 15'
NW North Wilmurt 7.5'
OH Ohio 15'
OS Oswegatchie 15'
PL Port Leyden 7.5'

Miscellaneous abbreviations

meg mineral present as megacrysts (Appendix C only)
mg Niggli mg index, i.e., the molecular $Mg/(Mg + Fe)$ ratio.



The New York State Museum is a program of
The University of the State of New York
The State Education Department

ISBN 1-55557-171-9



9 781555 571719

Metamorphosed Intrusive or Volcanic Rocks

Metamorphosed Intrusive or Volcanic Rocks

- [illegible]

Metamorphosed Sedimentary Rocks










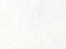






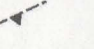
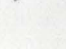

- [illegible]

Mixed Units

- KZn:** White to pink, waxy foliated (magnetite) + hornblende – (garnet) – biotite leucocrysts with interlayered amphibole and lesser amounts of biotite or hornblende granitic grains, basaltic clasts, (garnet) – biotite – quartz – plagioclase grains, and biotite schist.
- BM:** White to buff, pink, or grey waxy foliated (fluorite) – (magnetite) – (biotite) – (garnet) – (sillimanite) – (plagioclase) – quartz – albite foliated leucocrysts with subordinate layers of calcite/granite grains. (fluorite) – sillimanite – garnet – quartz – K feldspar – biotite or biotite + hornblende granitic grains. Contains stannite beds of stannite and arsenobismite that are weakly separated as JA where sufficiently thin.
- LD:** (Lake Dorset Sequence). White to grey or pink, waxy to foliated, (magnetite) – biotite – quartz – K feldspar protomylon and leucocrysts with subordinate but locally common layers of (magnetite) – biotite – quartz – plagioclase grains, biotite schist, (magnetite) – biotite – quartz – plagioclase grains, hornblende granitic protomylon, and calcite/granite grains.

Note: Phases in parentheses may or may not be present. For more complete unit descriptions, see the accompanying text.

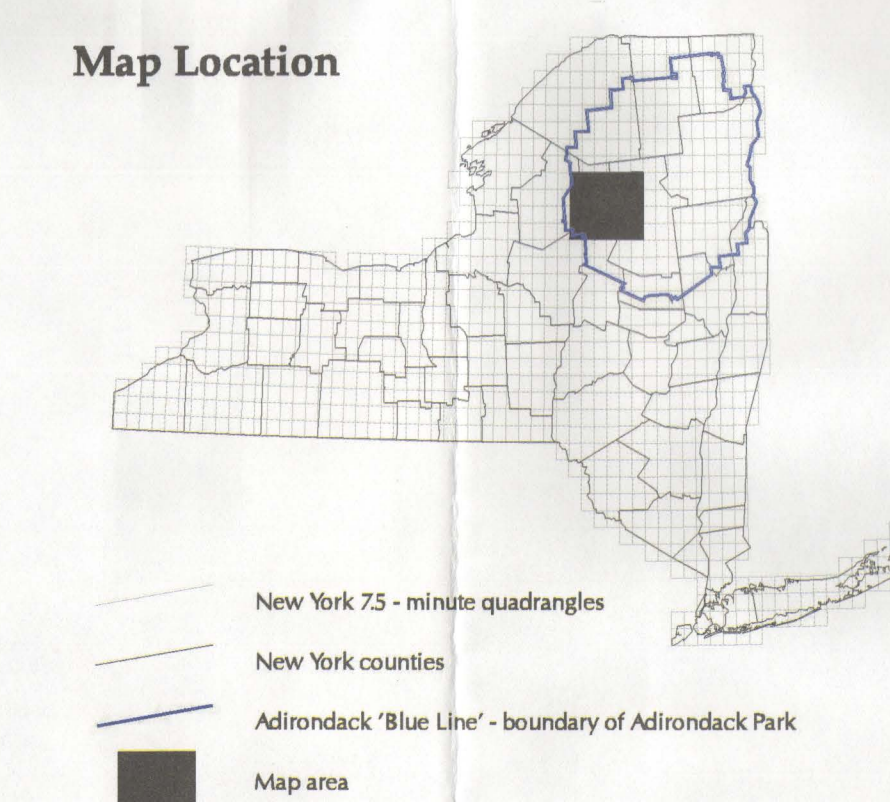
Structure Symbols

- | | | | |
|---|----------------------------------|---|----------------------------------|
|  | Contact, approximate |  | Vertical foliation |
|  | Contact, inferred |  | Horizontal foliation |
|  | Contact, concealed |  | Bearing and plunge of lineation |
|  | Fault, defined |  | Horizontal lineation |
|  | Fault, approximate |  | Bearing and plunge of minor fold |
|  | Fault, inferred |  | Anticline |
|  | Thrust fault, approximate |  | Syncline |
|  | Thrust fault, normal fault |  | Overturned anticline |
|  | Low-angle normal fault, inferred |  | Overturned syncline |
|  | Strike and dip of foliation | | |

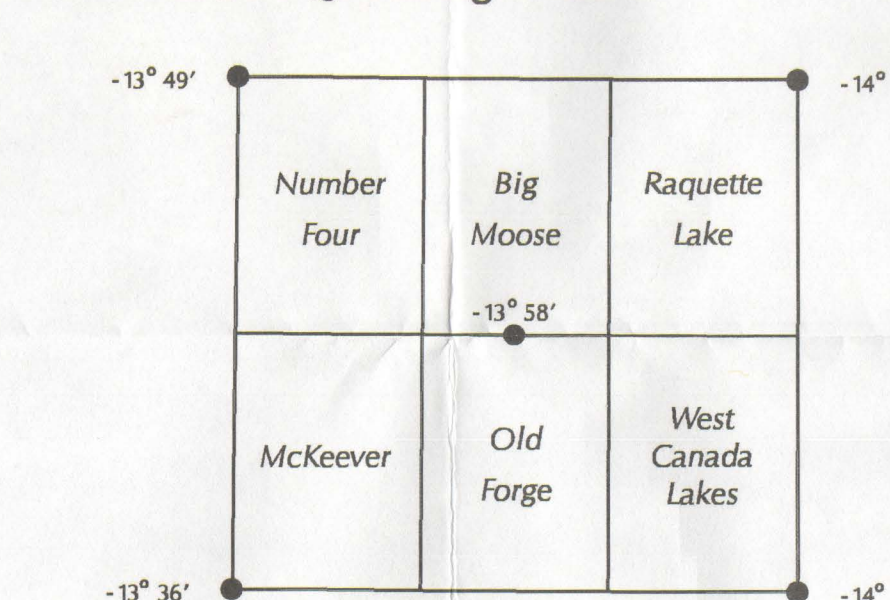
Other Symbols

- | | | | |
|---|-----------|---|----------------|
| | Roads | | State Route 28 |
| | Railroads | | 75-minute time |

Map Location



15 - Minute Quadrangle Index



Magnetic declination values for the year 2002 for the four corners and center (43° 45' N, 78° 52' 30" W) of the map are shown. Values are generally accurate to 30 minutes. Declination values were obtained from the National Geophysical Data Center's Geomagnetic website (<http://www.ngdc.noaa.gov>) and are based on the International Association of Geomagnetism and Aeronomy's International Geomagnetic Reference Field - 2000.

NOTICE

While every effort has been made to insure the integrity of this map and text, and the factual data upon which it is based, the New York State Education Department ("NYSED") makes no representation or warranty, expressed or implied, with respect to accuracy, completeness, or suitability for any particular purpose. NYSED assumes no liability for damages resulting from the use of any information, apparatus, method, or process disclosed in this map and text, and urges independent site-specific verification of the information contained herein. Any use of trade, product, or firm names is for descriptive purposes only and is not endorsement by NYSED.

Philip R. Whitney, Robert H. Fakundiny, & Yngvar W. Isachsen

2002

Map & Chart Series 44
New York State Museum

